


Technical Report No. 215

004860-1-T

A MIMI PROPAGATION STUDY: COHERENT SPECTRA OF  
WIDEBAND UNDERWATER ACOUSTIC RECEPTIONS IN THE  
STRAITS OF FLORIDA, 25 NOVEMBER 1970

by

Gerald N. ~~Cederquist~~

Approved by   
Theodore G. Birdsall

COOLEY ELECTRONICS LABORATORY  
Department of Electrical and Computer Engineering  
The University of Michigan  
Ann Arbor, Michigan

for

Contract No. N0014-67-A-0181-0035  
Office of Naval Research  
Department of the Navy  
Arlington, Va. 22217

May 1973

THE UNIVERSITY OF MICHIGAN  
ENGINEERING LIBRARY

Approved for public release; distribution unlimited.

en8n

UMR0917

## ABSTRACT

In an underwater acoustic propagation experiment conducted in November 1970 a periodic broadband signal, centered about 420 Hz, was transmitted across the Straits of Florida continuously for 19 days. This report presents the preliminary results from spectral analysis of the acoustic reception of this signal at Bimini, Bahamas, during a 7.61-hour period on 25 November 1970. The spectra are noteworthy for their slow rate of change during this period. Plots of the spectral amplitude and phase of the reception are presented for a 50 Hz bandwidth centered about 420 Hz.

## FOREWORD

Underwater acoustic propagation experiments of the past few years have verified that the general features of long-range, single frequency reception are complicated amplitude fluctuations with deep fades, relatively stable phase and frequency, accompanied by surface scattered energy.

The next level of experiment should establish how close two frequencies have to be to behave "similarly," and how far apart two frequencies have to be to behave "independently." The work reported here is at this level. Sixty-one signal frequencies with spacing of  $5/6$  hertz that were transmitted simultaneously for over seven hours were analyzed and preliminary results are given in this report.

T. G. Birdsall

## TABLE OF CONTENTS

	<u>Page</u>
ABSTRACT	iii
FOREWORD	iv
LIST OF ILLUSTRATIONS	vi
AUTHOR'S PREFACE	viii
1. INTRODUCTION	1
2. THE MIMI PROPAGATION EXPERIMENT OF NOVEMBER 1970	3
2.1 The Miami-Bimini Range	3
2.2 The Transmitted Signal	6
2.3 The Quantities Measured	9
3. THE PROCESSING OF THE BIMINI RECEPTION	12
3.1 The Equipment Configuration at Bimini	12
3.2 On-Site Digital Filtering and Recording	12
3.3 Selection of Data for Spectral Analysis	17
3.4 The Spectral Analysis	18
4. PRELIMINARY ANALYSIS AND CONCLUSIONS	21
4.1 The On-Line Power Measurements	21
4.2 Spectral Plots	23
4.3 Preliminary Conclusions	28
APPENDIX A: Constant Time Plots	31
APPENDIX B: Constant Frequency Plots	78
REFERENCES	110
DISTRIBUTION LIST	111

## LIST OF ILLUSTRATIONS

<u>Figure</u>	<u>Title</u>	<u>Page</u>
1	The Miami-Bimini range: (a) physical layout, (b) bottom profile	4
2	Sound speed vs depth, Miami to Cat Cay, 28-29 November 1961	6
3	Sound ray paths along $25^{\circ}44'$ on 28-29 November 1961	7
4	A complement-phase modulated signal (a) a portion of the modulating waveform (b) the resulting CM transmission	8
5	The RMS spectrum of a complement-phase modulated signal for $L = 15$ and $D = 8$	10
6	Equipment configuration at Bimini	13
7	Complex demodulation of the hydrophone reception	14
8	The carrier and sideband filters used on the November 1970 reception	16
9	On-line power measurements for 25 November 1970	22
10	Prototype constant time plot	24
11	Prototype constant frequency plot	27
12	Spectrum at $t_0 = 1118$ hours, 25 November 1970	29
13	Spectrum at $t_0 + 1$ minute, 40 seconds	29
14	Spectrum at $t_0 + 10$ minutes	30

LIST OF ILLUSTRATIONS (Cont.)

<u>Figure</u>	<u>Title</u>	<u>Page</u>
15	Spectrum at $t_0 + 1$ hour, 3 minutes, 20 seconds	30

## AUTHOR'S PREFACE

This report presents preliminary results rather than the polished conclusions of a completed investigation. No attempt has been made to draw conclusions from the data or to analyze it. A more substantial report on spectral analysis of Project MIMI transmissions is planned for a later date.



## 1. INTRODUCTION

In November 1970 an underwater acoustic propagation experiment (Project MIMI) was conducted jointly by the Acoustics Group of the Rosenstiel School of Marine and Atmospheric Sciences at The University of Miami (Florida) and the Signal Processing Group of the Cooley Electronics Laboratory at the University of Michigan. A periodic broadband signal centered about 420 Hz was transmitted continuously across the Straits of Florida for 19 days. In the on-site portion of the experiment, the power and phase angle of the carrier, the power in the signal sidebands, and the noise power in the signal band were measured at two receiving sites. In addition, the total power and the power spectrum in a narrow band about the carrier frequency were computed to measure signal modulation due to forward-scattered surface reverberation. The received signal was also correlated with a pulse compression reference signal to measure the multipath structure of the acoustic channel.

During the course of the experiment, approximately 9 million digital words of the reception were recorded for later processing. Portions of these recordings were complex-valued demodulates of a comb-filtered version of the reception. A period of 7.61 hours on 25 November 1970 for which such recorded demodulates were available from Bimini, Bahamas, was selected for spectral analysis.

Chapter 2 presents background information on the acoustic range and equipment configuration used. Chapter 3 details the processing of the reception at Bimini and the methods used to transform the recorded receptions to frequency domain, and Chapter 4 presents plots of the spectra of the reception.

## 2. THE MIMI PROPAGATION EXPERIMENT OF NOVEMBER 1970

### 2.1 The Miami-Bimini Range<sup>1</sup>

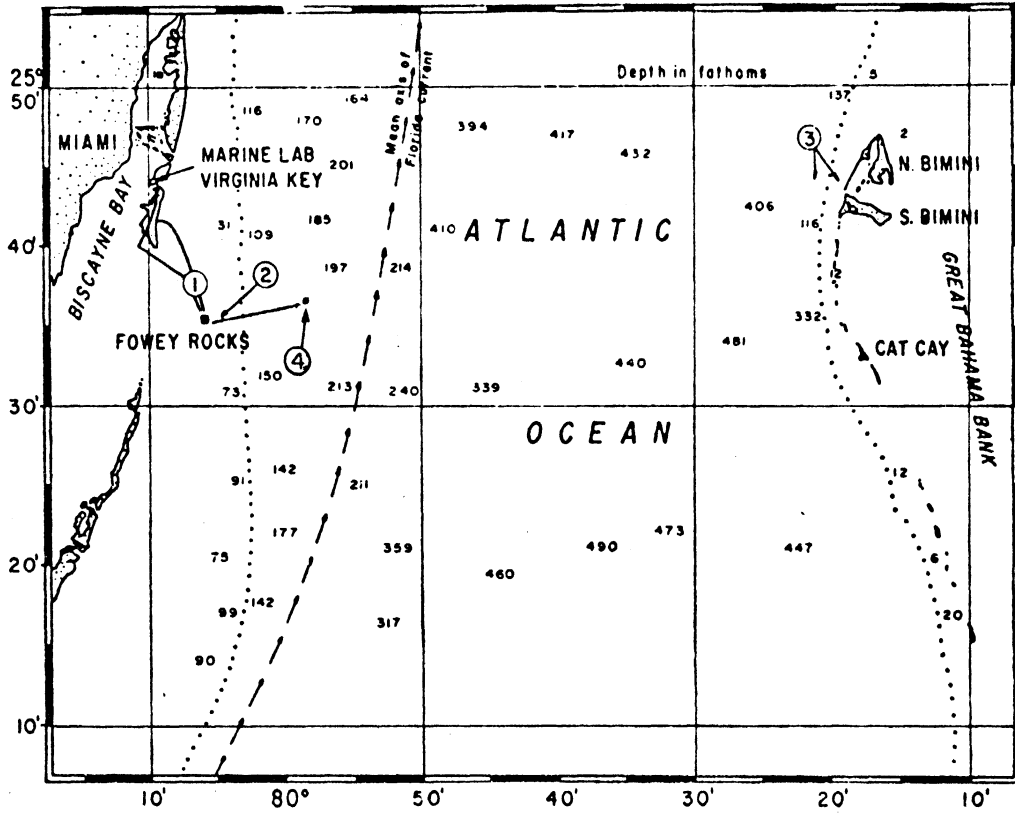
The Miami-Bimini range, illustrated in Fig. 1, is part of the facilities of the Acoustics Group of the Rosenstiel School of Marine and Atmospheric Sciences (RSMAS) of The University of Miami. It extends across the Straits of Florida from Miami to Bimini, Bahamas.

The transmitting site is located at Fowey Rocks [point 2, Fig. 1(a)] approximately 12 miles (19 km) from the RSMAS laboratory and is connected to the laboratory by telephone lines (point 1, Fig. 1). At Fowey Rocks a bottom-mounted projector is located in 72 feet (22 m) of water at the focal point of a 24-foot (7.3 m) compliant tube parabolic reflector. It has a maximum source level of 120 dB/ $\mu$ bar at 1 m with a nominal bandwidth of 100 Hz. The source level for the November test was 110 dB/ $\mu$ bar/meter. The 30<sup>0</sup> beamwidth is directed toward Bimini, a distance of 43 nautical miles (78.6 km).

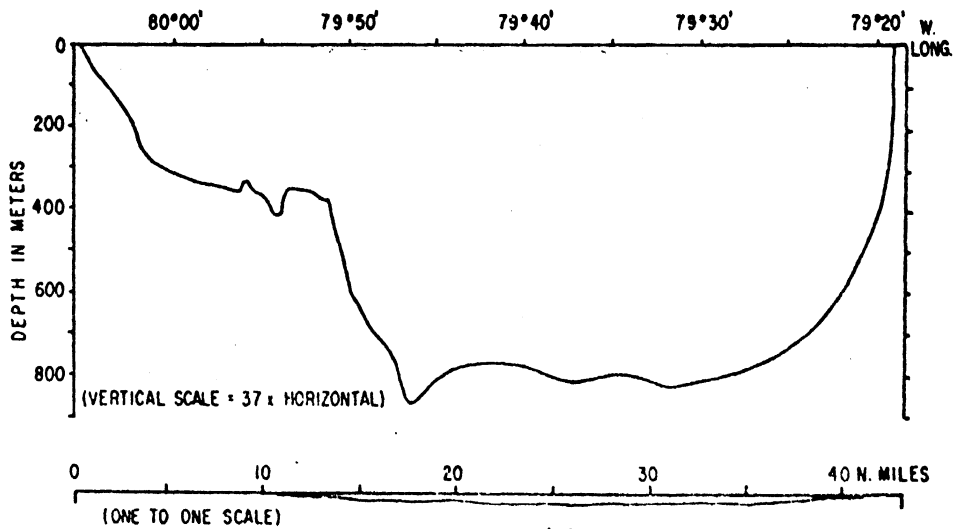
Two receiving sites were used in the experiment. At the first, a bottom-mounted hydrophone is located in 1000 ft (305 m) of water (point 4, Fig. 1) approximately 7 $\frac{1}{2}$  nautical miles (12 km) from the source. The reception from this hydrophone is transmitted to the

---

<sup>1</sup>The material in this section is taken from Ref. 1. A more complete discussion on the Miami-Bimini range can be found there.



(a)



(b)

Fig. 1. The Miami-Bimini range: (a) physical layout, (b) bottom profile

RSMAS laboratory by marine cable. The second receiving site is located off Bimini (point 3, Fig. 1). There, two bottom-mounted hydrophones are cable-connected to a laboratory on Bimini. These hydrophones are located at 100 and 1200 feet depth (30 m and 366 m), 1 and 2 miles (1.8 and 3.6 km) off-shore and are referred to as the shallow and deep hydrophones, respectively.

The bottom profile of the Miami-Bimini range is illustrated in Fig. 1(b). A shelf extends out from Miami about 15 miles (28 km) to a depth of 400 m followed by a sharp drop-off to a depth of 800 m. Thirty miles (56 km) beyond, the Grand Bahamas bank rises abruptly from this depth.

A sound speed profile, obtained during November 1961, appears in Fig. 2. This profile is characterized by a mixed layer which extends to the relatively constant depth of 100 m followed by a region of negative velocity gradient. It is noted that the velocity gradient becomes increasingly negative as the Florida shore is approached.

The ray diagram corresponding to the sound speed profile of Fig. 2 is shown in Fig. 3. This diagram shows sound being propagated by reflections from surface and bottom, by refraction and reflection from the bottom and by refraction and reflection from the surface. This latter mode of propagation does not appear in ray diagrams calculated from sound-speed profiles obtained in the spring and summer.

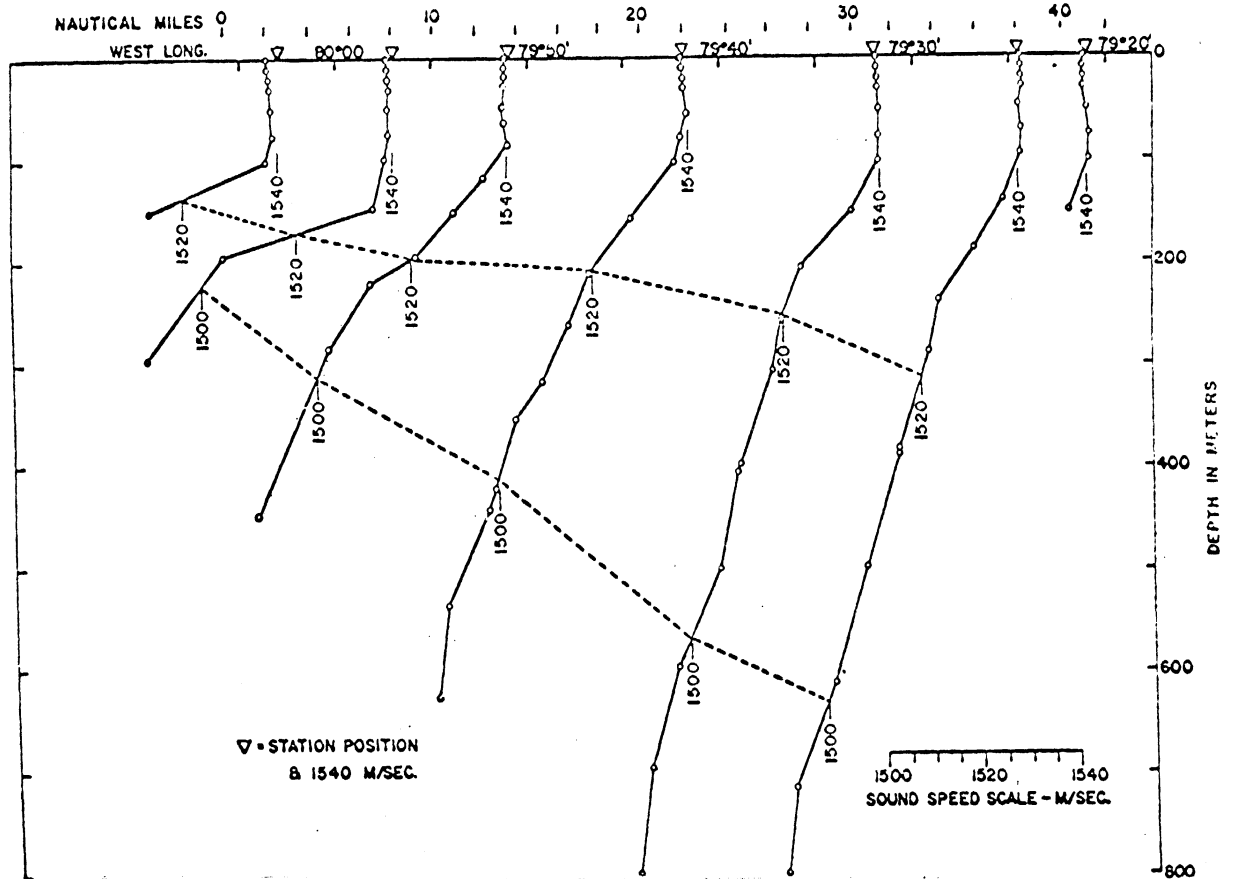


Fig. 2. Sound speed vs. depth, Miami to Cat Cay,  
28-29 November 1961

## 2.2 The Transmitted Signal

The transmitted signal, complement-phase modulate (CM), consisted of a carrier wave at 420 Hz modulated by a linear-maximal, pseudorandom sequence. The phase of the carrier was shifted to either  $+45^{\circ}$  or  $-45^{\circ}$  depending on the value of the binary digit in the modulating sequence. A portion of such a CM signal is shown in Fig. 4 where

$$f_c = \text{carrier frequency in hertz}$$

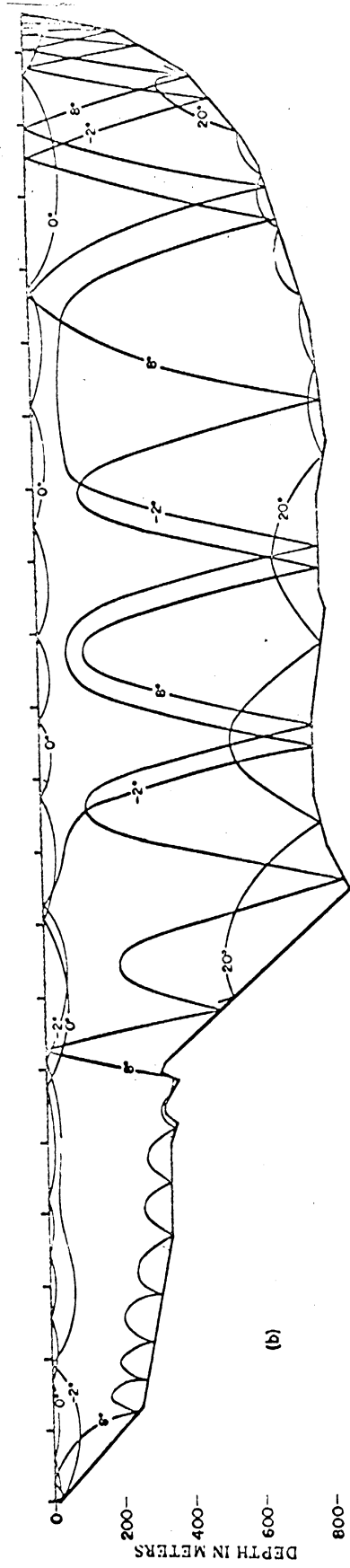


Fig. 3. Sound ray paths along 25° 44' on 28-29 Nov. 1961

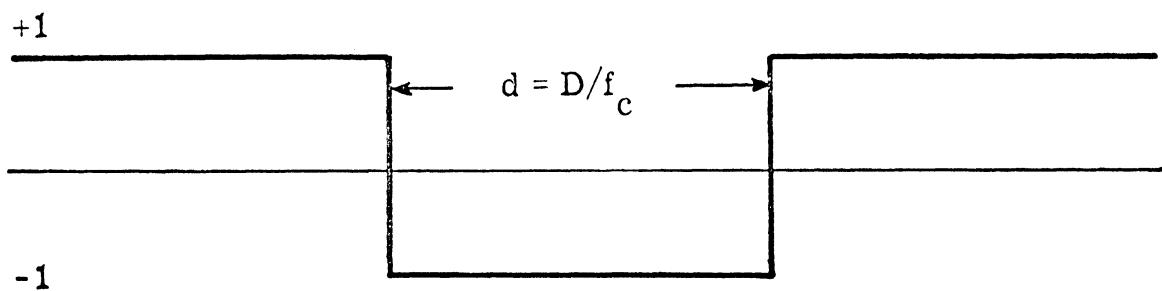
$d$  = duration of the sequence digit in seconds

$D$  = number of cycles of carrier per sequence digit.

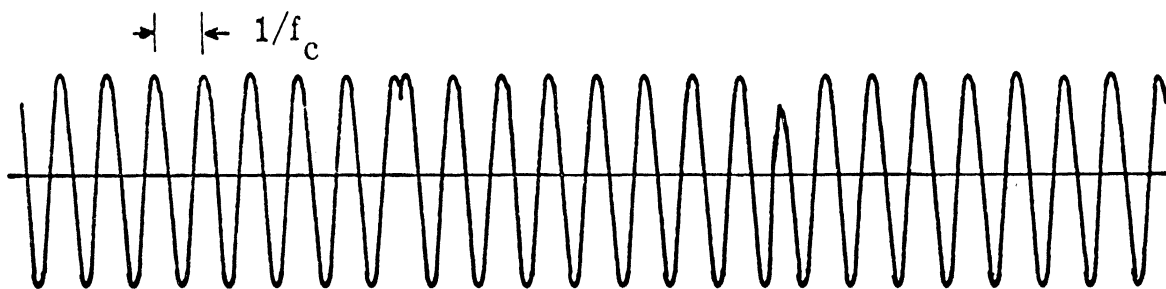
For all MIMI experiments, the number of cycles of carrier per digit  $D$  is chosen to be integer-valued; thus the CM signal is periodic with period

$$T = Ld = LD/f_c$$

where  $L$  is the number of digits in one period of the modulating sequence.



(a)



(b)

Fig. 4. A complement-phase modulated signal  
 (a) a portion of the modulating waveform  
 (b) the resulting CM transmission



The RMS power spectrum of a typical periodic signal of CM type is shown in Fig. 5. For all such signals, the spectrum has a  $\sin(x)/x$  envelope except at the carrier frequency. Approximately half of the total power is contained in the carrier line with the other half contained in the sideband lines.

The signal used in the November experiment had

$$f_c = 420 \text{ Hz}$$

$$D = 8 \text{ cycles/digit}$$

and  $L = 63 \text{ digits}$

with the result that the digit duration and the period were

$$d = 0.019 \text{ seconds}$$

and  $T = 1.2 \text{ seconds}$

The spacing  $\Delta f$  between adjacent lines in the transmitted spectrum is

$$\Delta f = 1/T = 5/6 \text{ Hz}$$

Finally, there are 127 spectral lines lying within the nominal transducer bandwidth of about 105 Hz. The bandwidth of the main lobe of the transmitted spectrum is also 105 Hz.

### 2.3 The Quantities Measured

The quantities measured on site during the November 1970

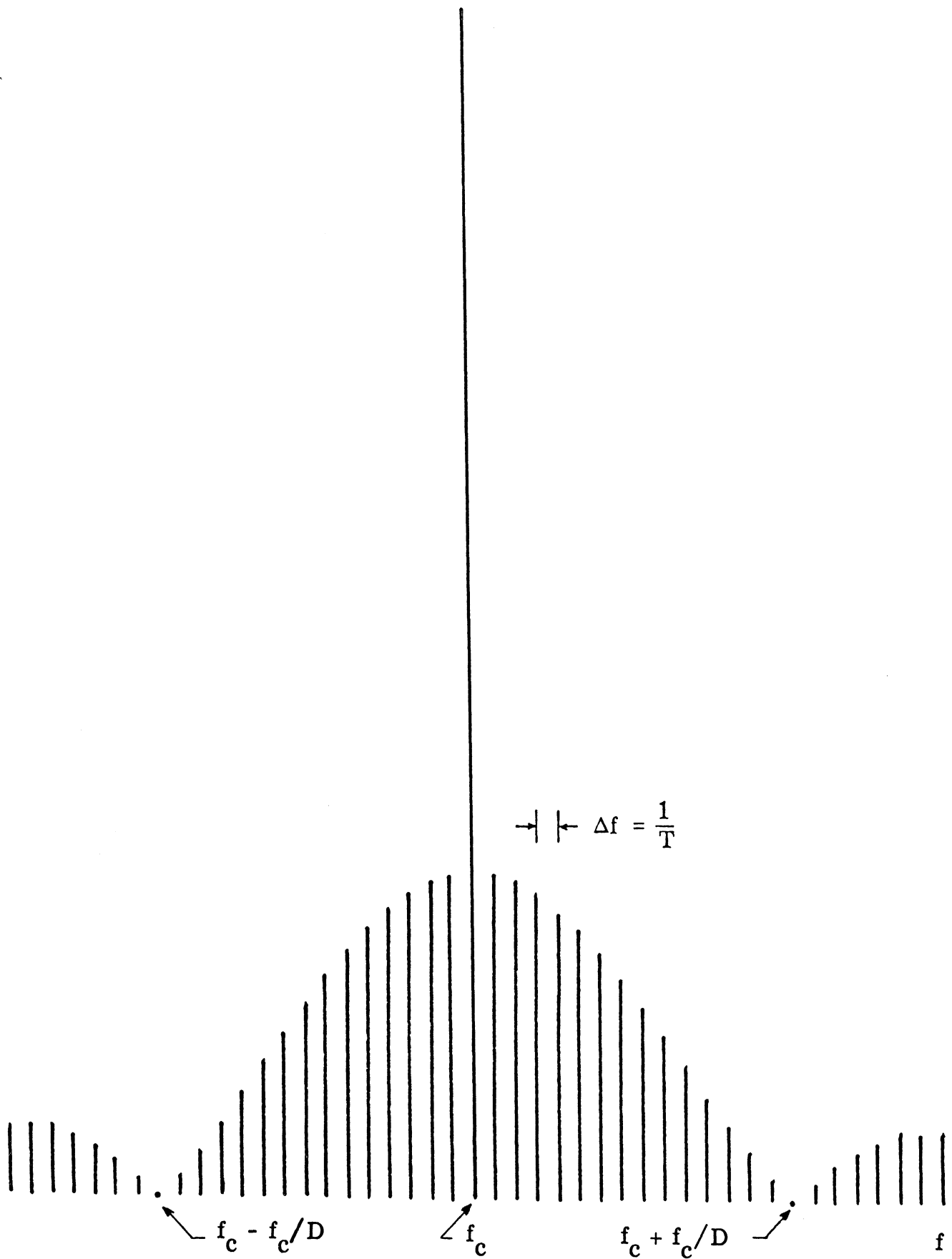


Fig. 5. The RMS spectrum of a complement-phase modulated signal for  $L = 15$  and  $D = 8$

experiment can be grouped into three categories: (1) signal power, noise power and carrier angle measurements, (2) forward-scattered surface reverberation measurements, and (3) multipath structure measurements. These measurements were obtained using digital processing techniques implemented by a digital computer located at each receiving site. Each of the measurements was computed and recorded every 100 sec on the basis of 80 sec of reception. (The remaining 20 sec were used solely for computations.) As each 80 sec of reception was digitized, it was effectively passed through a comb-filter before being stored in the memory of the computer. This filtered reception was recorded on magnetic tape for later processing at Cooley Laboratory, and the spectra contained in this report are derived from this reception.

A discussion relating the spectra and the simultaneous measurements from categories (1) and (2) above is given in Chapter 4. For a detailed discussion of the on-site measurements, the reader is referred to Ref. 2.

### 3. THE PROCESSING OF THE BIMINI RECEPTION

#### 3.1 The Equipment Configuration at Bimini

The equipment configuration at Bimini is shown in Fig. 6. A frequency standard accurate to 1 part in  $10^{10}$  provides a reference signal that is converted to a 1680 Hz (equal to 4 times carrier frequency) clock signal by a frequency synthesizer. After passing through an isolation amplifier, the clock signal controls the analog-to-digital conversion circuitry on the computer.

The receptions from both the shallow and the deep hydrophones are passed through signal conditioning bandpass filters and amplifiers and brought to a patch panel. There the operator selects which hydrophone signal is to be connected into the A/D converter on the computer. Because of an equipment failure on the deep hydrophone link, the shallow hydrophone reception was used for the data covered in this report. (Recall that the shallow hydrophone is in 100 ft of water 1 mile offshore.)

#### 3.2 On-Site Digital Processing and Recording

The computer is programmed to demodulate the input at the A/D converter from a real-valued, bandpass signal centered at 420 Hz to a complex-valued, lowpass signal centered about dc (i. e., zero Hz). The processing is effectively shown in Fig. 7. The input signal

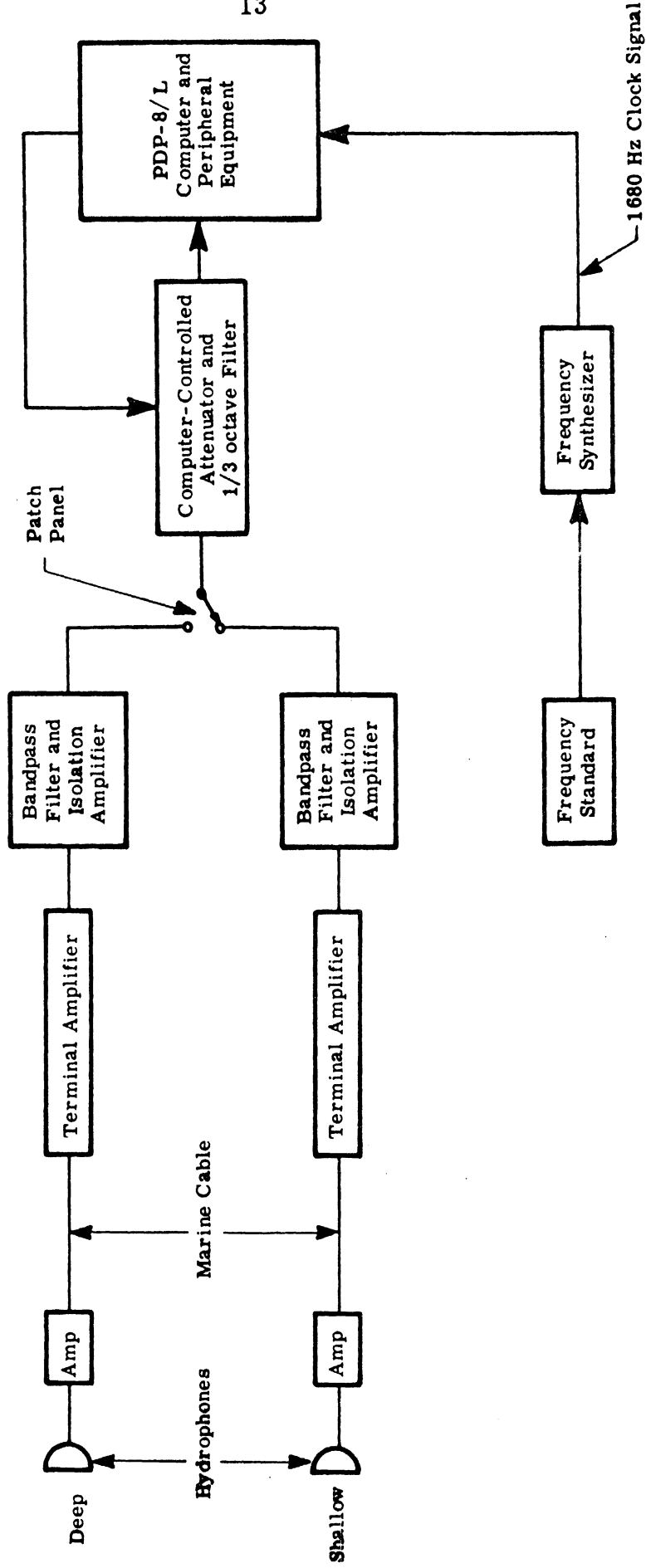


Fig. 6. Equipment configuration at Bimini

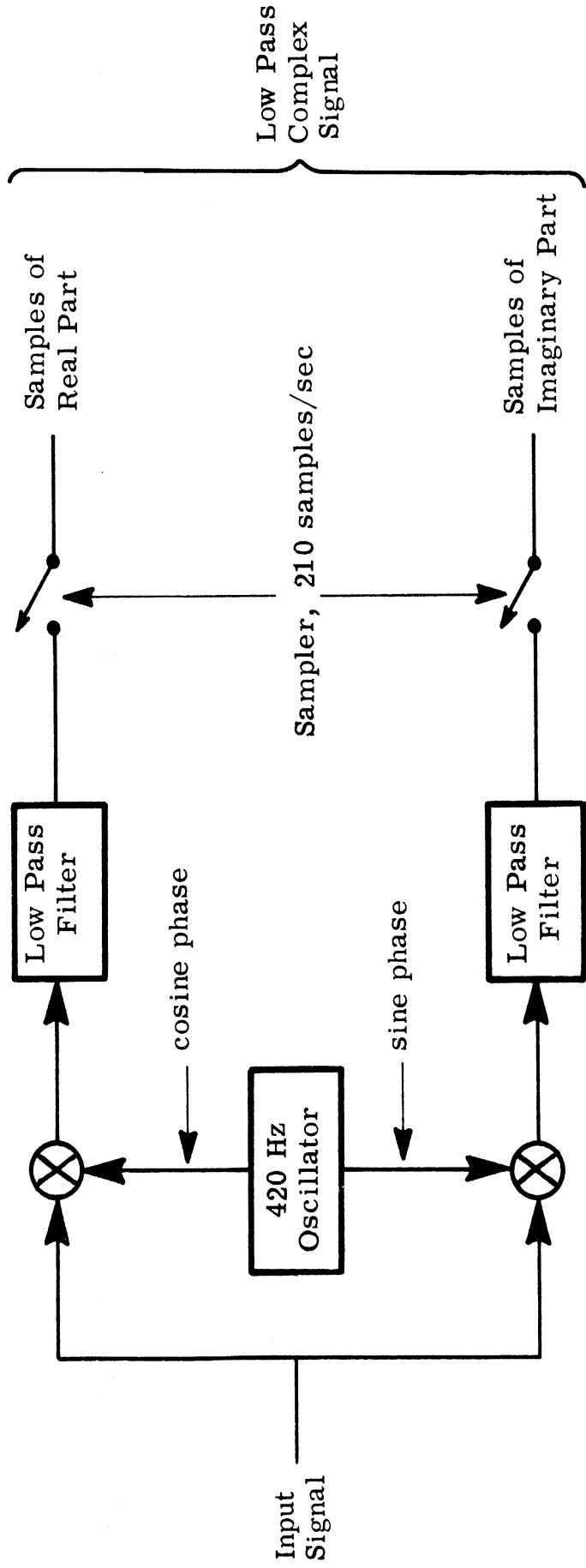


Fig. 7. Complex demodulation of the hydrophone reception

is demodulated by multiplication with both sine and cosine phase of a 420-Hz reference signal. A lowpass filter on the output of each multiplier passes only the difference-frequency components to the samplers, which provide 210 samples/sec of each channel. If the output from the cosine phase channel is called the real-part of the demodulated signal and the output of the sine channel is called the imaginary-part, then this real-imaginary pair can be thought of as a complex-valued representation of the input bandpass waveform.

In point of fact, no information is lost in this process, and each signal processing operation that can be performed on the bandpass signal can also be performed on the lowpass complex signal to yield the same results (Ref. 3). An advantage of the complex representation in this case is that the number of samples per second which must be dealt with depends only upon the bandwidth of the signal and not upon its center frequency.

Inside the computer, the complex samples are passed through a number of digital filters to perform the on-line measurements described in Section 2.3. The spectral characteristics of the filters germane to this current investigation are shown in Fig. 8. These filters separate the line spectrum of the transmission into two disjoint pieces: the carrier alone, and the sidebands excluding the carrier. Of course, both filter outputs contain those noise components that are immediately adjacent to the signal lines. The sideband filter

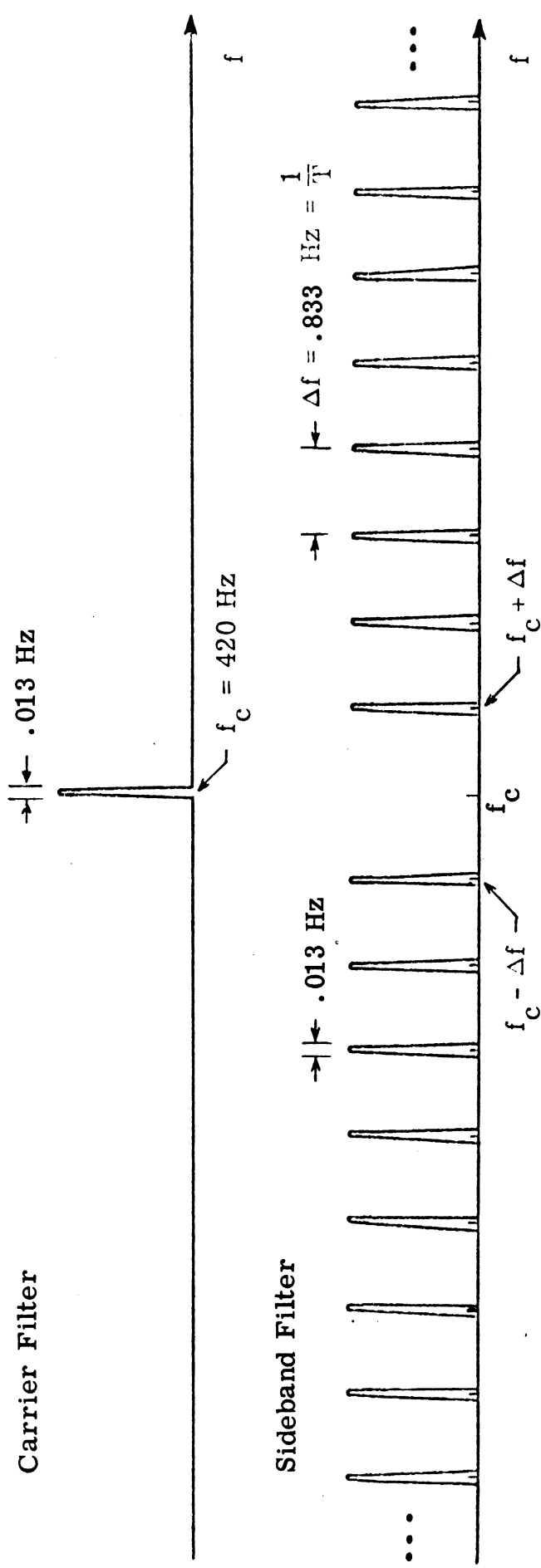


Fig. 8. The carrier and sideband filters used on the November 1970 reception



produces a time series of 252 complex points every 80 sec, and the carrier filter produces one complex point every 80 sec. The outputs of these filters are written onto magnetic tape after each 80-sec segment of reception is collected.

### 3.3 Selection of Data for Spectral Analysis

The record data from the Bimini receiving site span a period of 19 days. The data from the period from ~1130 hours to ~1900 hours local time, 25 November 1970, were selected for spectral analysis for the following reasons:

(1) Recordings of sideband filter and carrier filter outputs are available for that period from the 7-mile hydrophone cabled back to RSMAS (point 4 on Fig. 1).

(2) The receiving and transmitting frequency standards were closely matched in frequency during that period. (Inadvertently for some parts of the experiment, they were approximately 2 millihertz apart, which is enough to compromise the phase structure of the wideband spectra.)

(3) The wideband, sideband power shows two distinct modes of behavior during the period, one of lower, constant power and another of higher, varying power. This behavior had been observed in past years on the carrier power measurement at the end of November, and a more thorough investigation was sought.

The data for analysis consisted of

(1) 274 time series, each containing 252 complex points, and being the lowpass representation of an average (i.e., comb-filtered) period of the reception with the carrier removed.

(2) 274 complex points yielding carrier amplitude and phase.

Each (time series, carrier) pair was produced on the basis of 80 sec of data taken over a 100-sec time span. Thus the data spans  $274 \times 100$  sec =  $456 + 2/3$  min = 7.61 hrs.

### 3.4 The Spectral Analysis

The spectral analysis proceeded in the steps outlined below.

#### (1) Fourier Transformation of the Time Series

Each 252-point time series  $Z(i)$  was discrete-Fourier-transformed according to the following definition:

$$H(k) = \sum_{i=0}^{251} Z(i) e^{j \frac{2\pi ik}{252}}, \quad k = 0, \dots, 251$$

where  $j = \sqrt{-1}$ . As expected, the frequency spectrum  $H(k)$  had an extremely low carrier value. (That the carrier value was not zero is attributed to the round-off errors in the computation.)

#### (2) Reinsertion of the Carrier

The large amplitude of the carrier in relation to the sideband lines  $H(k)$  called for some scaling of the carrier prior to its

reinsertion into  $H(k)$  and subsequent display. The scale factor chosen was such as to transform the transmitted spectrum of Section 2.2 into a pure  $\sin(x)/x$  curve; i.e., the carrier was attenuated exactly enough to fit into the smooth  $\sin(x)/x$  curve of the other lines.

The ratio of transmitted carrier power for the CM signal used to the carrier power in the equivalent  $[\sin(x)/x]^2$  power spectrum is  $P$ , where

$$P = 1 + L \left( \frac{L-1}{L+1} \right) = L - 1 + \frac{2}{L+1}$$

For the  $L = 63$  digit sequence used in the experiment,

$$P = 62 - \frac{1}{32} = 62.03125 = (7.875992)^2$$

Since the spectra are in volts and not power, each carrier line was attenuated by  $1/7.875992$  and reinserted into its corresponding spectrum  $H(k)$  as  $H(0)$ .

### (3) Removal of Phase Bias

The relative phase of each of the frequency lines in the transmitted signal is determined by the pseudorandom modulating sequence. In general, the phase angles of adjacent lines are not at all close, making visual determination of phase behavior for even closely spaced lines rather difficult. Consequently, the phase of each line in all 274 received spectra was modified by subtracting from it the phase of the same line in the transmitted spectrum. This allowed phase

plots for adjacent lines to reflect oceanic influences rather than the phase structure of the transmitted signal.

#### (4) Selection of Lines for Further Analysis

Inspection of the on-line sideband power measurements for the data under investigation indicates that the wideband signal plus noise-to-noise ratio from the sideband filter varied from a minimum of 10 dB to a maximum of 25 dB. The centermost lines of the transmitted spectrum contain the most power. Subject to cancellation due to interference phenomena, the signal plus noise-to-noise ratio of the centermost lines is greater than or equal to that of the sideband filter output.

Thirty lines to each side of the carrier, as well as the carrier itself, were selected for further analysis and display. The power transmitted in these lines varies from 1.008 to 2.166 times the average line power in the main lobe of transmission.

The effective length of the time series that were transformed was 1.2 sec, yielding an eigenfrequency spacing in the spectrum of  $5/6$  Hz. Since 61 lines were selected, the spectra spanned 50 Hz, i.e., 25 Hz either side of the carrier.

## 4. PRELIMINARY ANALYSIS AND CONCLUSIONS

### 4.1 The On-Line Power Measurements

The results of the on-line signal power measurements are shown in Fig. 9, which is drawn from Ref. 2. The sideband filter output, labeled S, and the carrier filter output, labeled C, clearly show the two distinct modes of behavior mentioned in Section 3.3. Before 1440 hours the S-output is lower and relatively constant; after that time it rises rapidly and is much more variable.

In general the carrier level tends to follow the sideband level. The substantial fluctuations in carrier level are probably caused by cancellation of the carrier due to interference phenomena occurring within the relatively narrow (13 millihertz) carrier tooth.

The trace on Fig. 9 labeled R is the output of a surface reverberation measurement filter and is the energy in a 5/6-Hz band about the carrier. The signal plus noise-to-noise ratio in dB of any of the C, S, or R outputs is simply the difference between it and the trace labeled N, which is a wideband noise measurement. For further information on the measurements shown on Fig. 9, refer to Ref. 2. The numeric labels on various features of the carrier level in Fig. 8 refer to the spectral plots and will be discussed in the next sections.

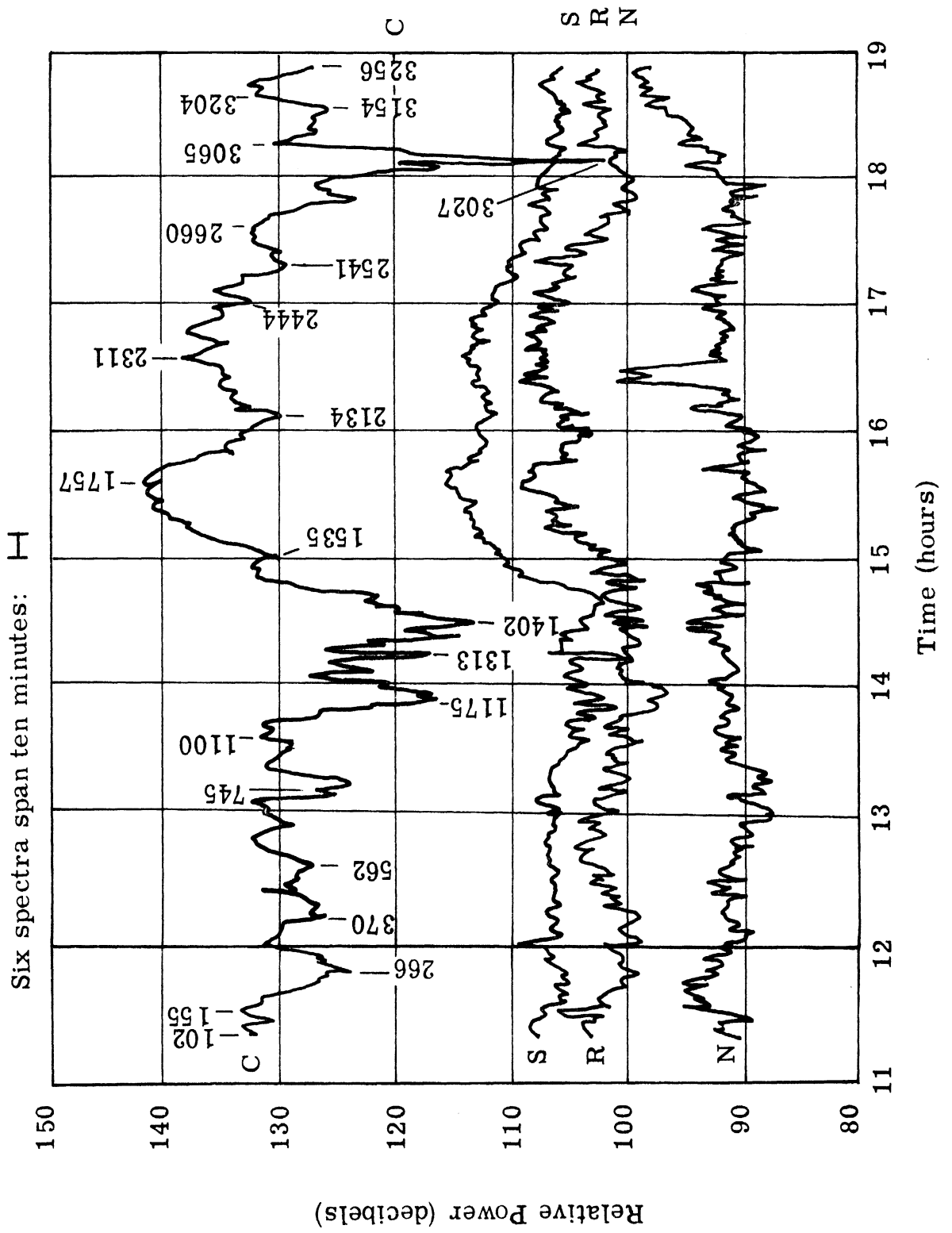


Fig. 6 On-line neuron measurements for SE NeuroLab 1070

## 4.2 Spectral Plots

Plots of the spectra are bound into the rear of this report. They are presented in polar coordinate  $r-\theta$  form to correspond to the amplitude-phase intuition of the electrical engineer (Appendixes A and B).

The spectra may be viewed as 274 samples of 61 complex-time series. They are denoted as

$$S(f, t), f = 1, \dots, 61; t = 1, \dots, 274$$

4.2.1 Constant Time Plots. Plots of  $S(f, t)$  holding  $t$  constant for each plot are shown in Appendix A. These correspond to 50-Hz wide spectra separated in time by 100 sec. A sample page is shown in Fig. 10. Six spectra spanning ten minutes in time are plotted on each page. Their time order is:

$$\begin{array}{ccc} 1 & 3 & 5 \\ 2 & 4 & 6 \end{array}$$

At each plot position, the amplitude  $|S(f, t)|$  is plotted above the phase angle  $\arg[S(f, t)]$  with frequency increasing to the right. The carrier frequency is marked with a tick. The phase is plotted between two horizontal lines, the top one of which also serves as the zero line for the amplitude plot. The range of the angle plot is one revolution (i.e., 360 degrees or  $2\pi$  radians).

The phase angles to be plotted were modified by the following transformation.

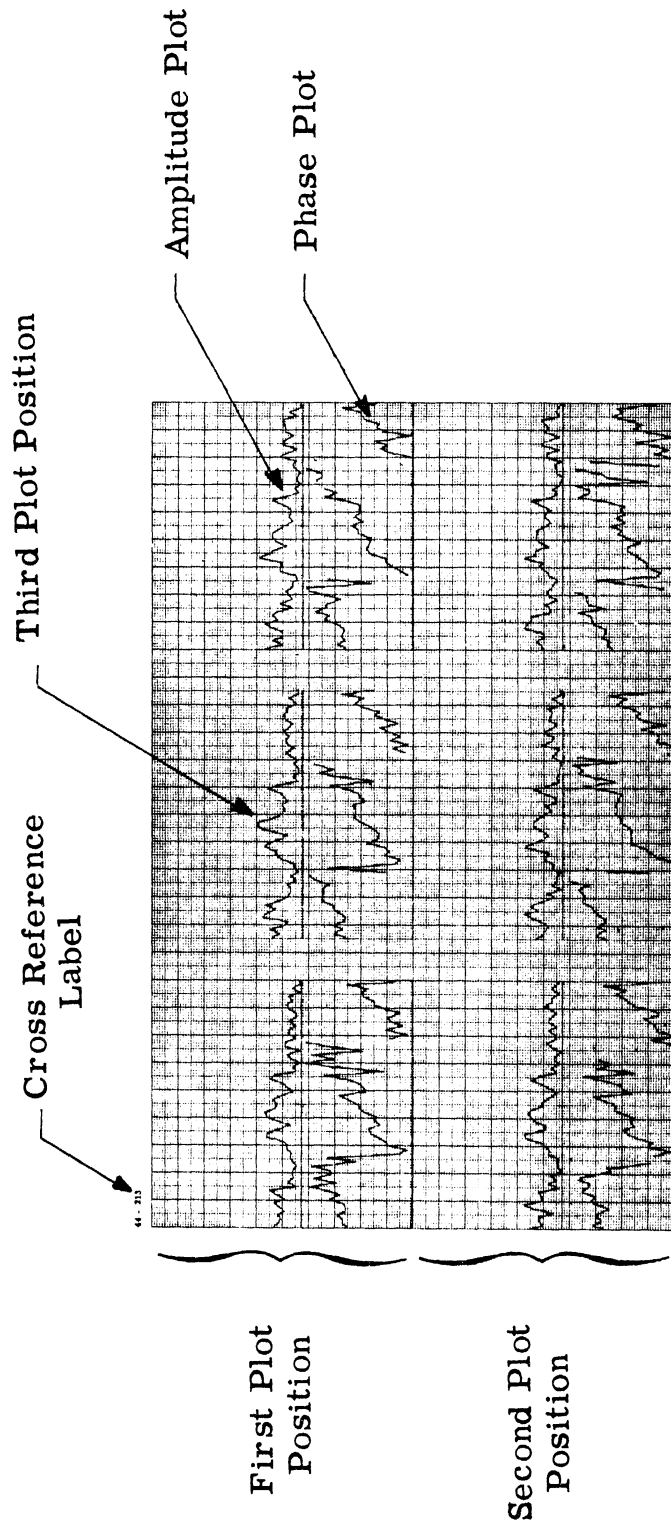


Fig. 10. Prototype constant time plot



$$\arg[\mathbf{S}(f, t)]_{\text{plot}} = \arg[\mathbf{S}(f, t)]_{\text{data}} - (af - b)$$

where the constants  $a$  and  $b$  were chosen empirically to be

$$a = 0.45507 \text{ revolution/frequency step}$$

$$b = 0.58593 \text{ revolution}$$

This transformation is equivalent to shifting the time origin 0.54608 sec and the phase origin 0.58593 revolutions. (The original time and phase origins were arbitrary since they were established by the instant-of-time at which the receiving processor began operating.)

The constants  $a$  and  $b$  were chosen to make the largest portions of all the 274 angle plots as flat (or alternately, as smoothly connected) as possible.

In those cases where the phase angle does cross the phase reference (zero revolution) axis, no attempt is made to draw a smooth line connecting adjacent angles. Rather the "offending" angle is plotted as a point instead of as a member of a line.

At the upper left of each page in Appendix A is a numeric label. This label is a computer data access code for the original recorded data that produced the spectrum in the upper left corner of the page, i.e., plot position 1. The second number in this label is the same as the numeric label on the C-power line of Fig. 9 and can be used to establish a time correspondence between power levels and spectral displays. The time duration of one page of spectra--ten minutes--is indicated on Fig. 9. (Hopefully these limited capabilities

for cross-referencing Fig. 9 and the plots in Appendix A will prove sufficient; the macroscopic rather than microscopic features are of interest here.)

4.2.2 Constant Frequency Plots. Plots of  $S(f, t)$  holding  $f$  constant for each plot are shown in Appendix B. These correspond to time series of signal amplitude and phase for each signal line in the 61-frequency ensemble selected in Section 3.4. Two  $r-\theta$  time series, each spanning 7.61 hours, are plotted on a page, one in the top half and the other in the lower half of the page. A sample page is shown in Fig. 11 with  $|S(f, t)|$  plotted above  $\arg[S(f, t)]$  with time increasing to the right. The vertical scaling is not the same as that of the constant time plots.

The angles portrayed in the constant frequency plots are computed directly via  $\arg[S(f, t)]$  and undergo no transformation. Again, as with the constant time case, angles which cross the phase reference axis are plotted as points instead of as members of a smooth line. At the upper left of each time series plot is a number indicating the  $f$  value for the time series shown. To convert the  $f$  value into a frequency in hertz, use the following relation:

$$\text{Frequency in hertz} = 420 + \frac{5(\text{integer } f \text{ value} - 31)}{6}$$

Accordingly, the carrier plot is labeled 31. Note that the C-power trace in Fig. 9 corresponds to time-series 31 when allowance is made for dB vs linear scales on amplitude.

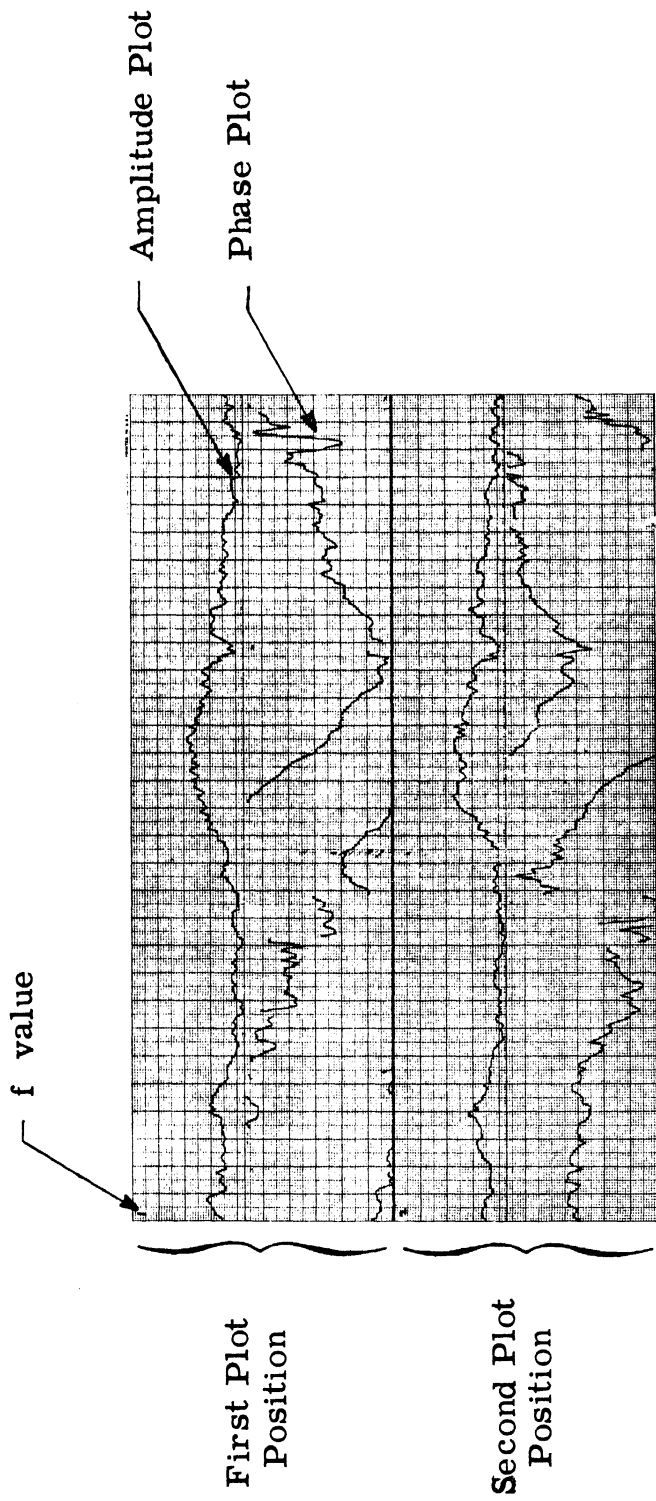


Fig. 11. Prototype constant frequency plot

### 4.3 Preliminary Conclusion

The most striking feature of the  $S(f, t)$  function is that it seems to change slowly both in frequency  $f$  and time  $t$ . Figures 12 to 15 show a sequence of spectra spanning over one hour. At the end of this time, the gross amplitude structure, especially the frequencies of the predominant nulls, has not changed appreciably. The frequency boundaries of the areas of linear phase angle behavior have also not shifted to an appreciable extent. Future work will consist of attempts to exploit the relative stationarity of the spectrum exhibited here, with some emphasis on better methods of display.

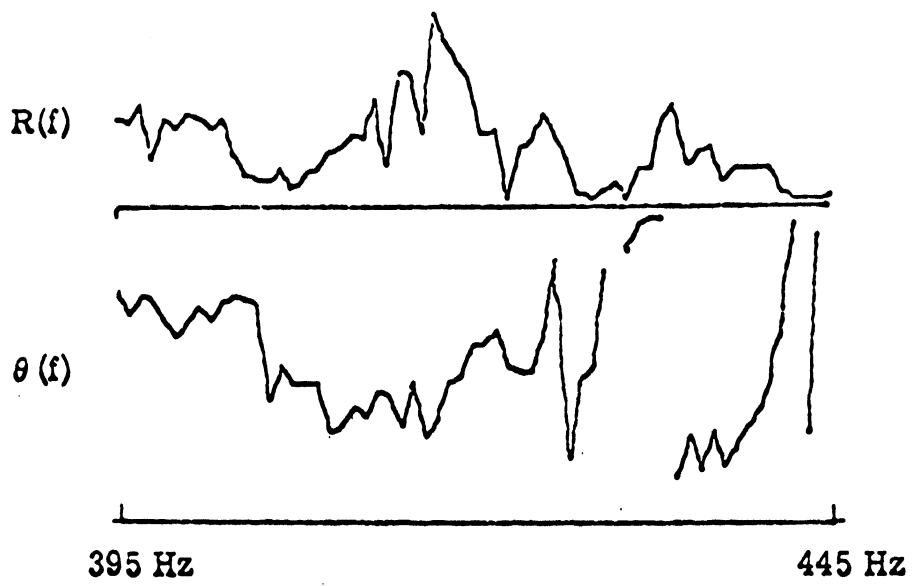


Fig. 12. Spectrum at  $t_0 = 1118$  hrs, 25 November 1970

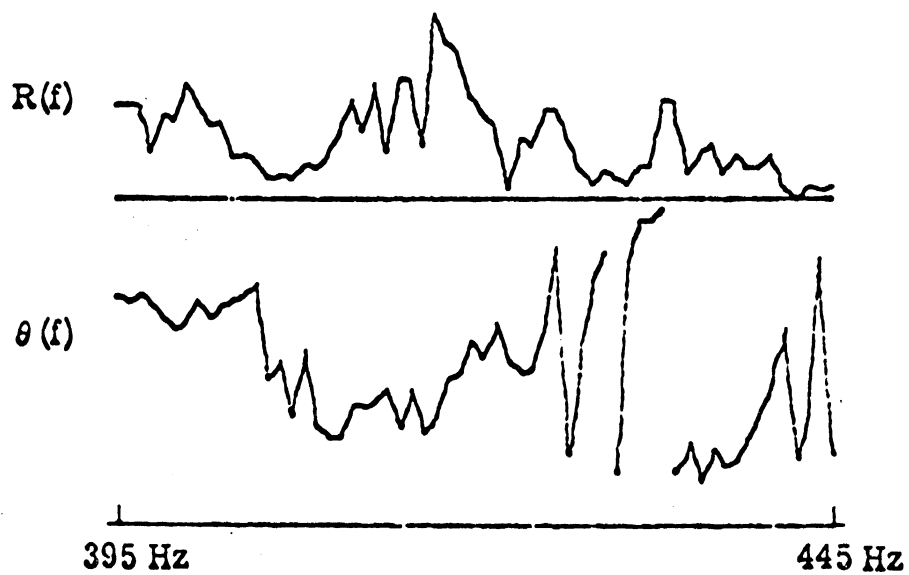


Fig. 13. Spectrum at  $t_0 + 1$  minute, 40 seconds

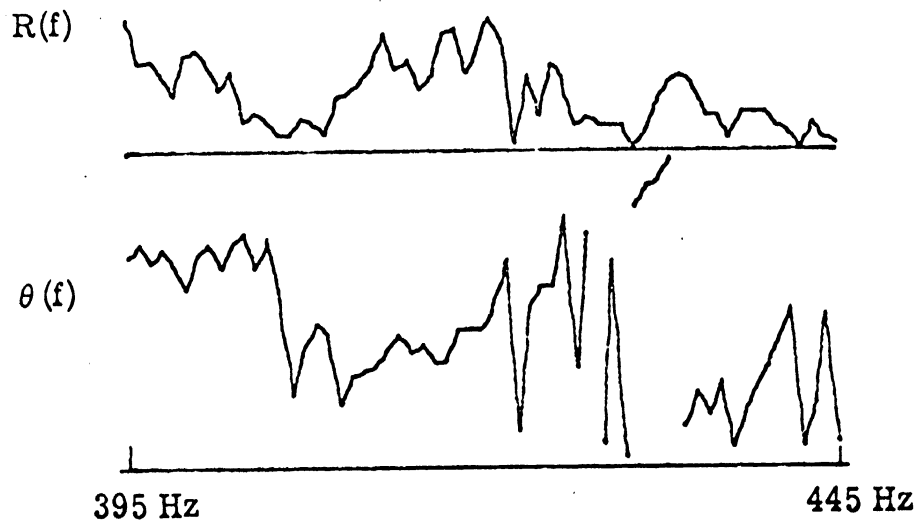


Fig. 14. Spectrum at  $t_0 + 10$  minutes

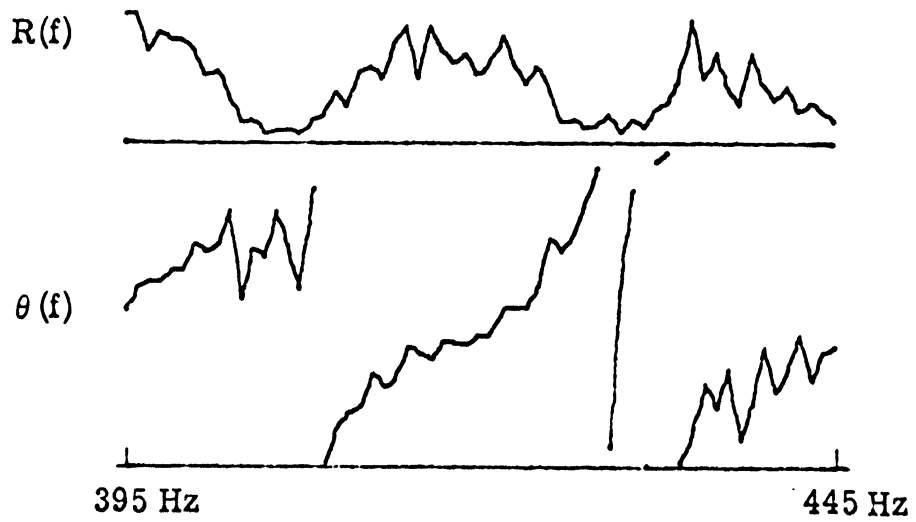


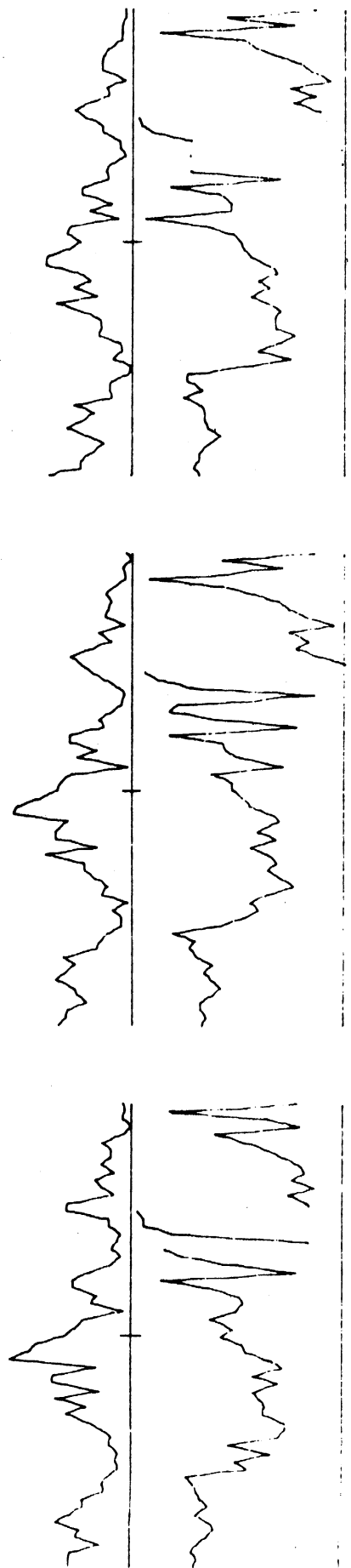
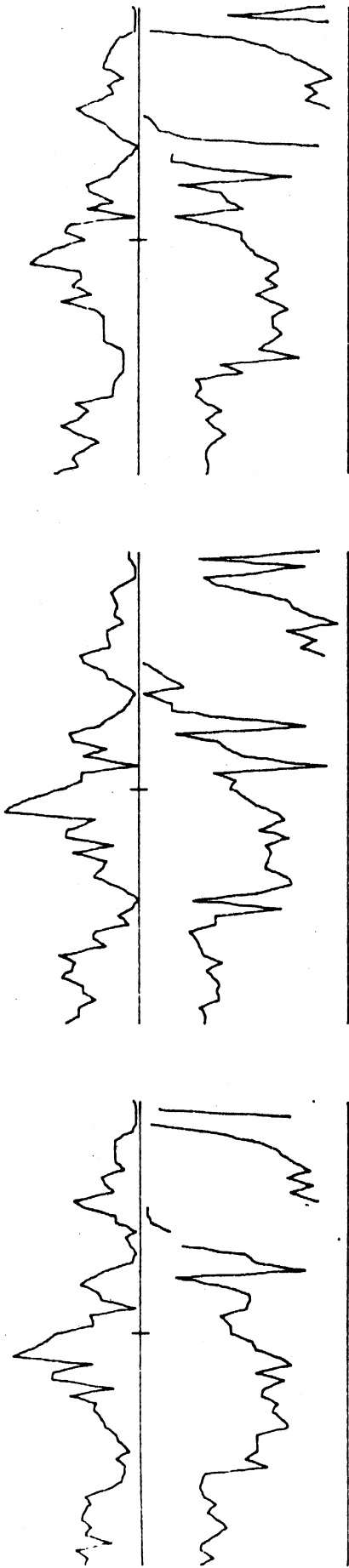
Fig. 15. Spectrum at  $t_0 + 1$  hour, 3 minutes, 20 seconds

## APPENDIX A

### Constant Time Plots

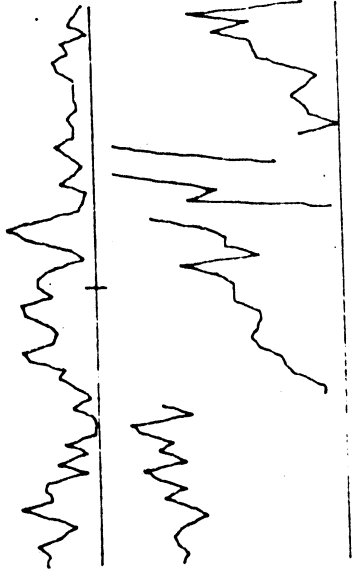
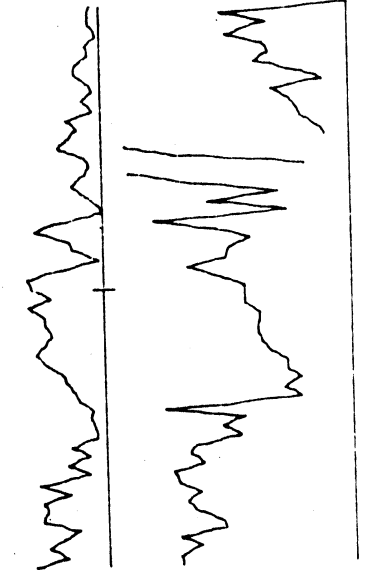
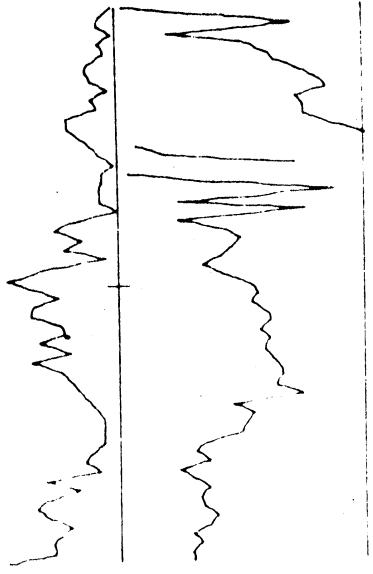
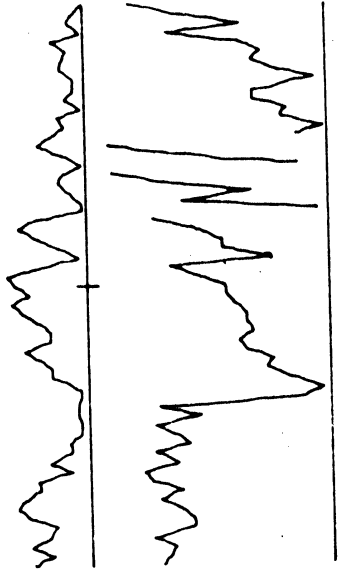
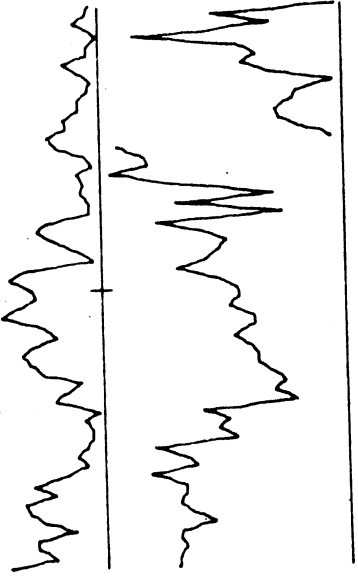
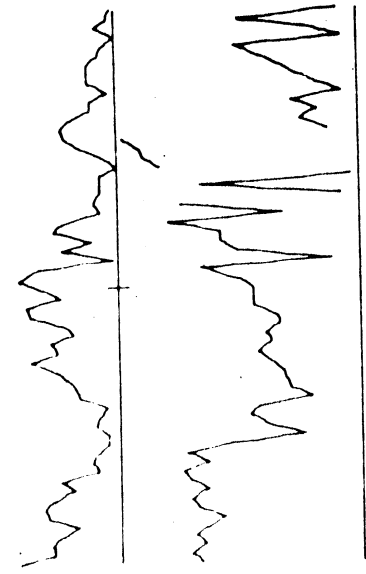
Section 4.2.1 explains how to interpret the constant time plots that follow.

44-102

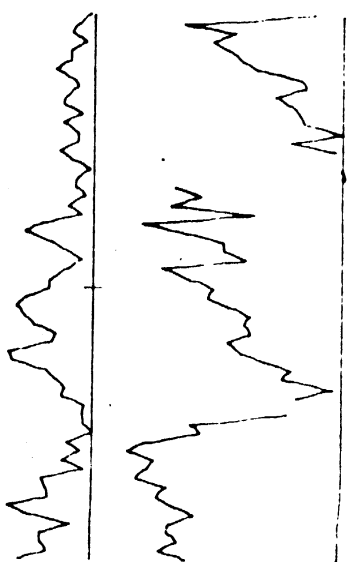
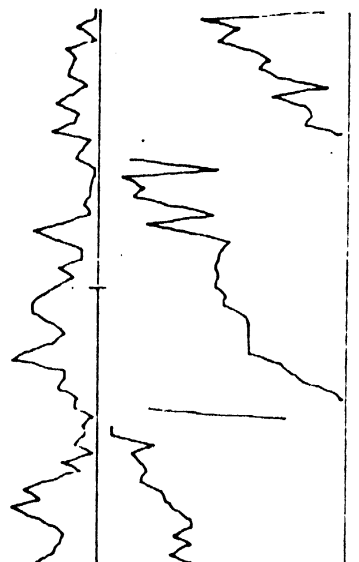
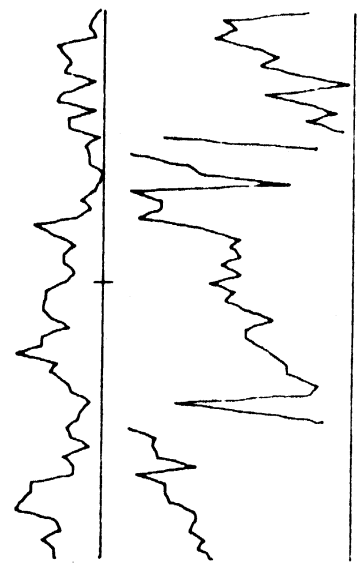
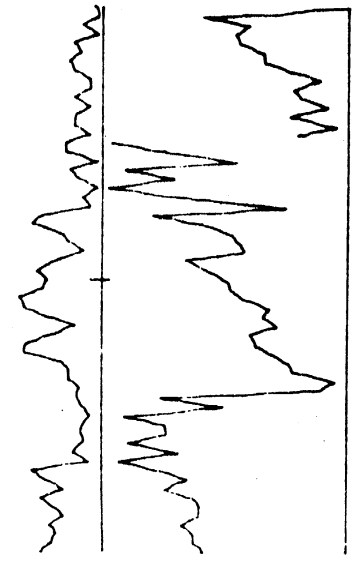
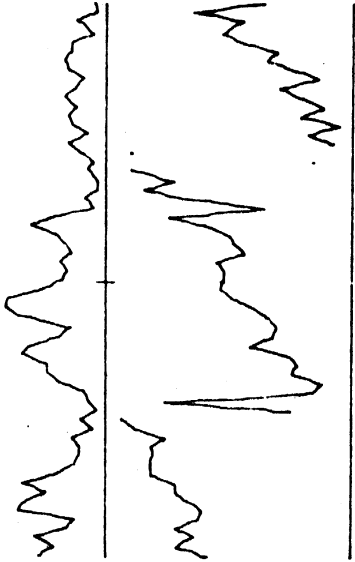
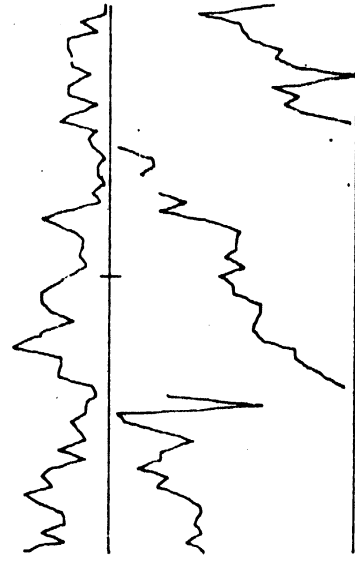




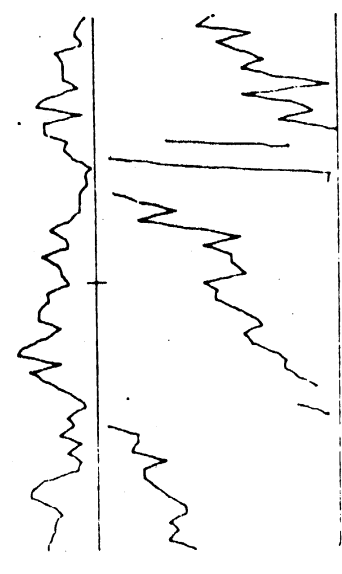
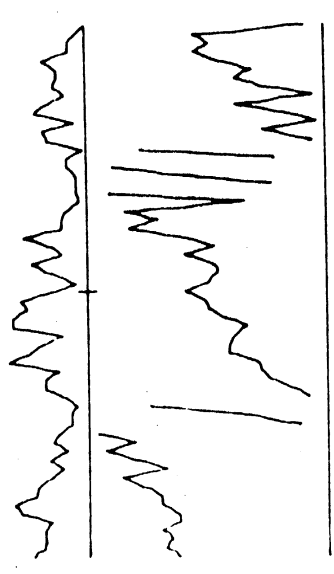
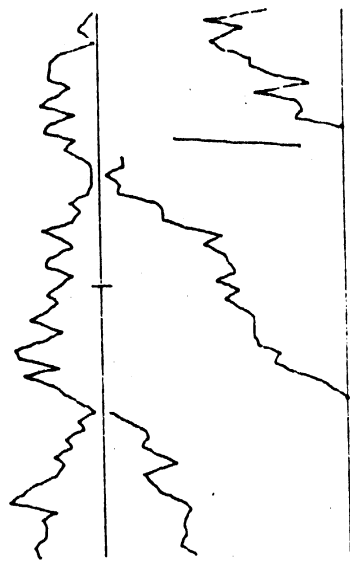
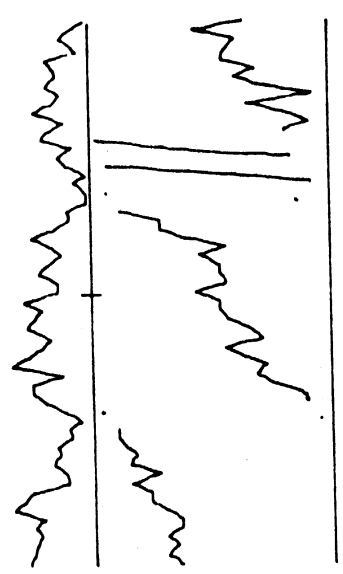
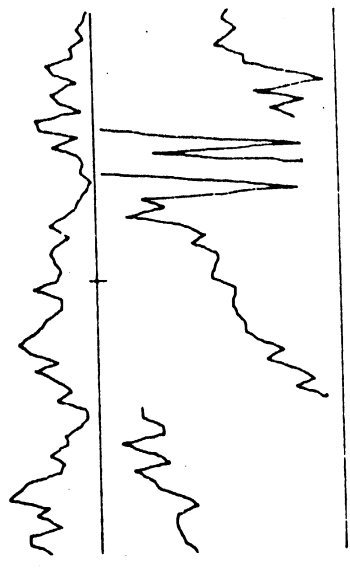
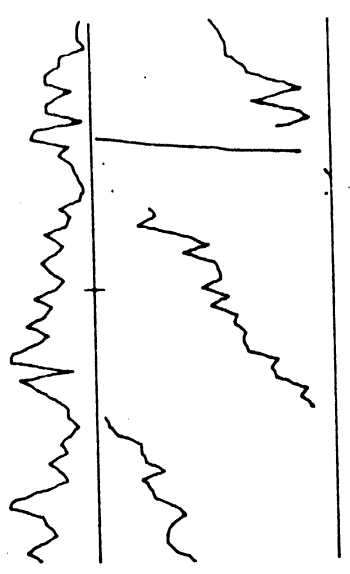
44-147



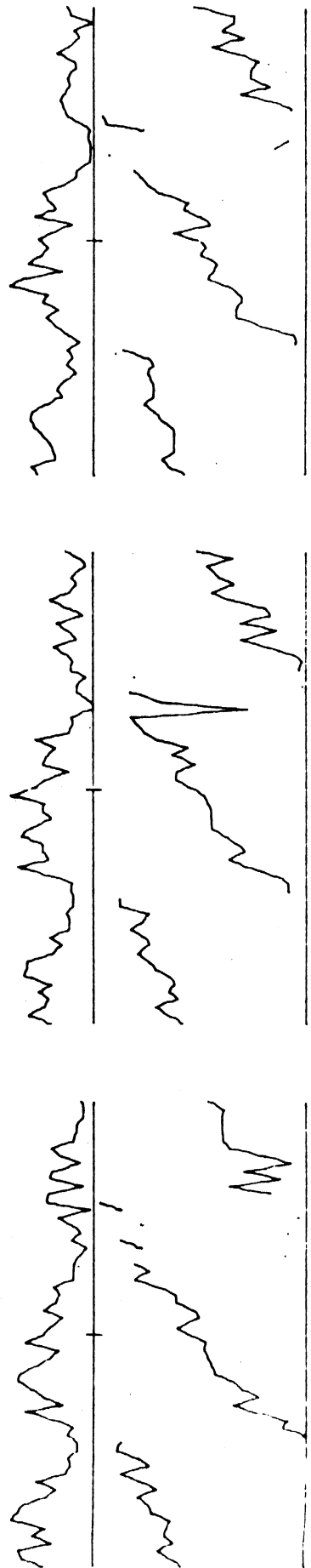
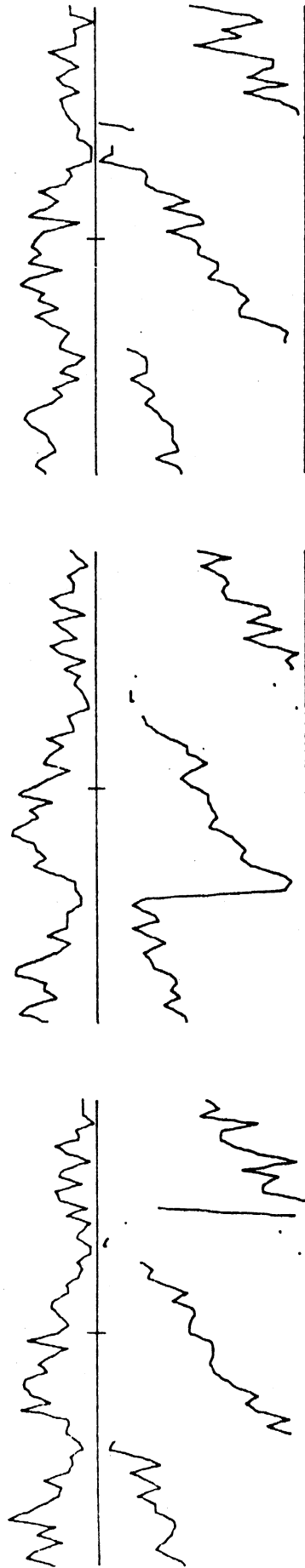
44-213



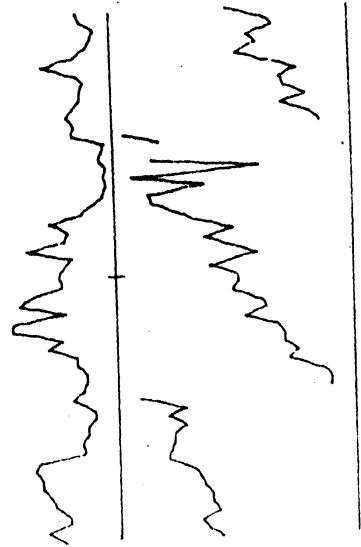
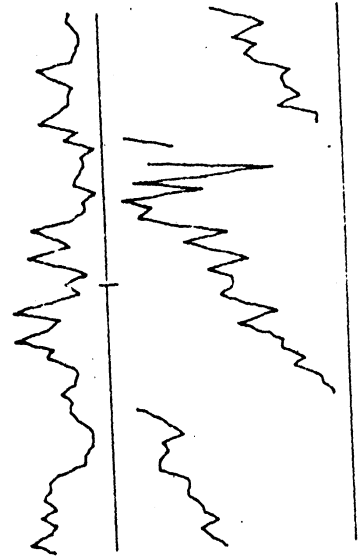
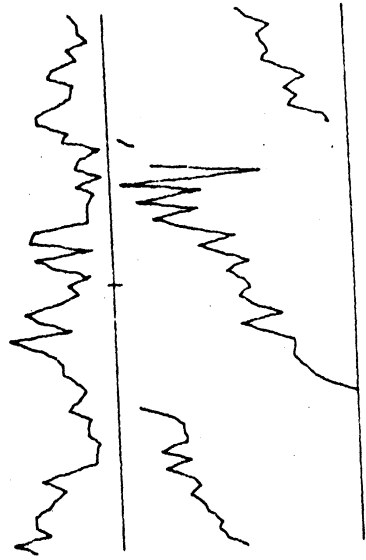
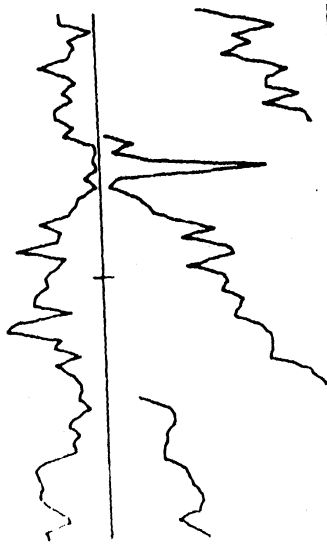
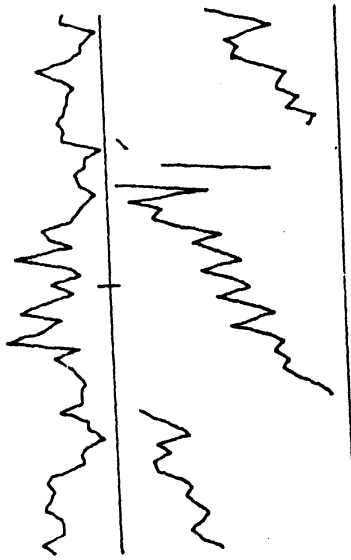
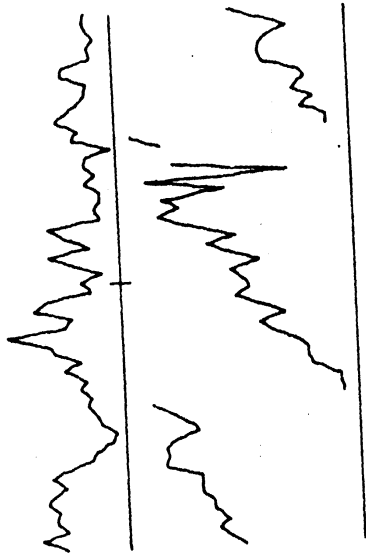
44-257



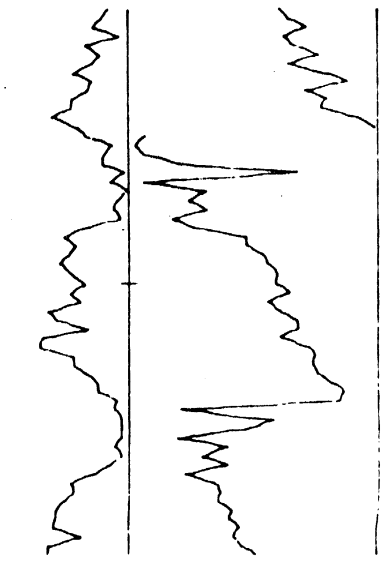
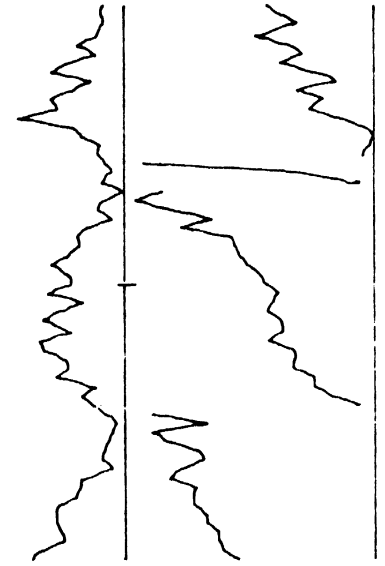
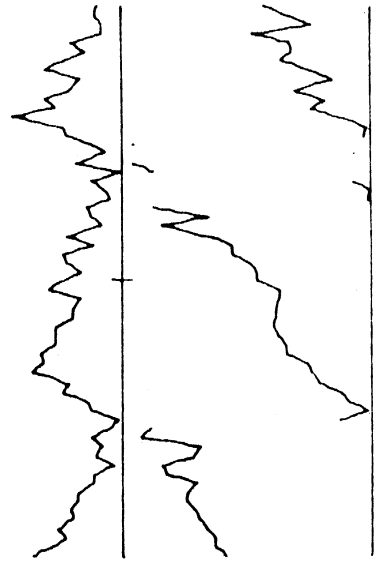
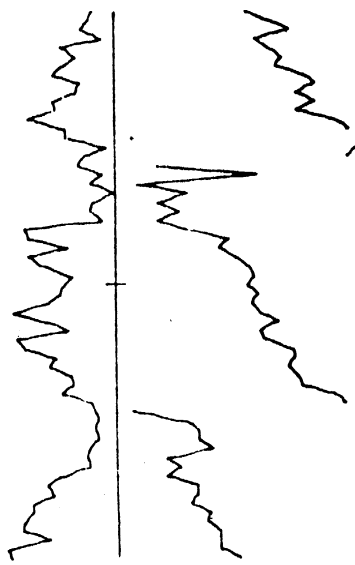
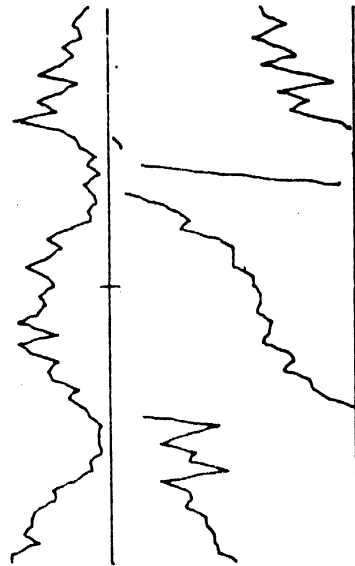
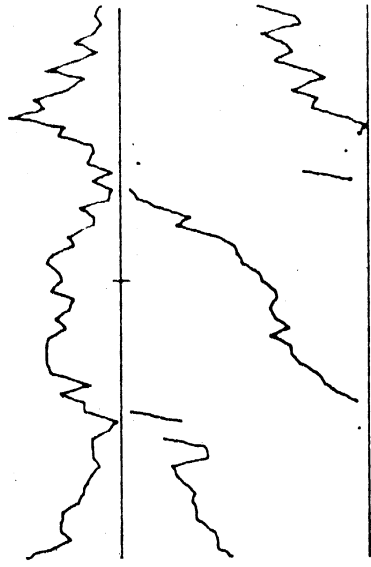
44-324

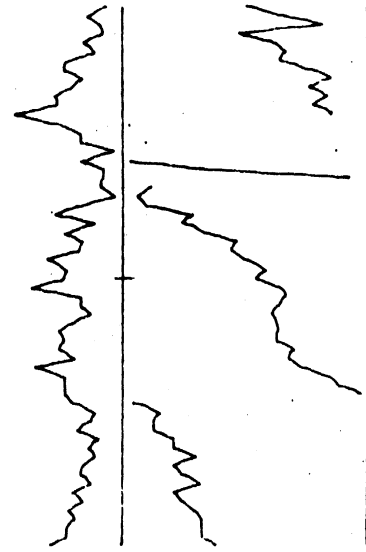
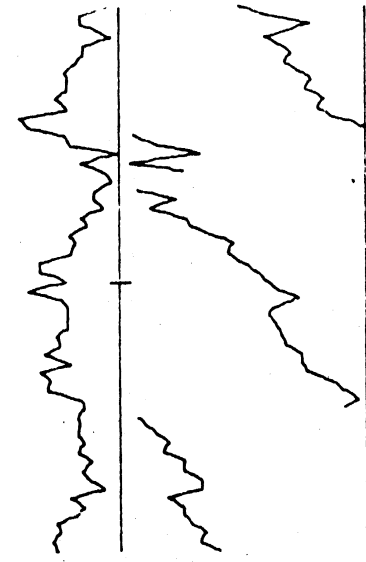
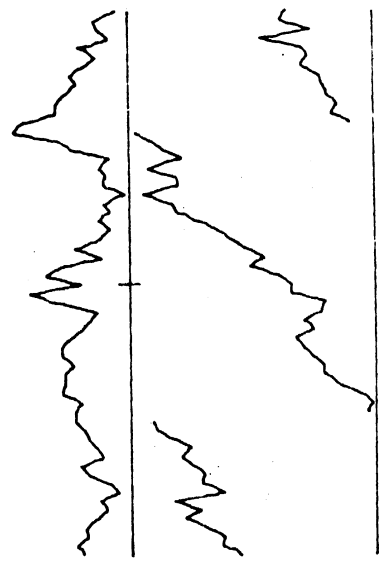
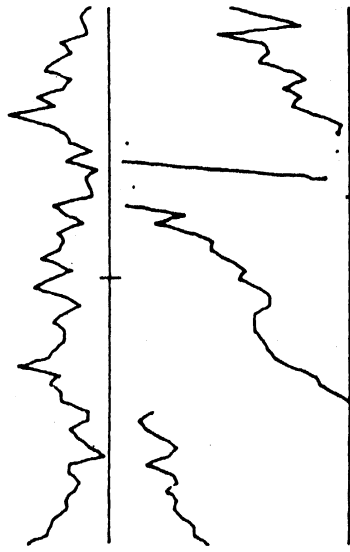
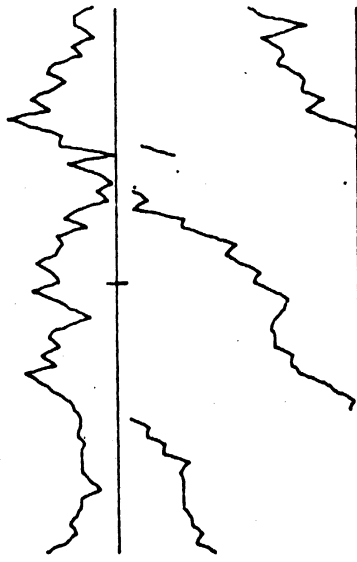
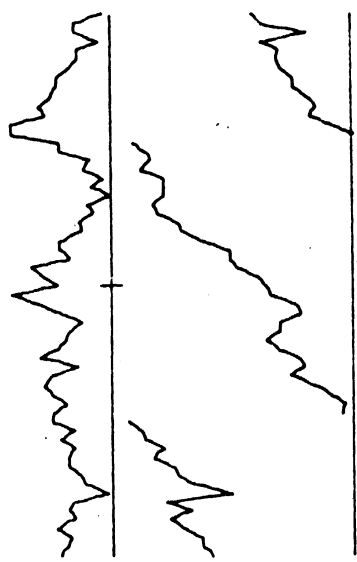


44-370

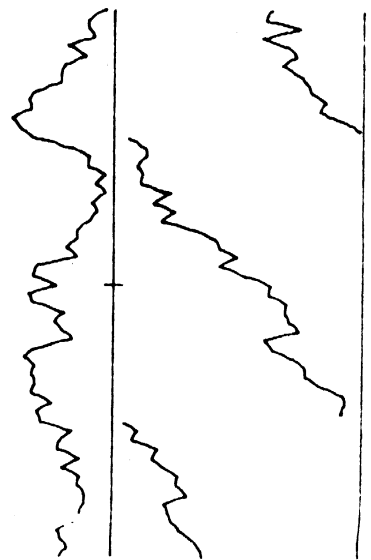
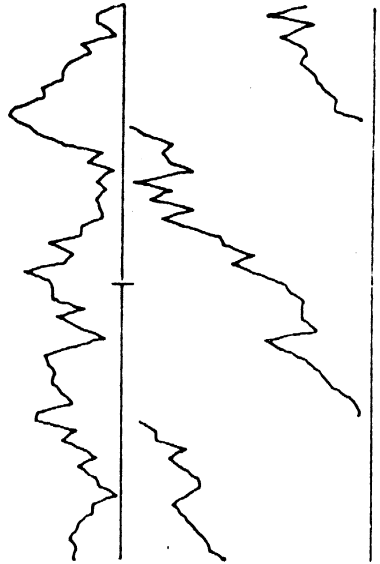
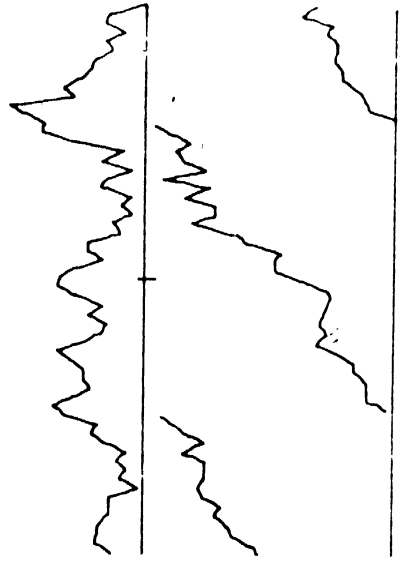
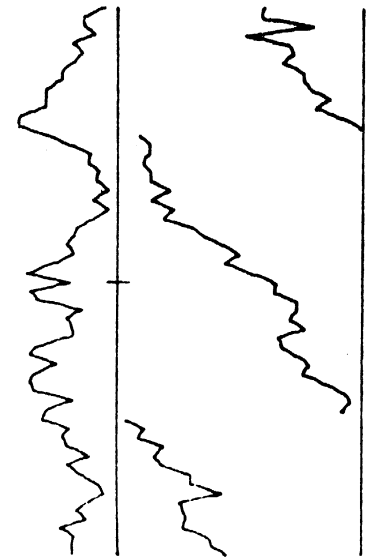
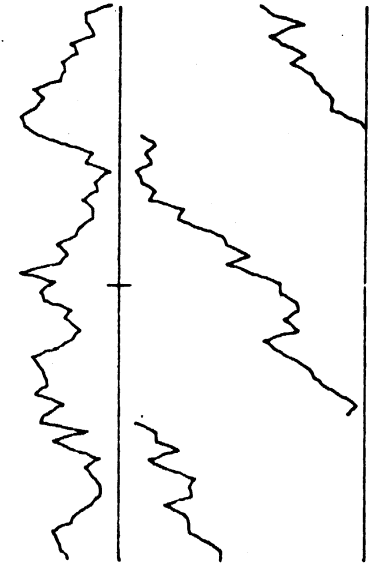
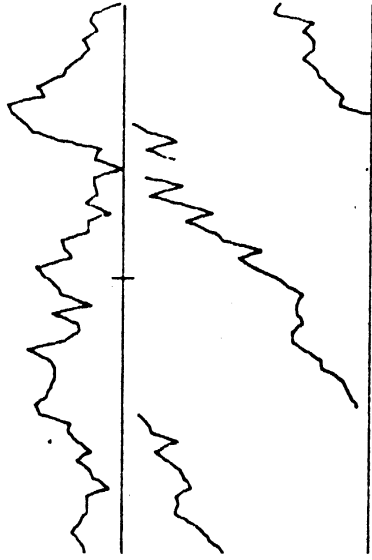


44-435



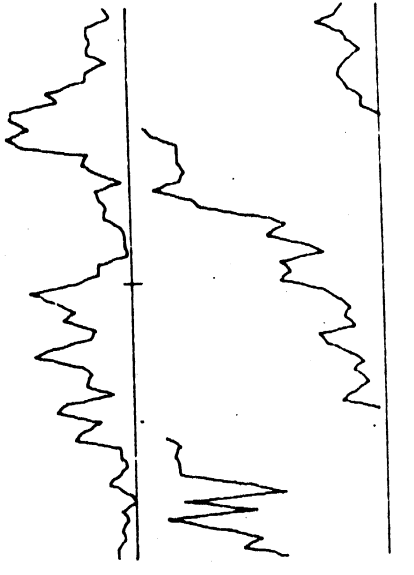
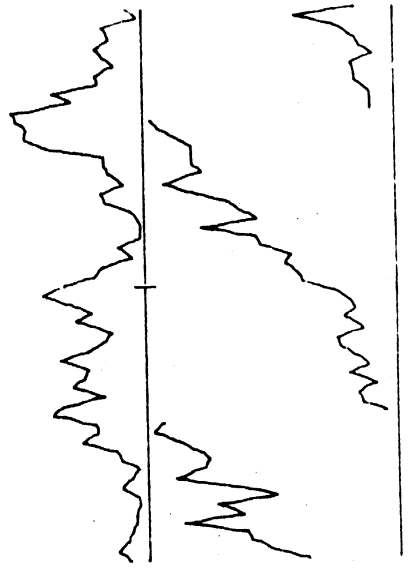
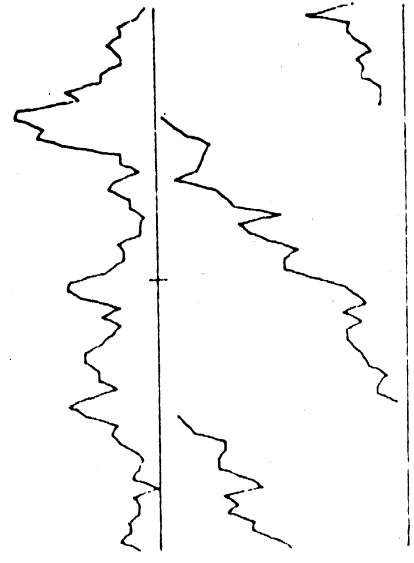
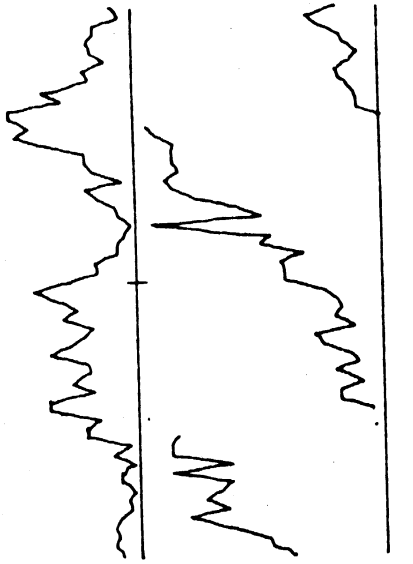
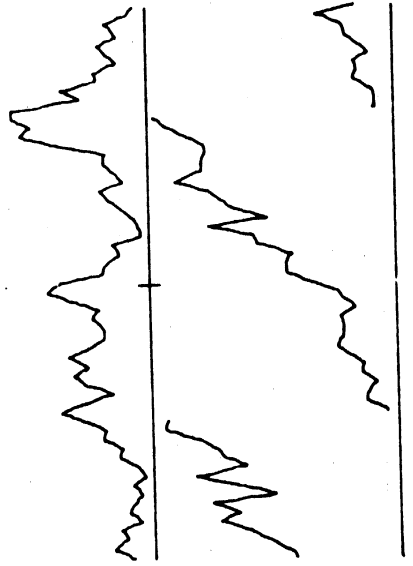
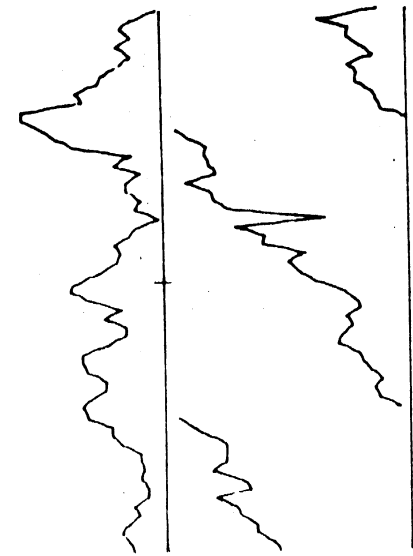


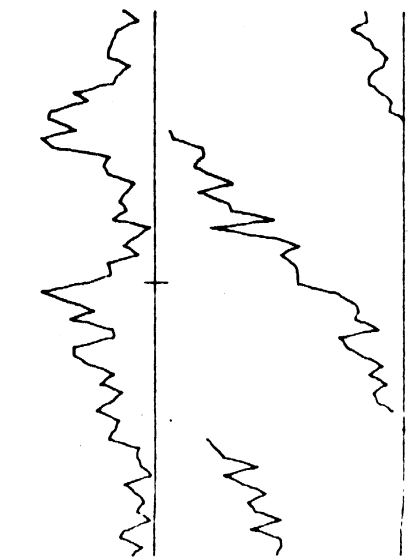
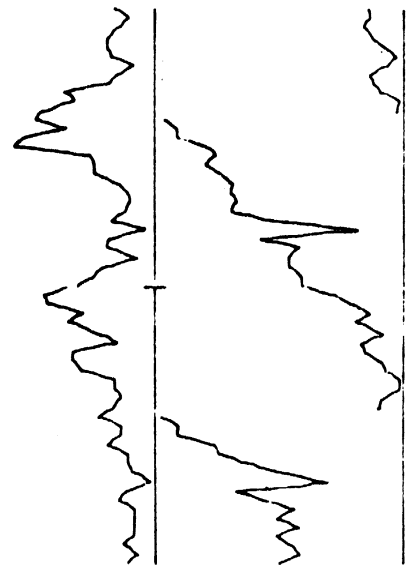
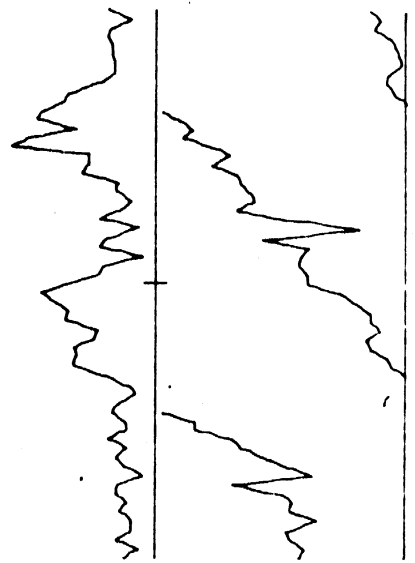
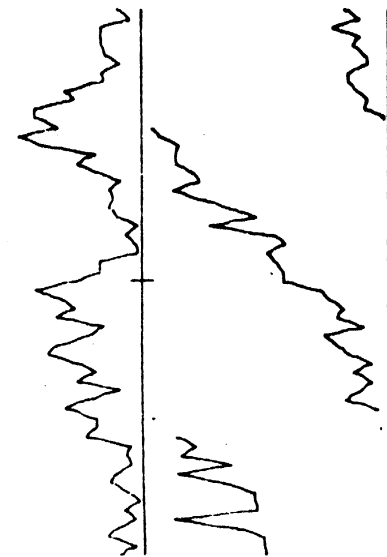
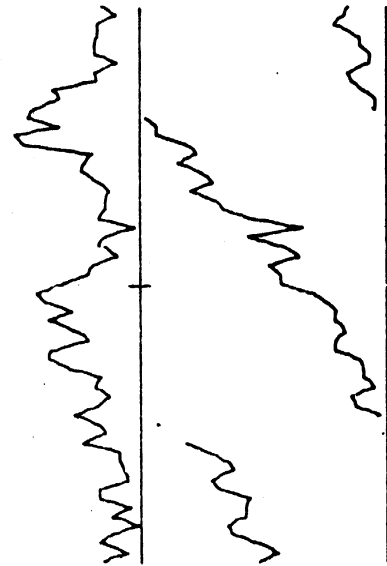
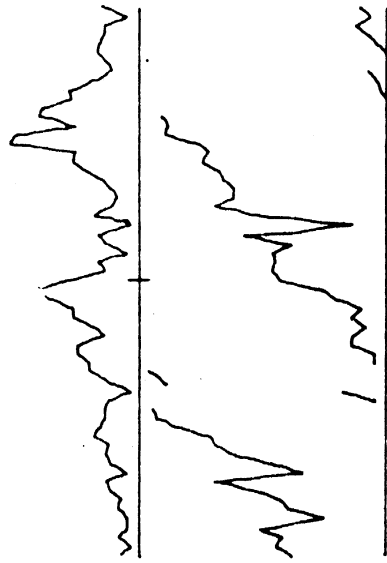
44-545



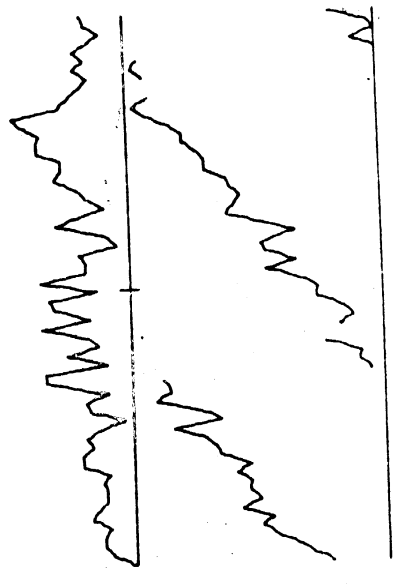
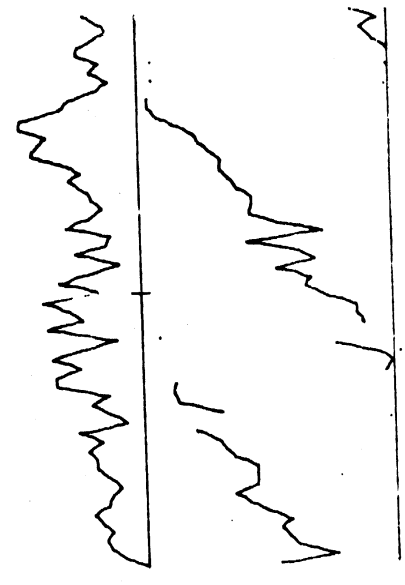
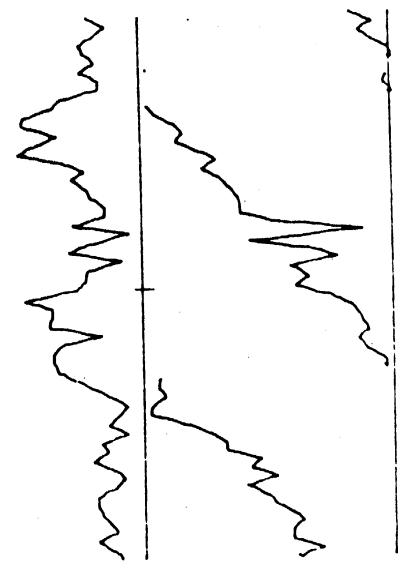
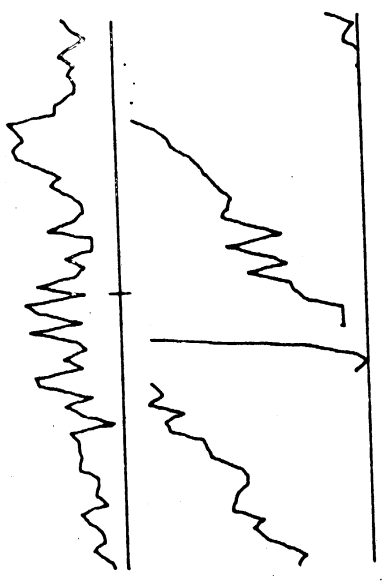
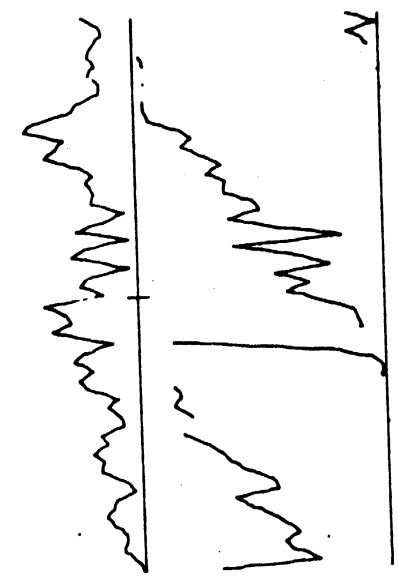
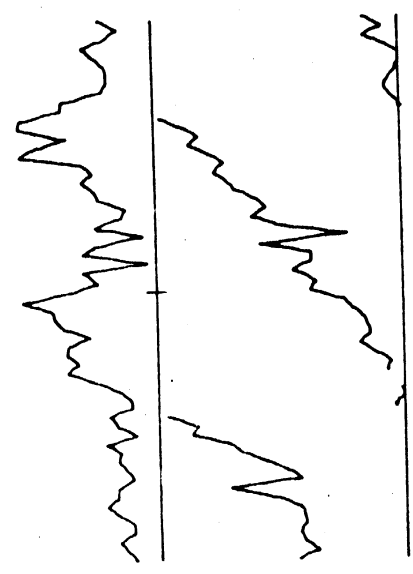


44-612

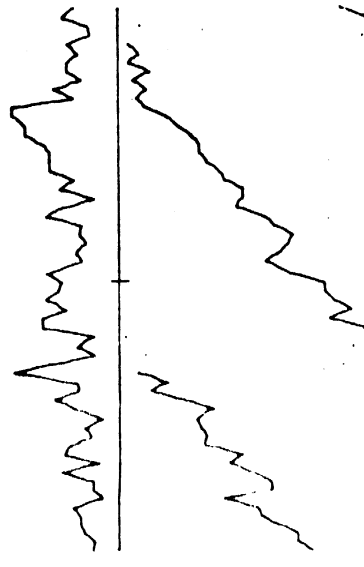
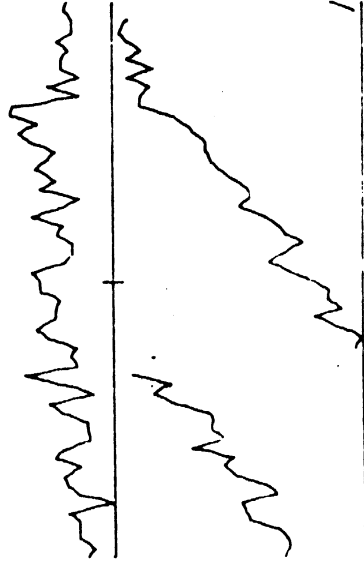
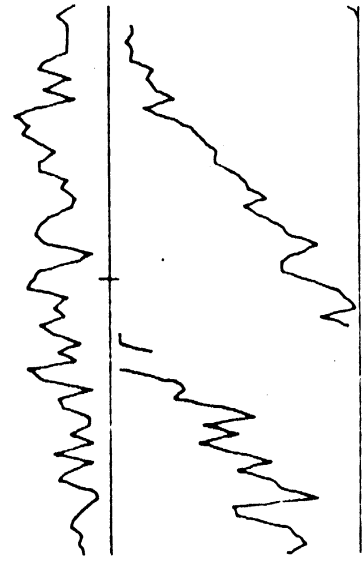
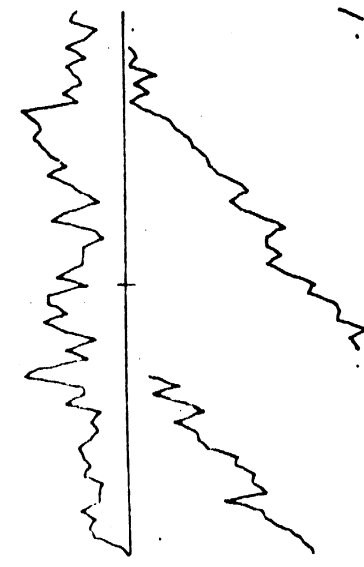
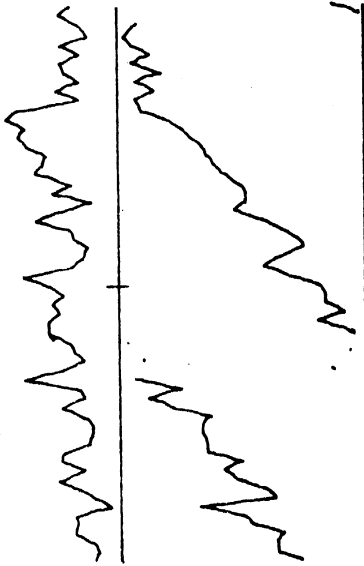
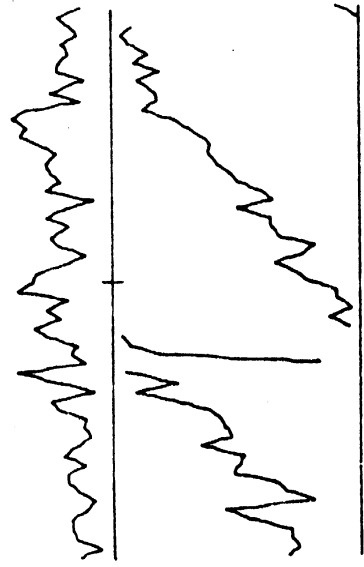




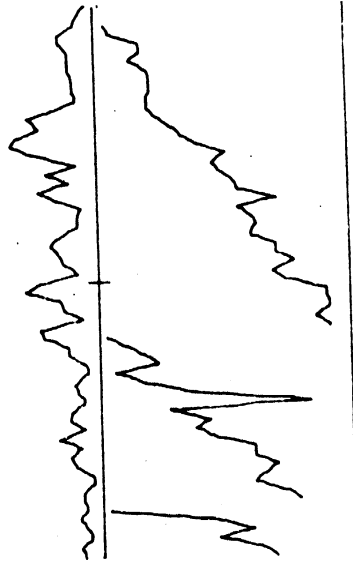
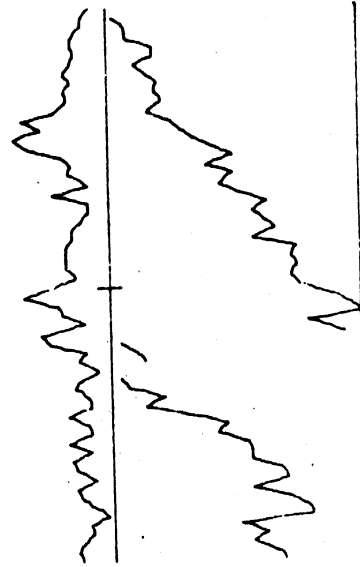
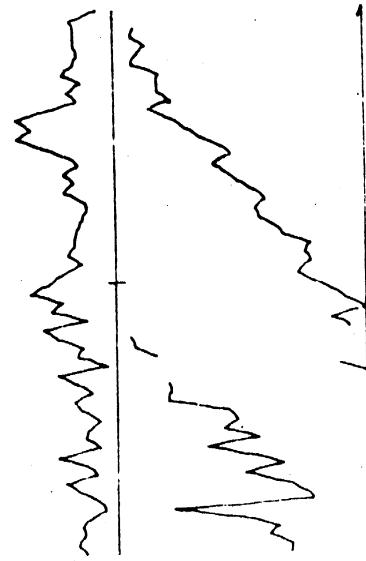
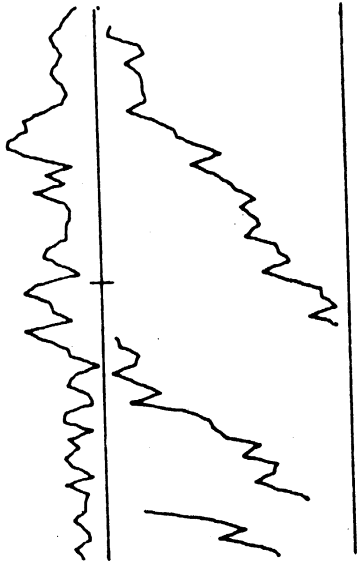
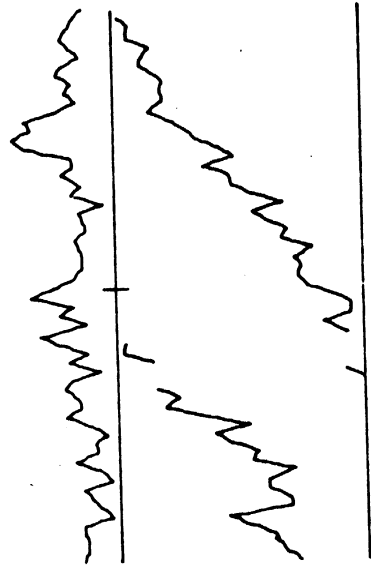
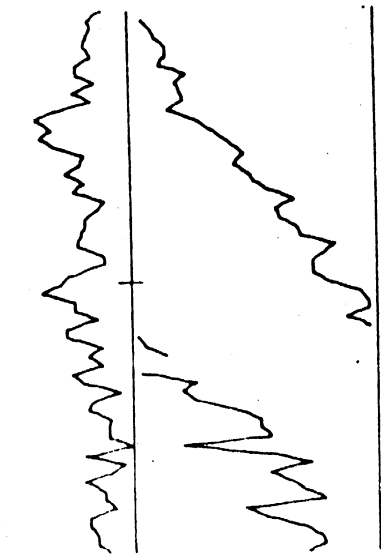
44-723



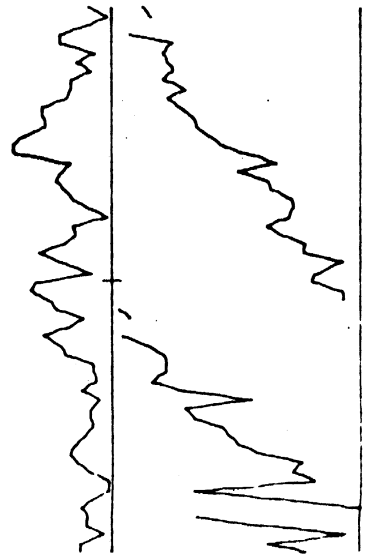
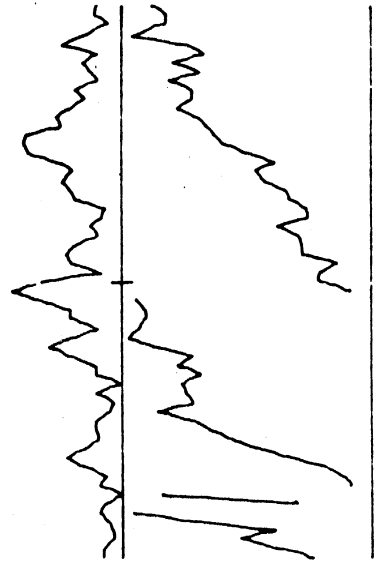
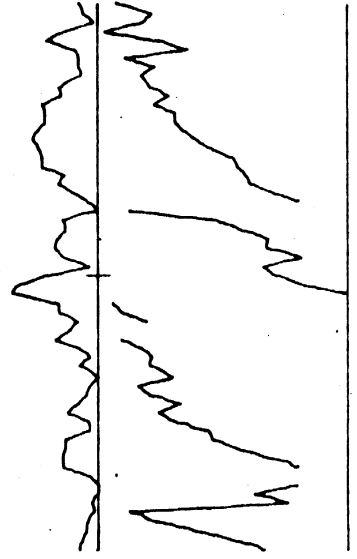
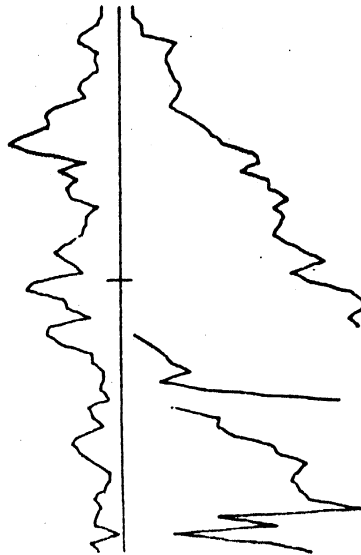
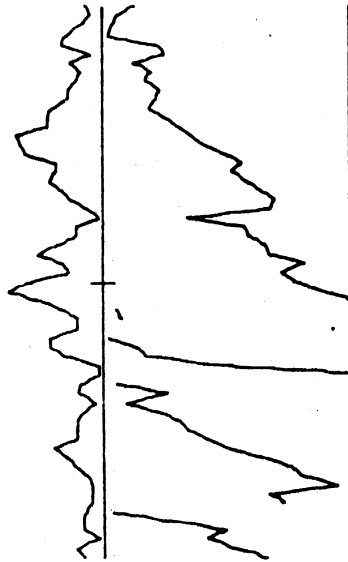
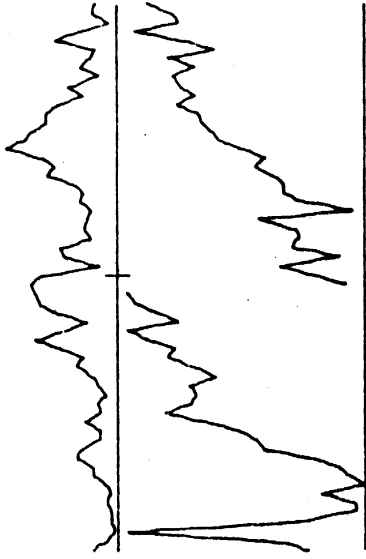
44-767



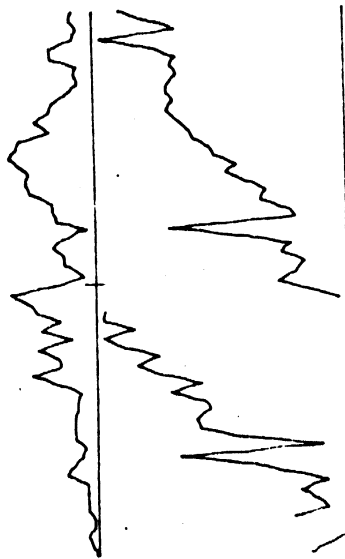
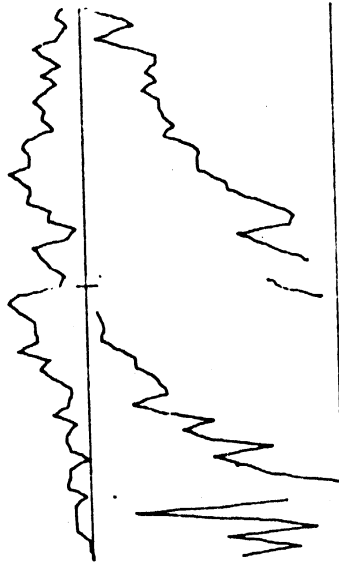
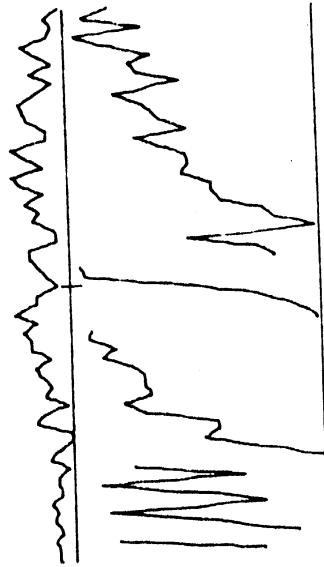
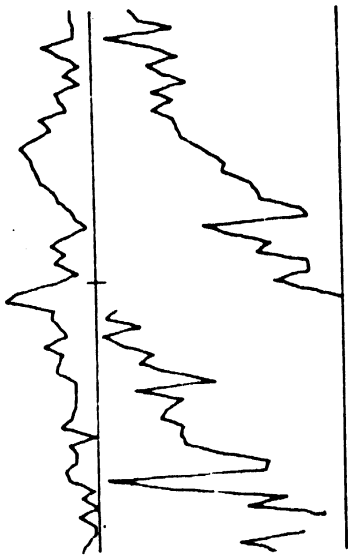
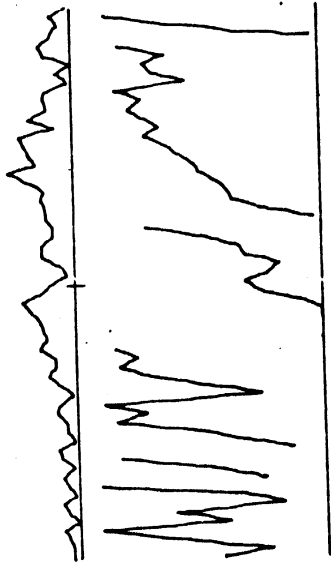
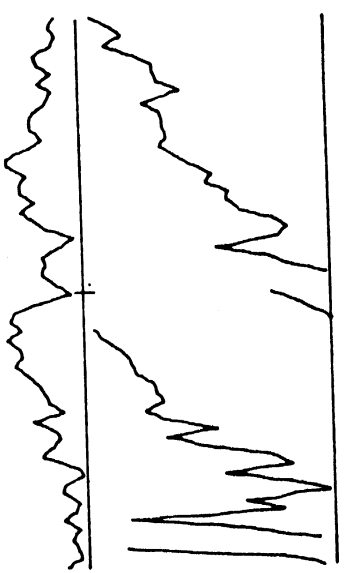
44-1033



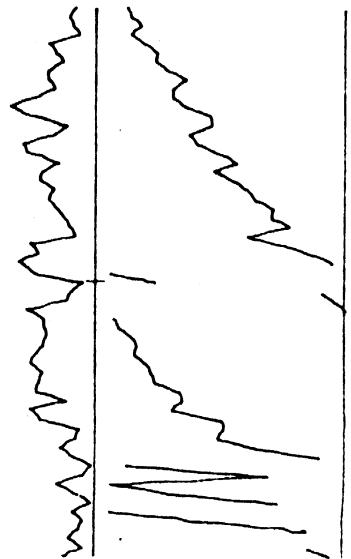
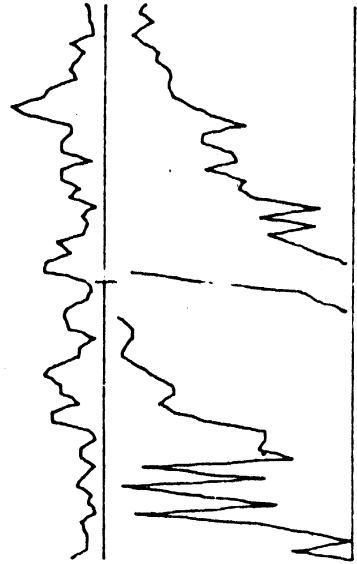
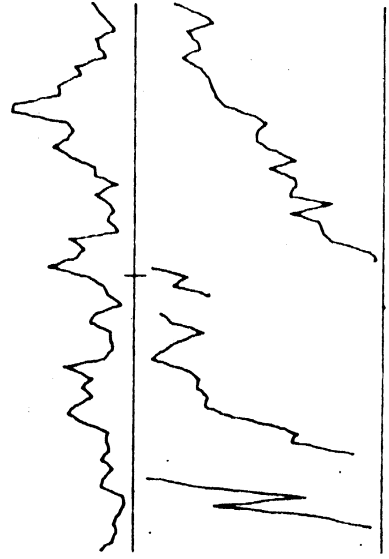
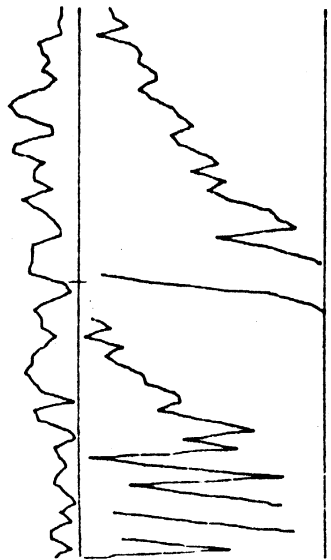
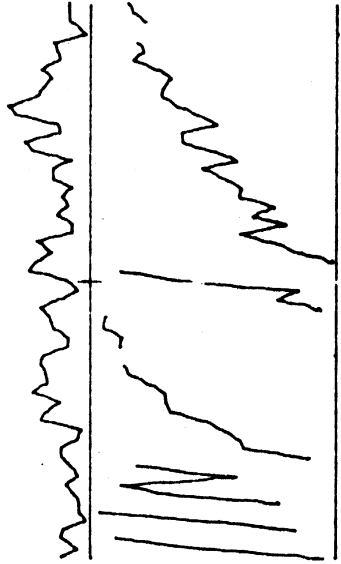
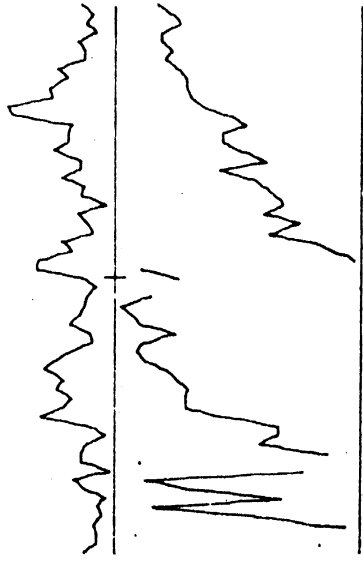
44-1100



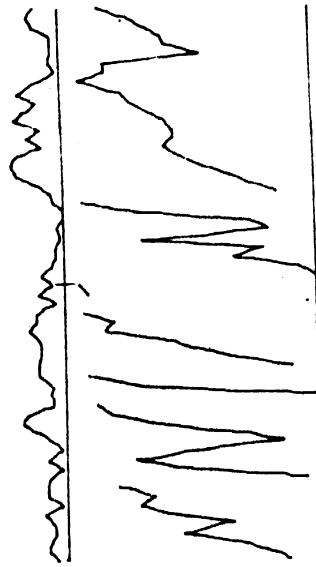
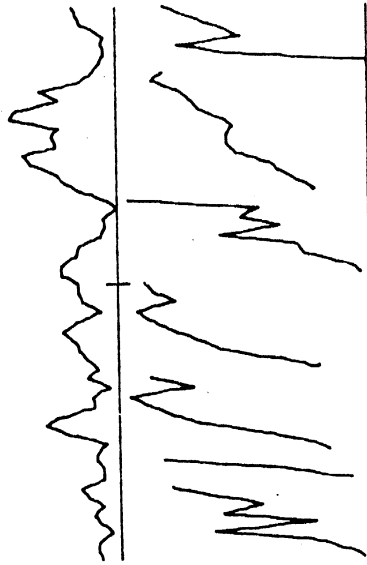
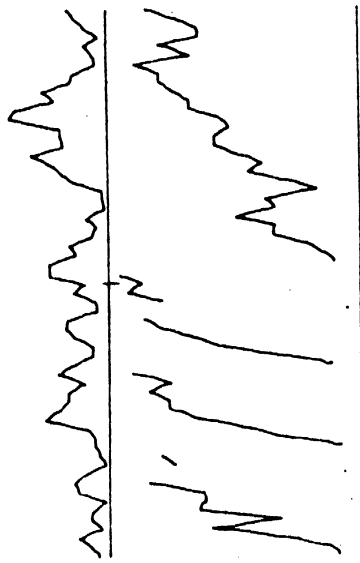
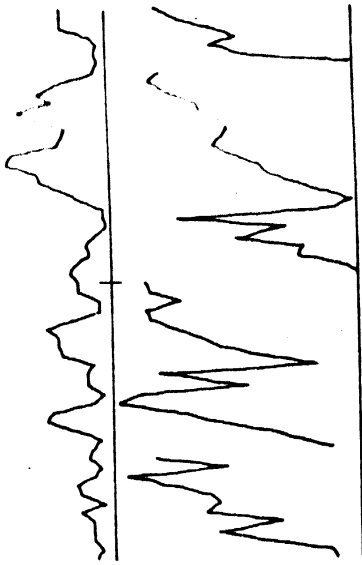
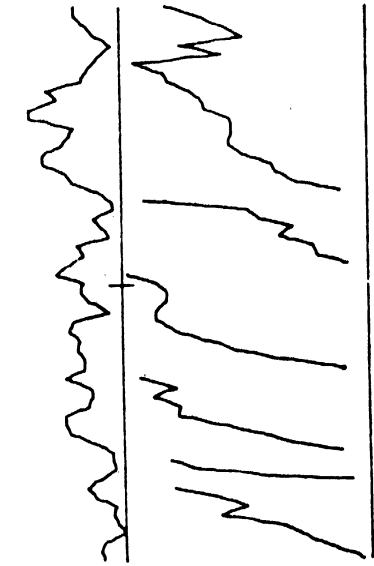
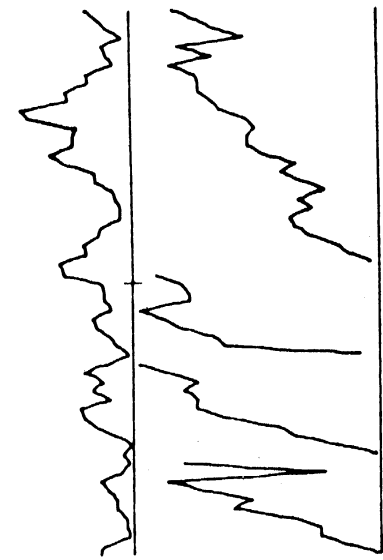
44-1144

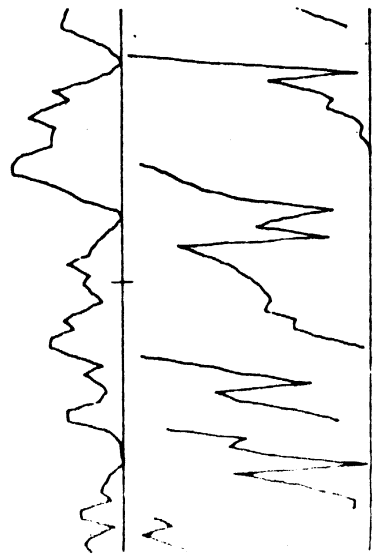
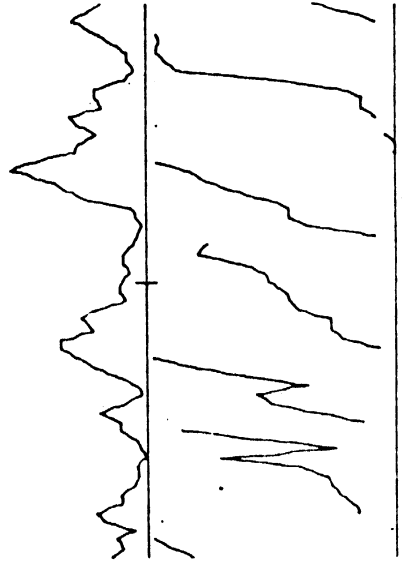
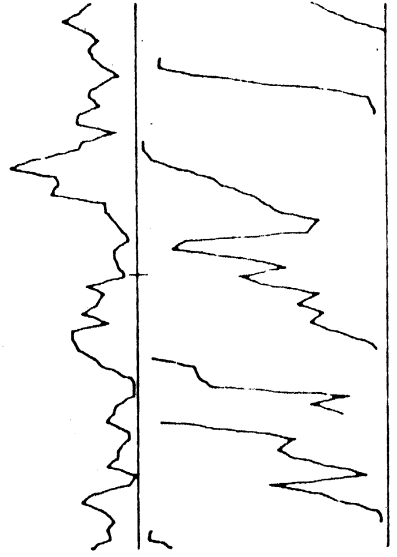
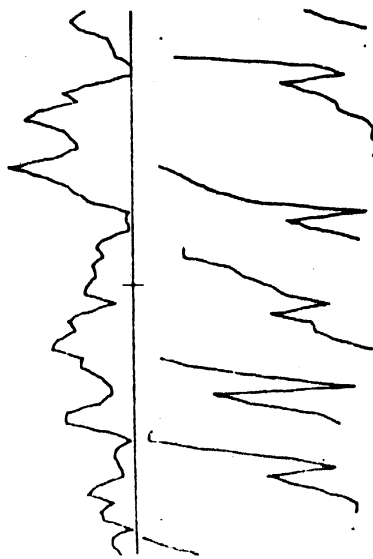
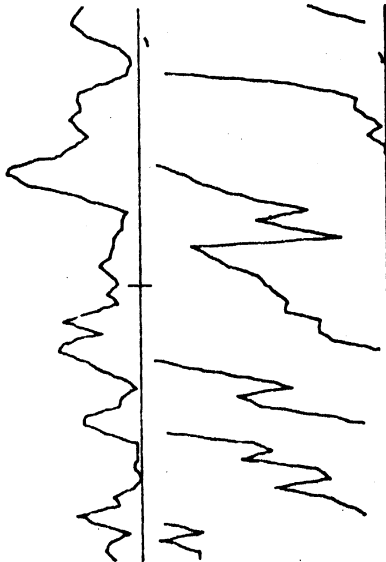
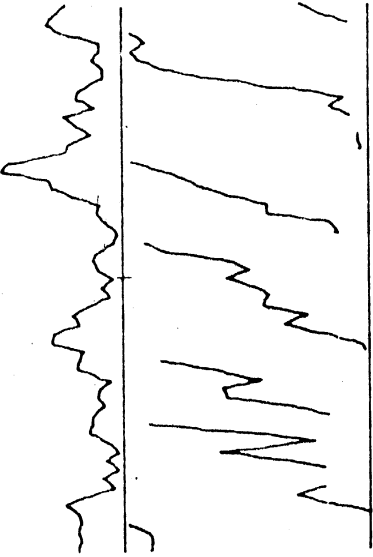


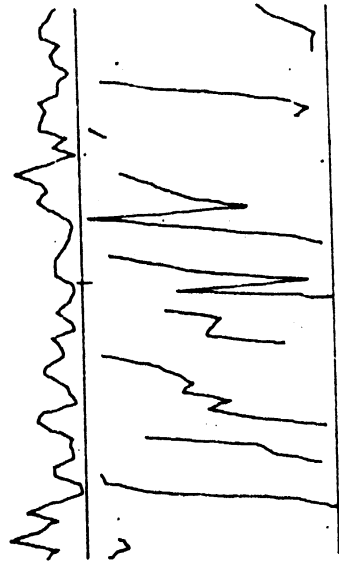
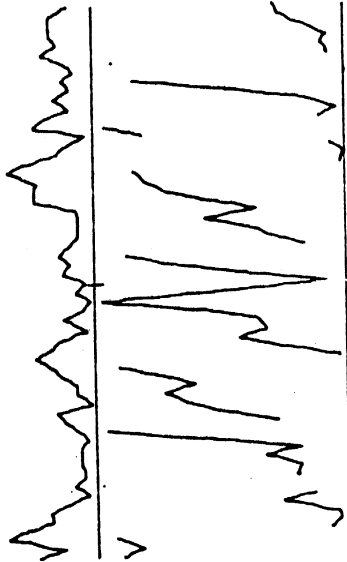
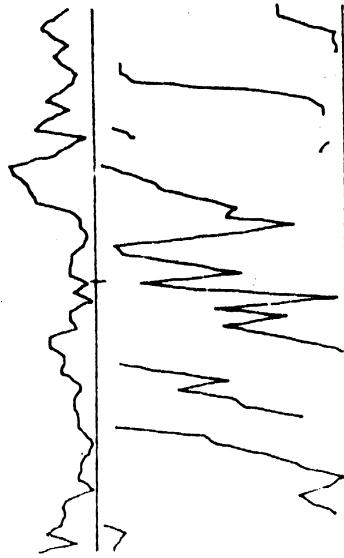
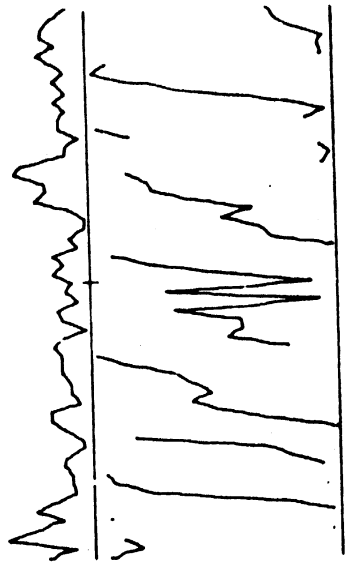
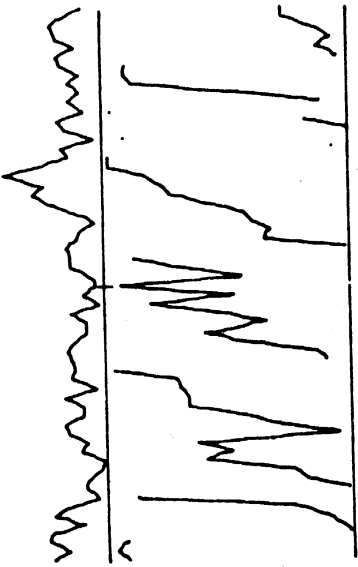
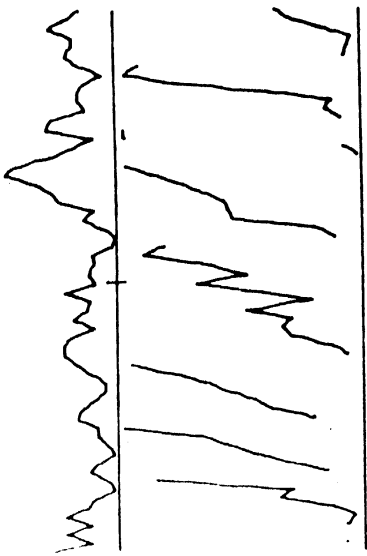
44-1211



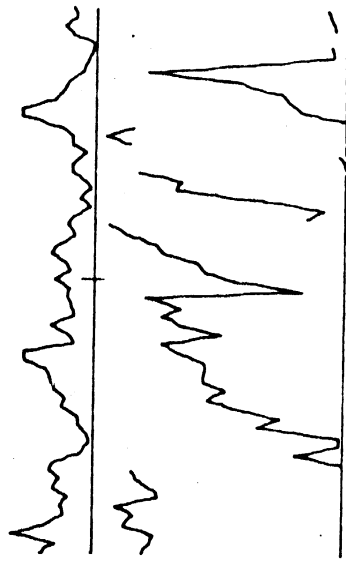
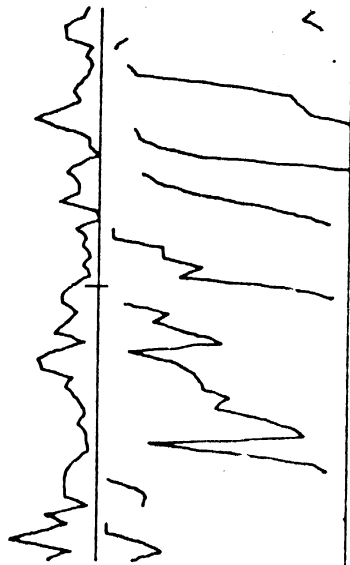
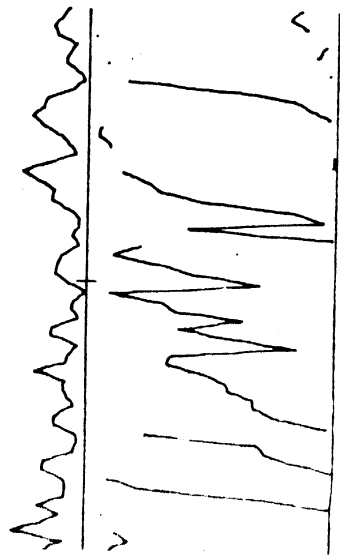
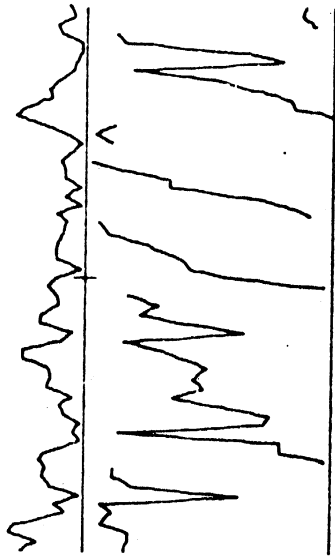
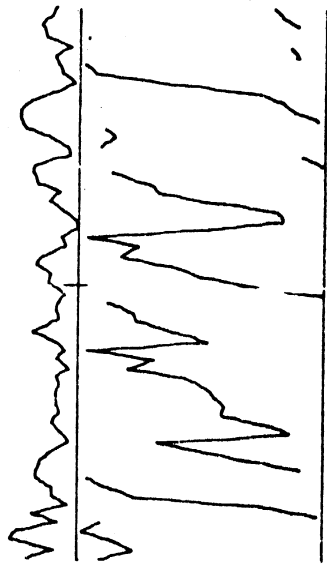
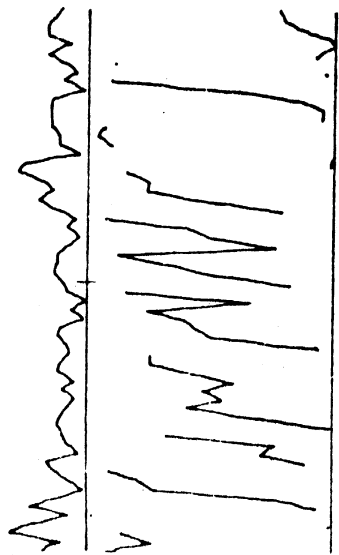




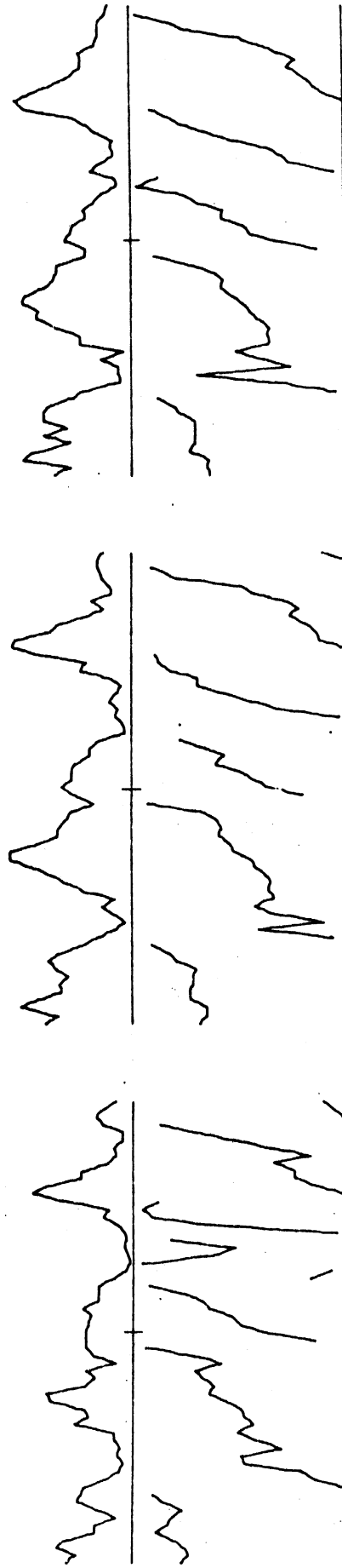
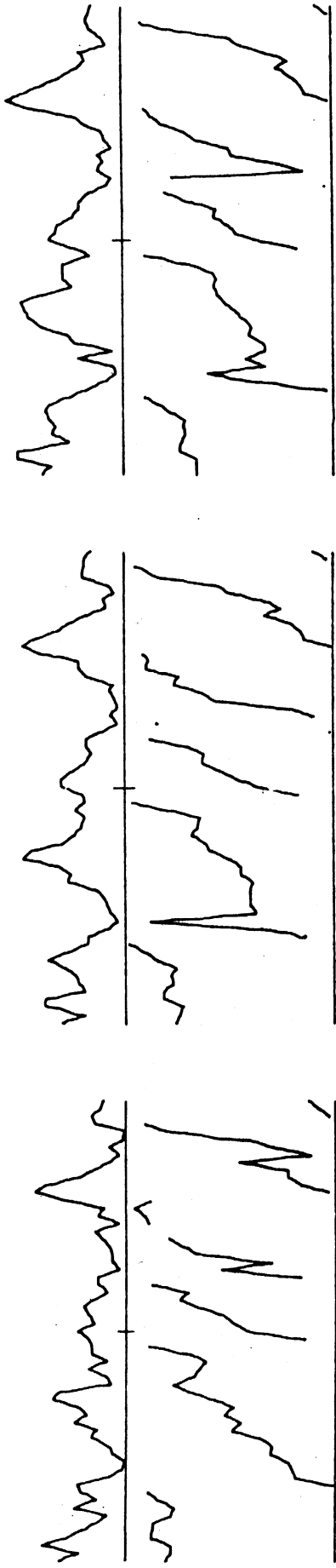




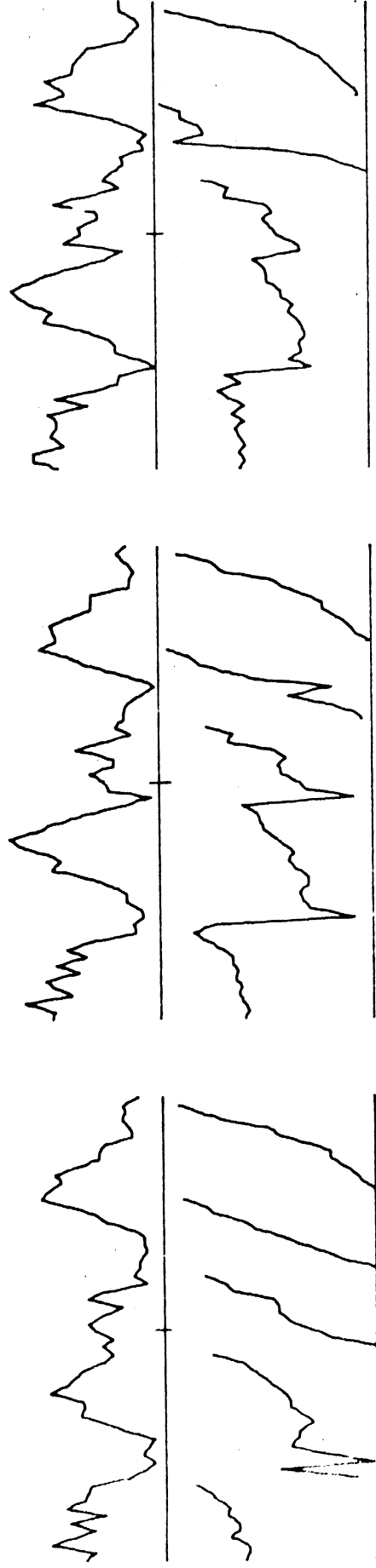
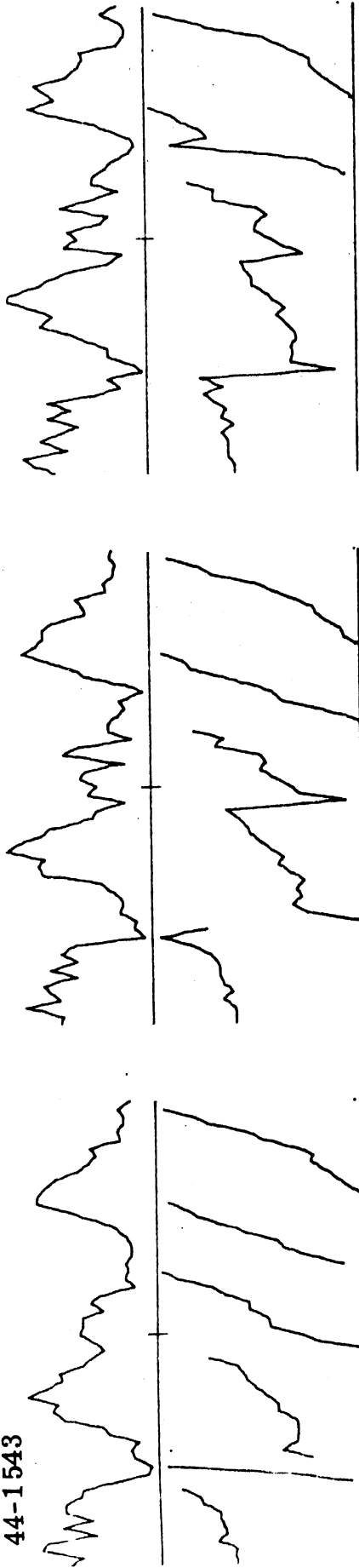
44-1432



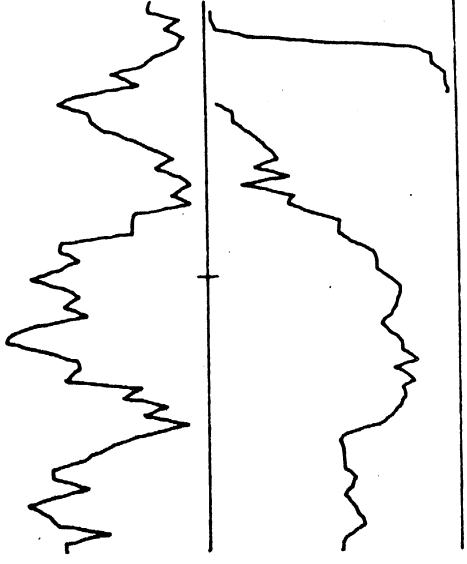
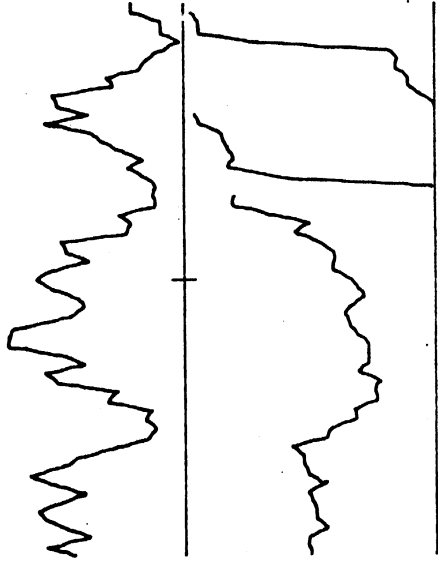
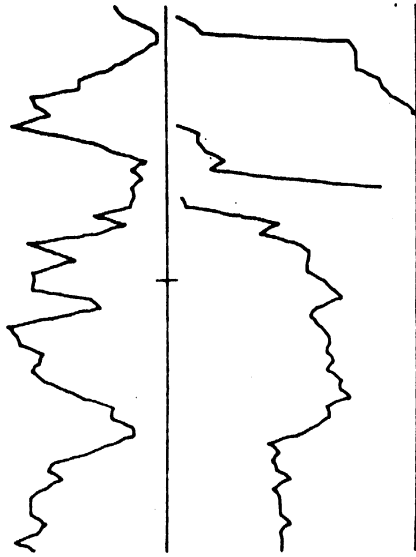
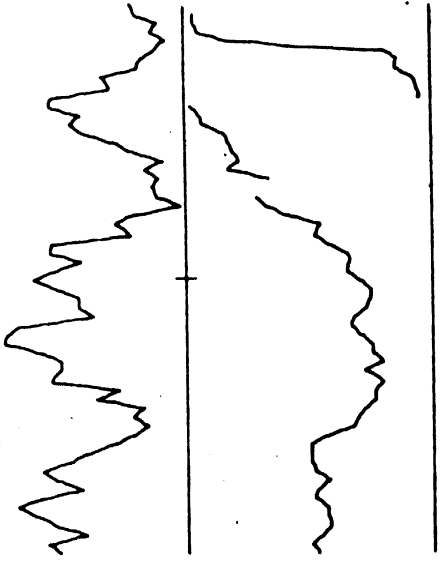
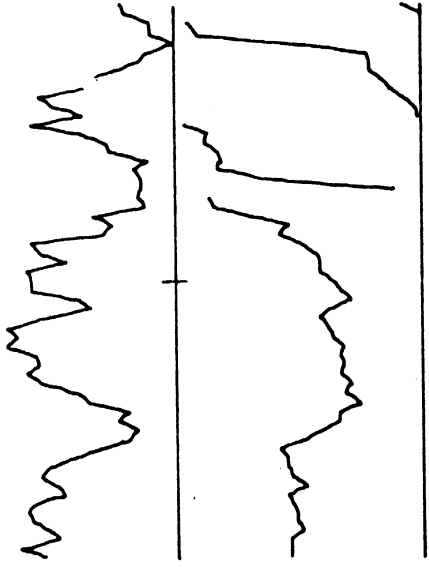
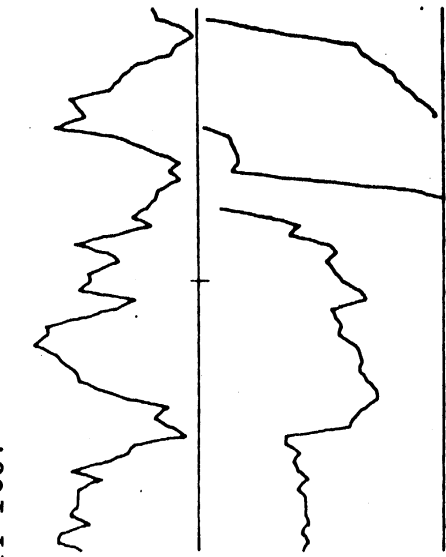
44-1471



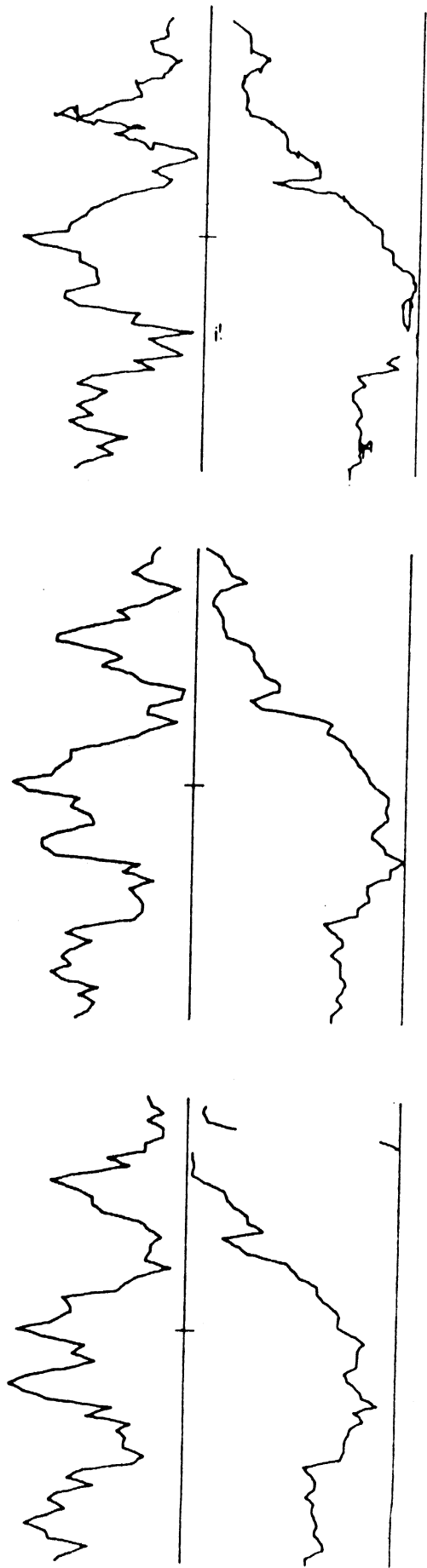
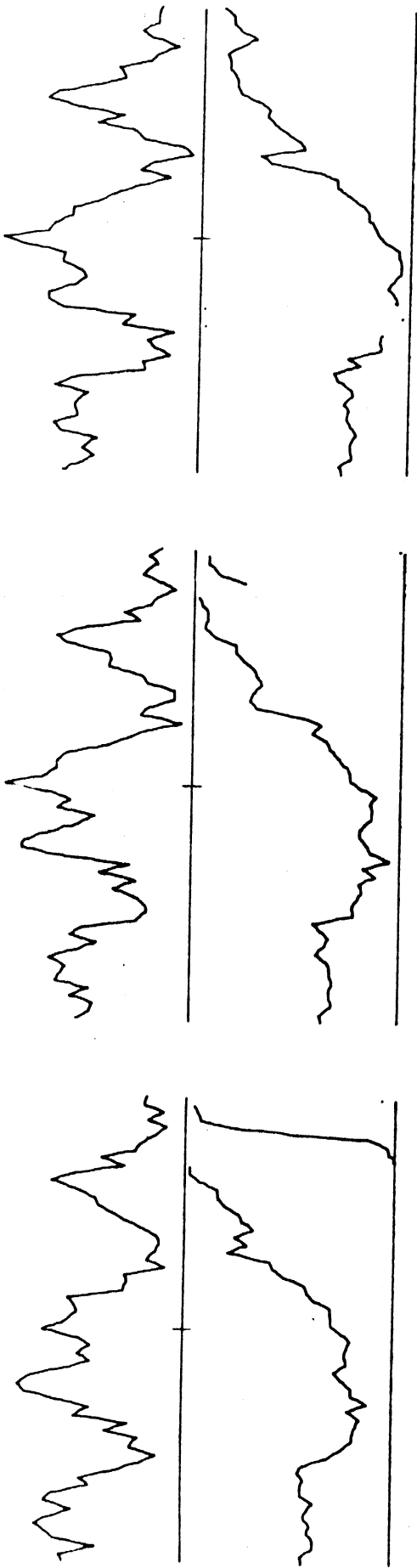
44-1543



44-1607

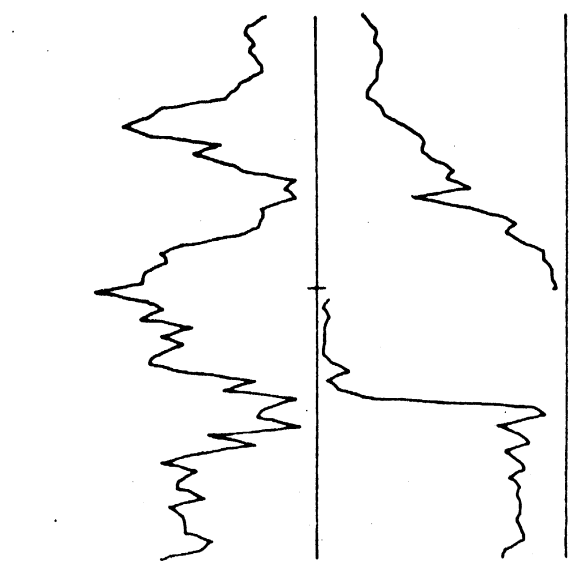
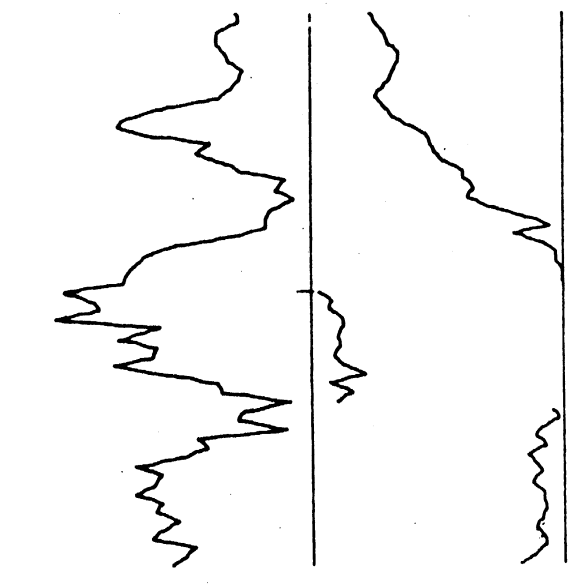
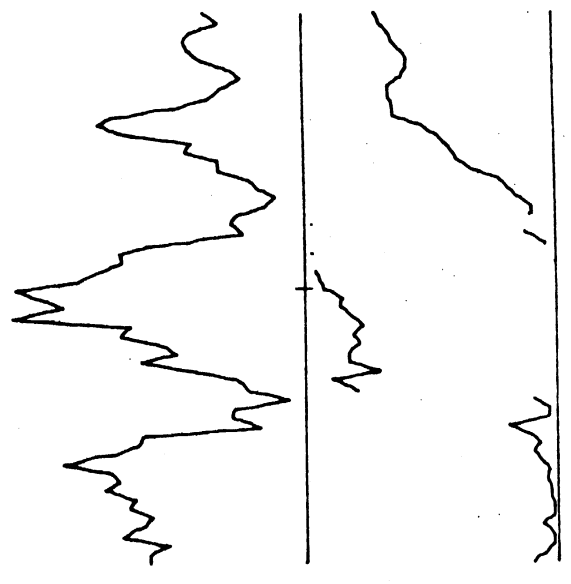
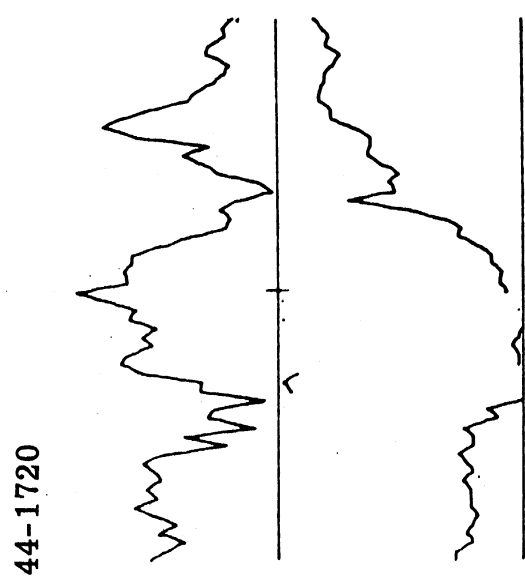
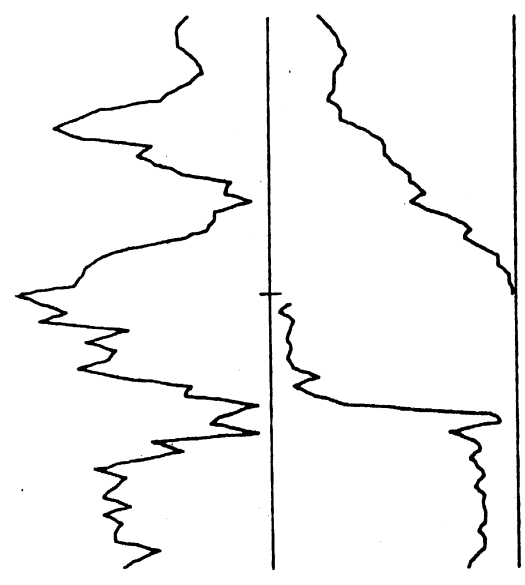
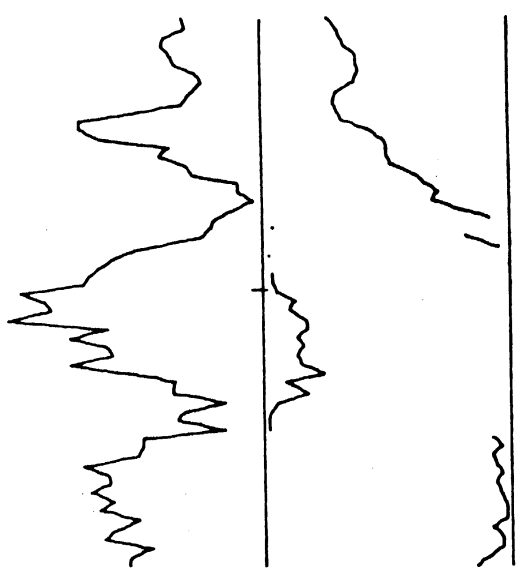


44-1654

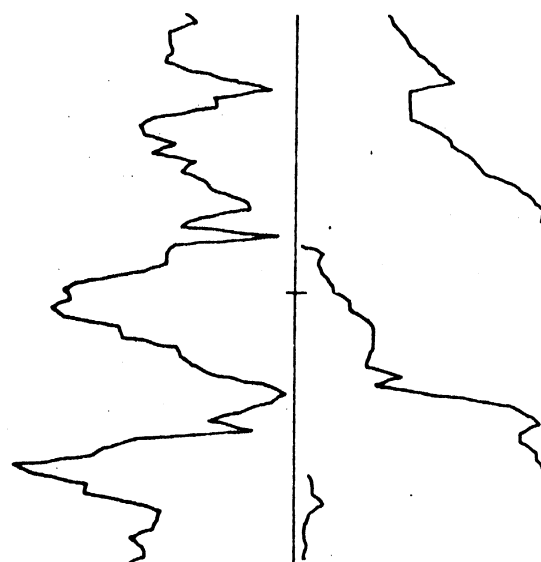
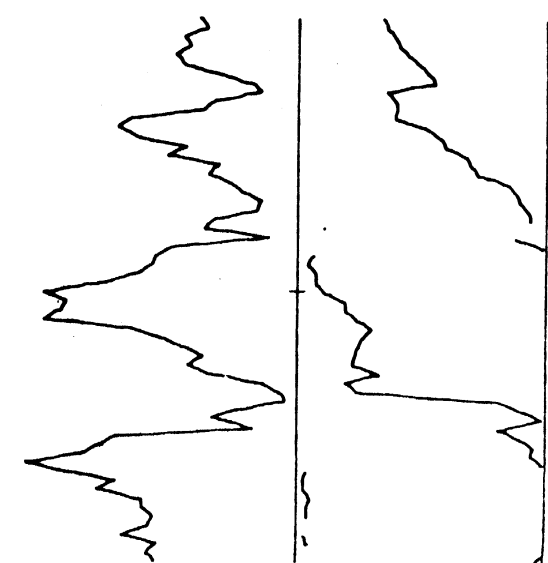
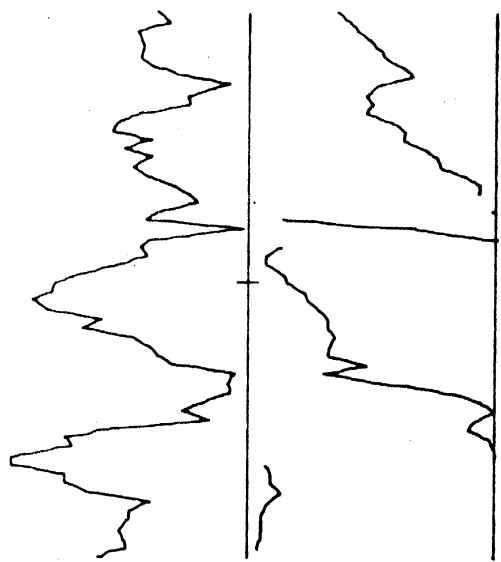
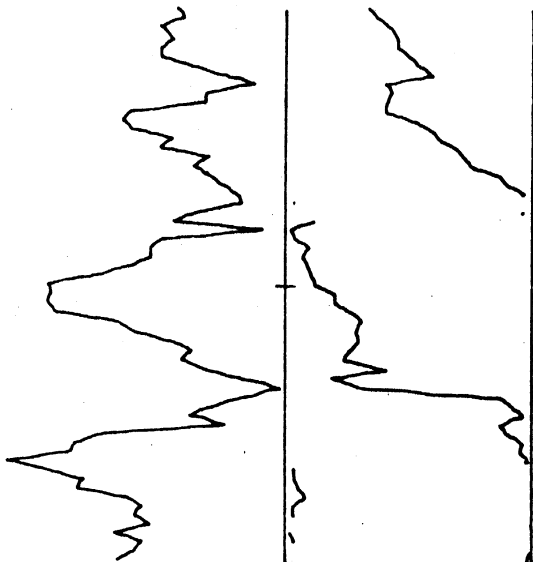
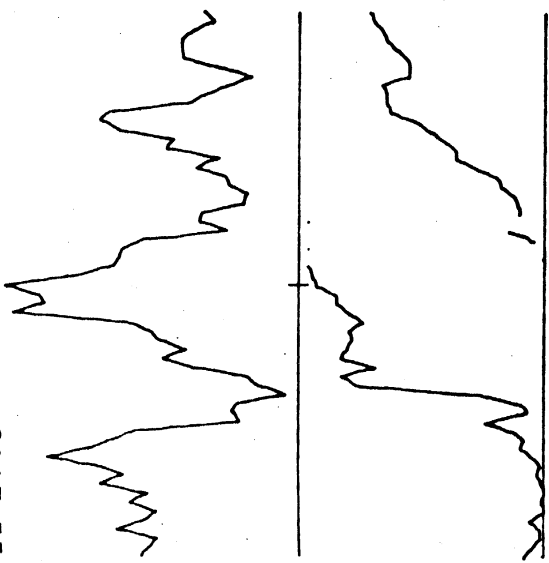




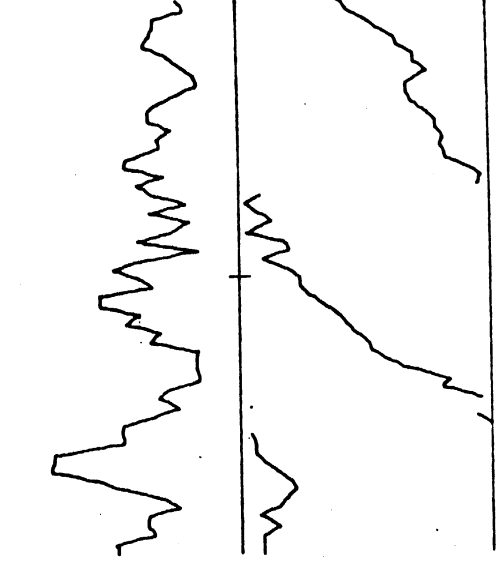
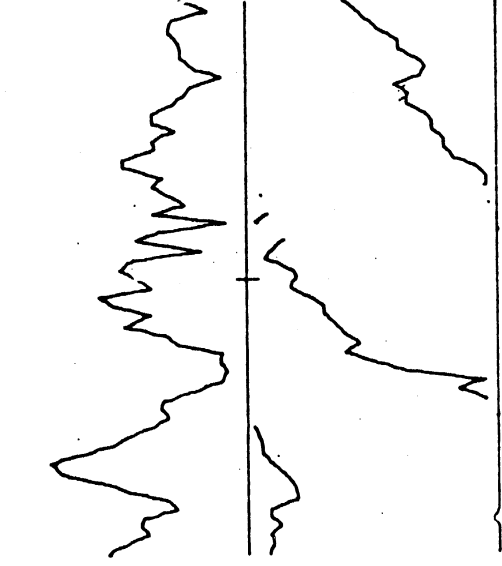
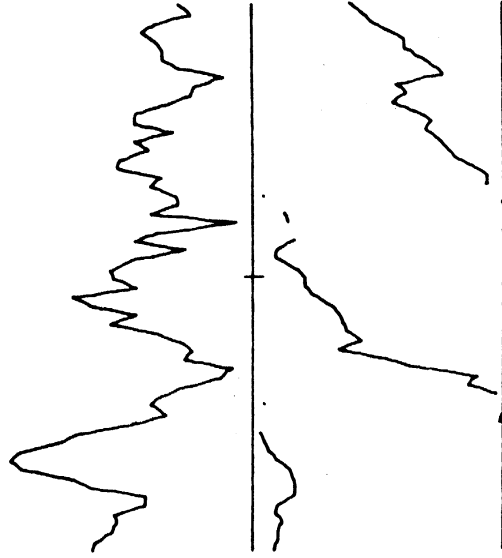
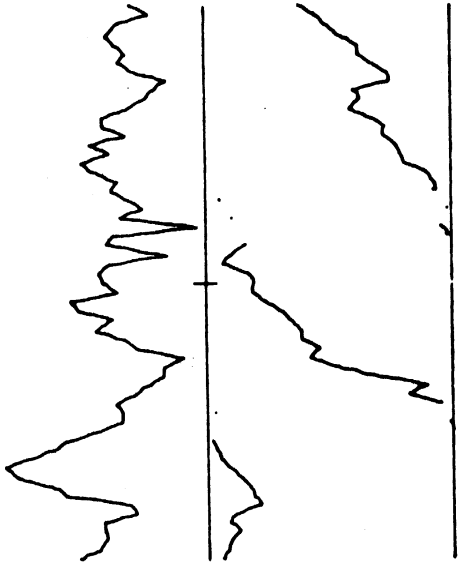
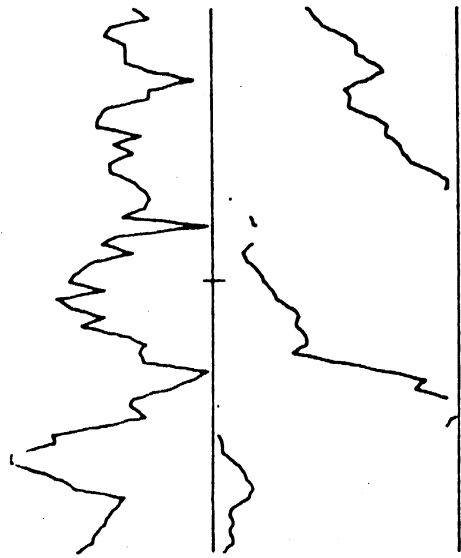
44-1720



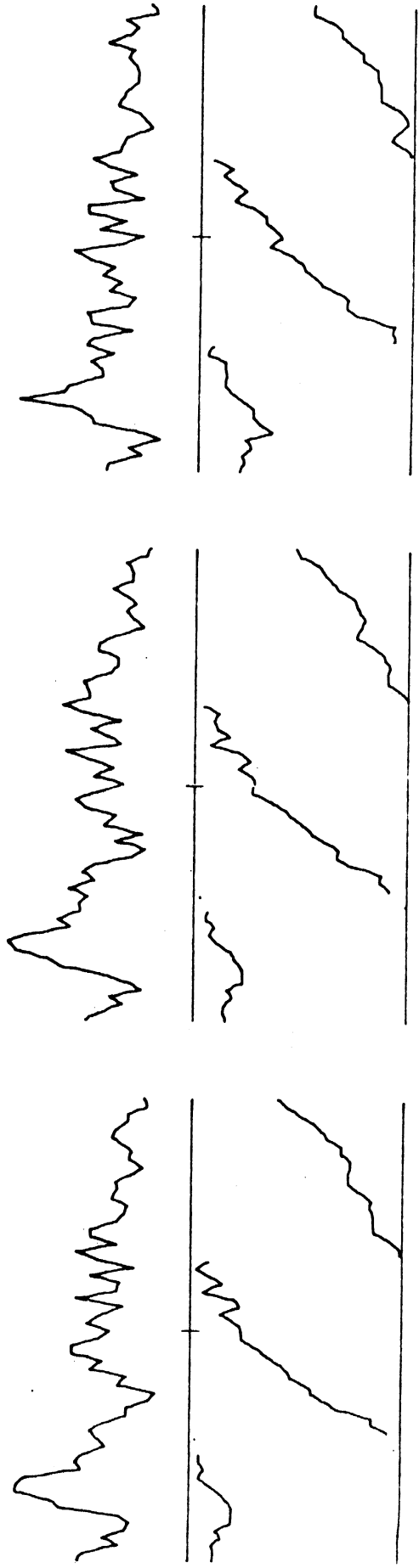
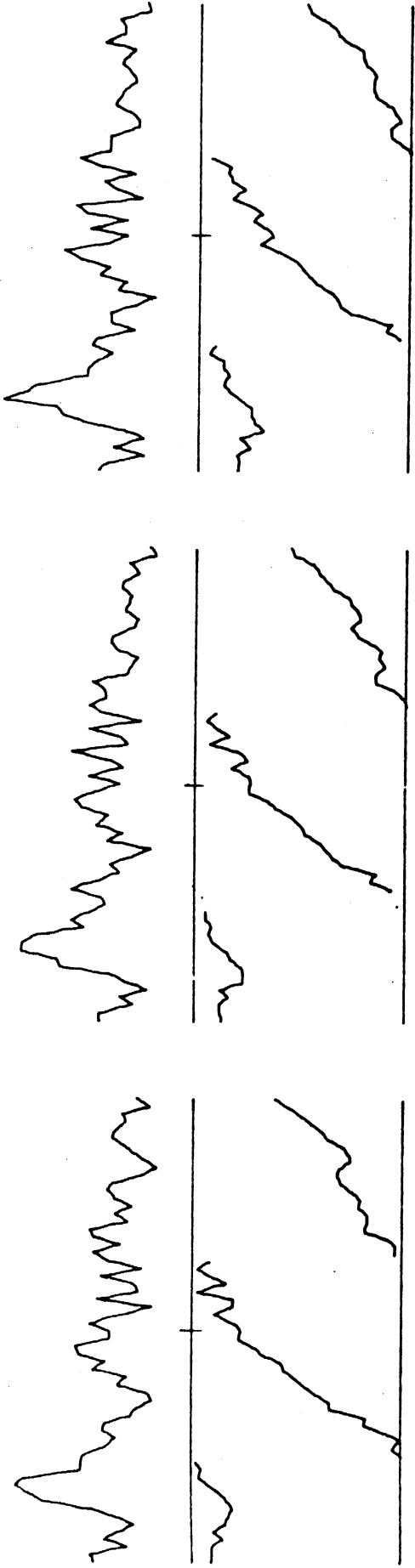
44-1765

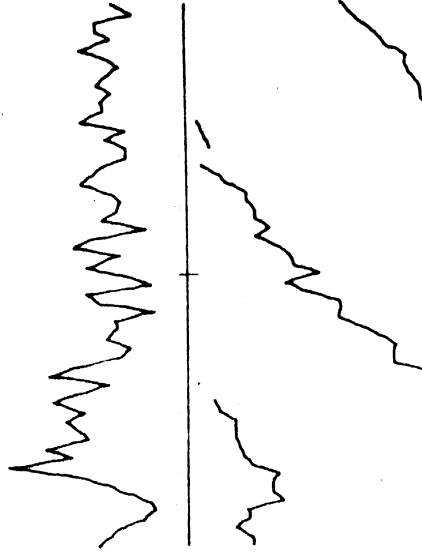
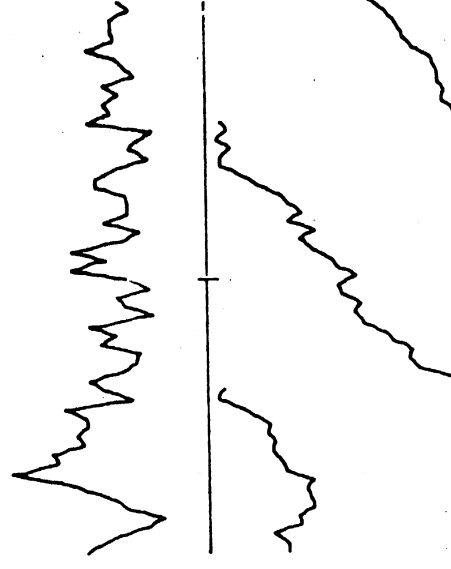
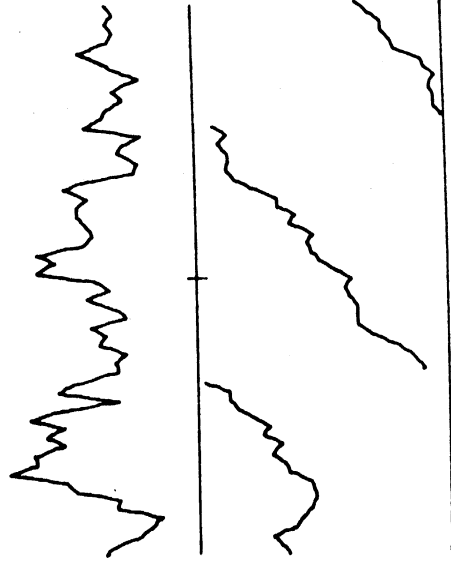
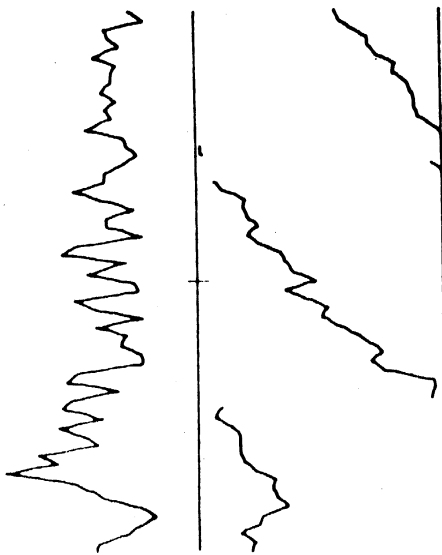
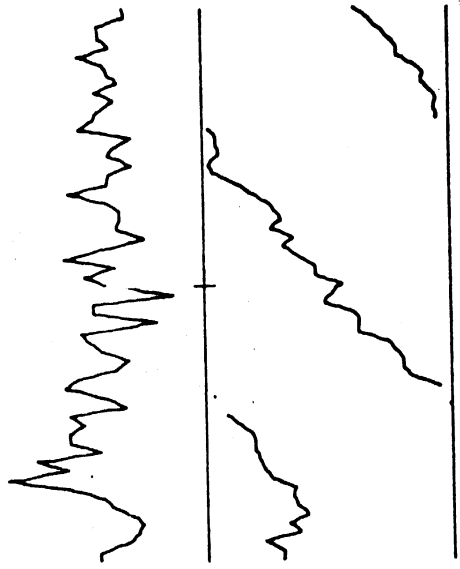
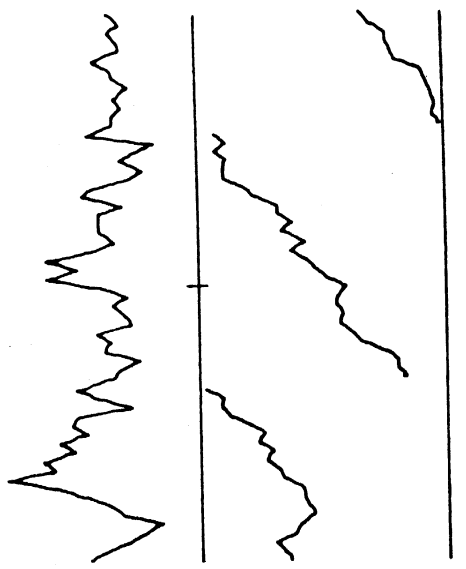


44-2031

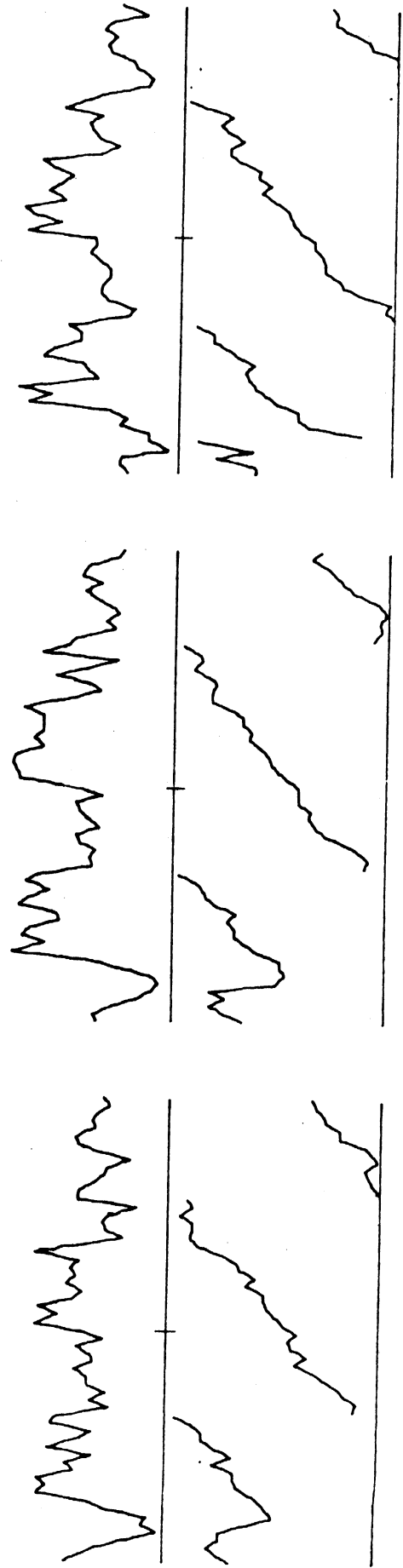
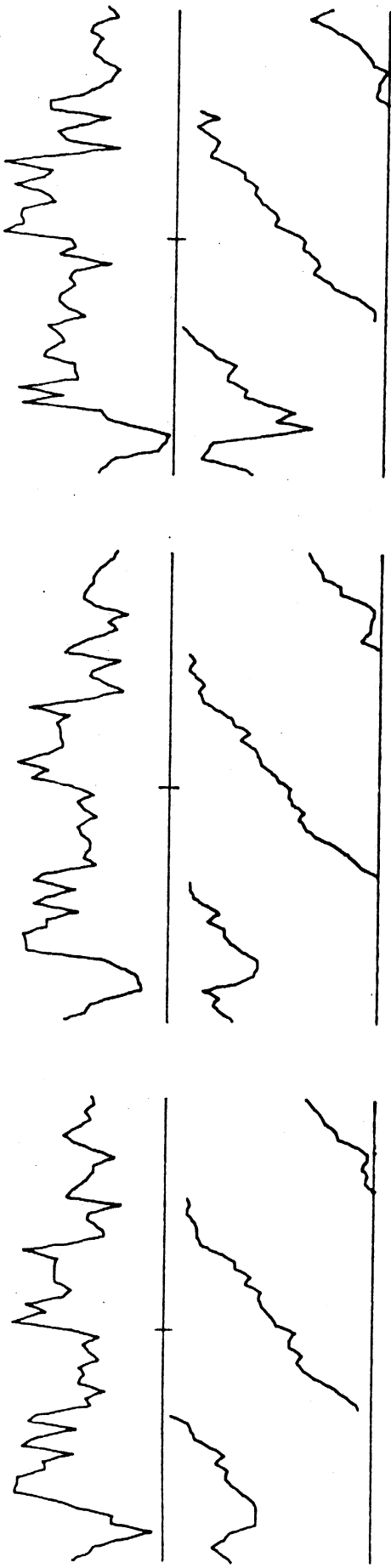


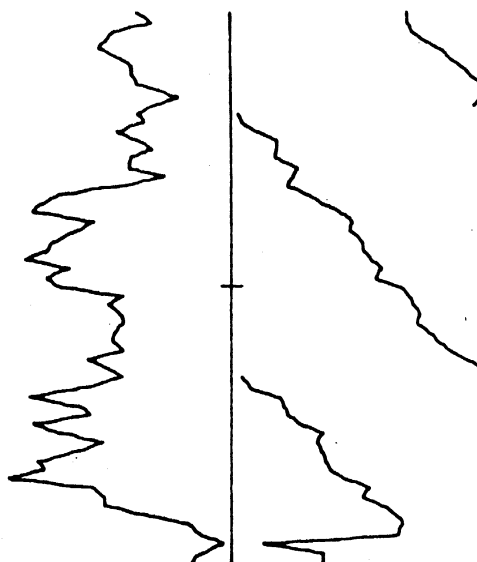
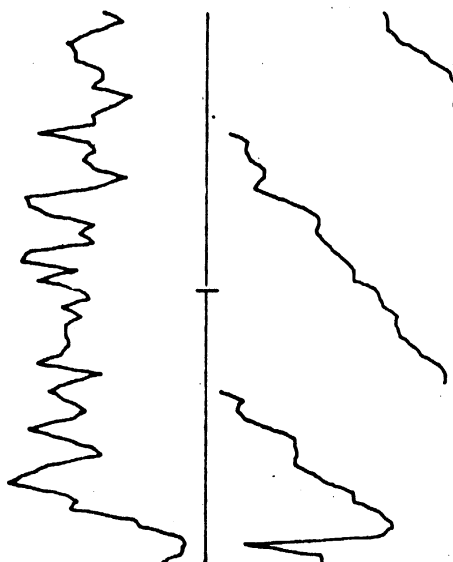
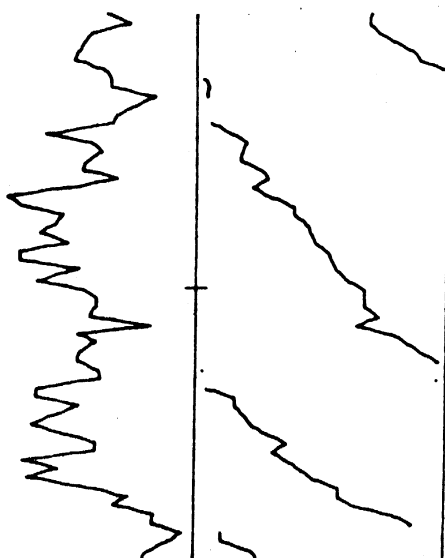
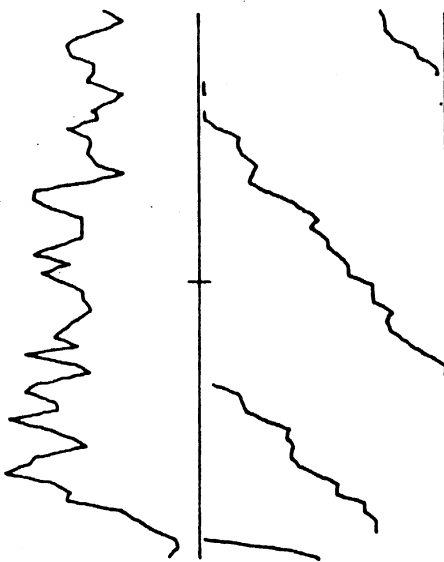
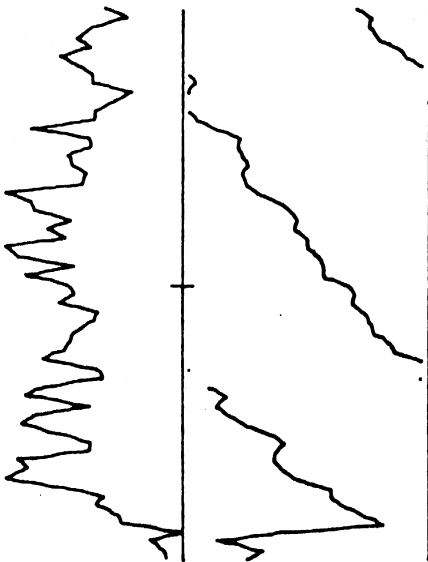
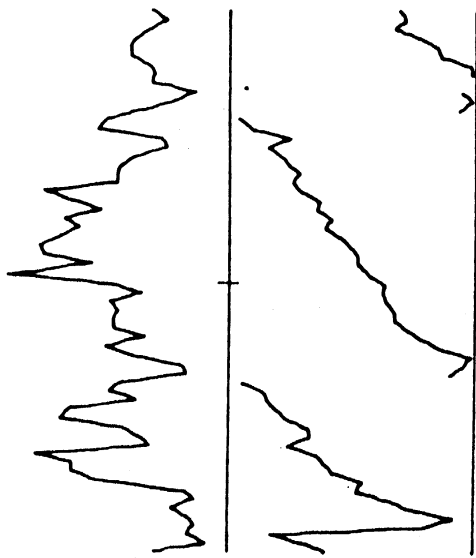
44-2075



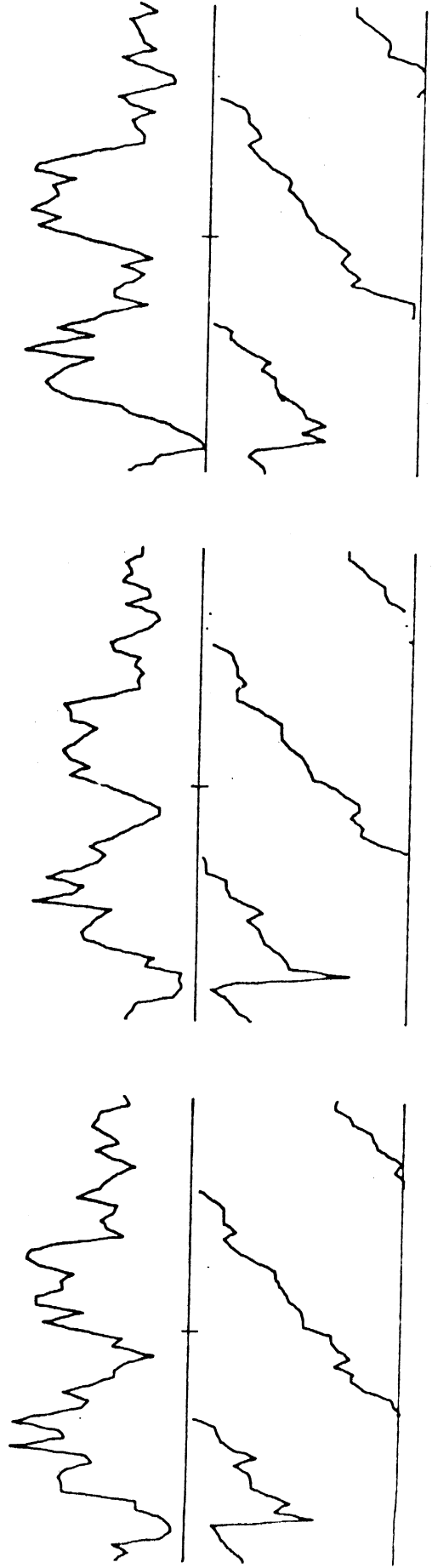
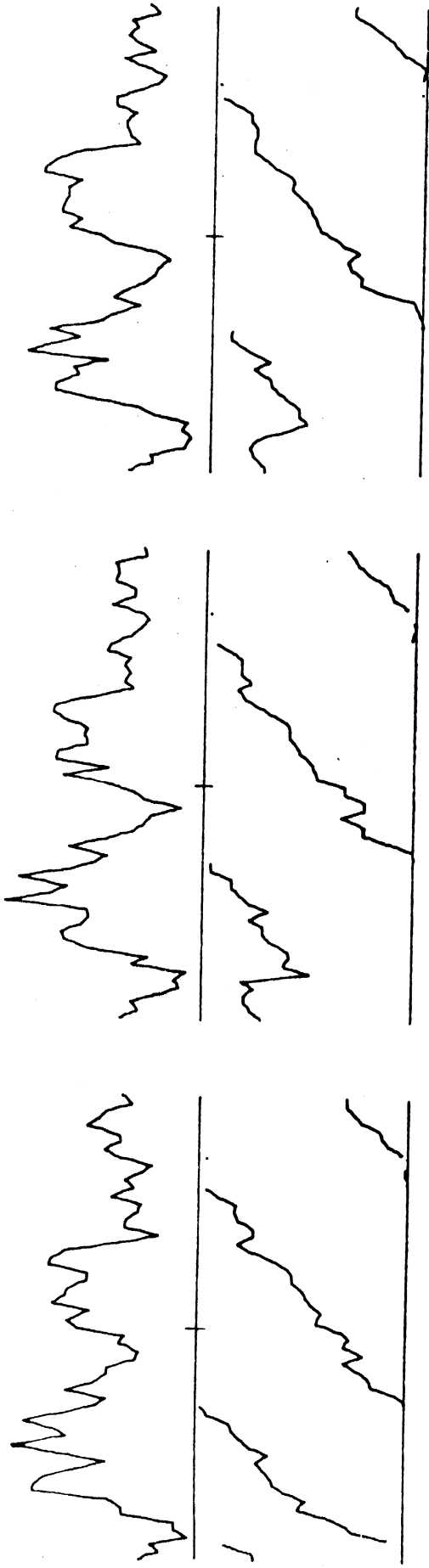


44-2206



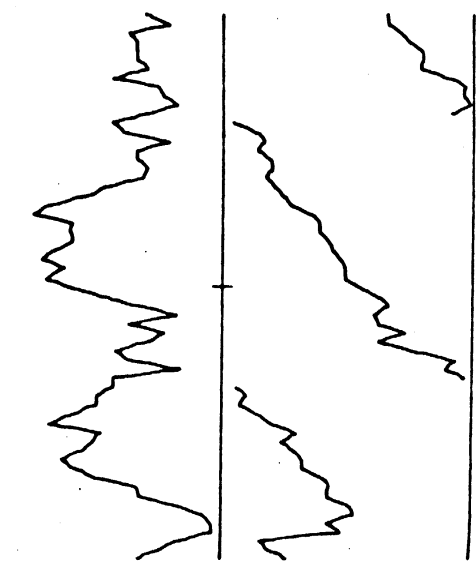
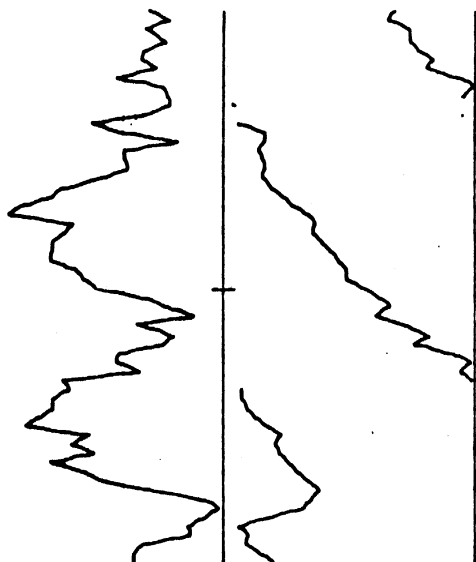
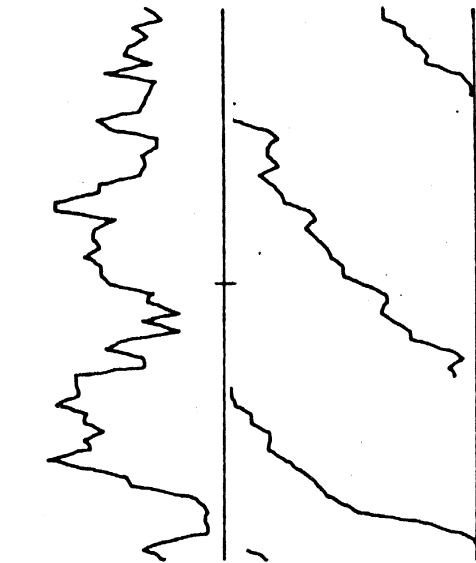
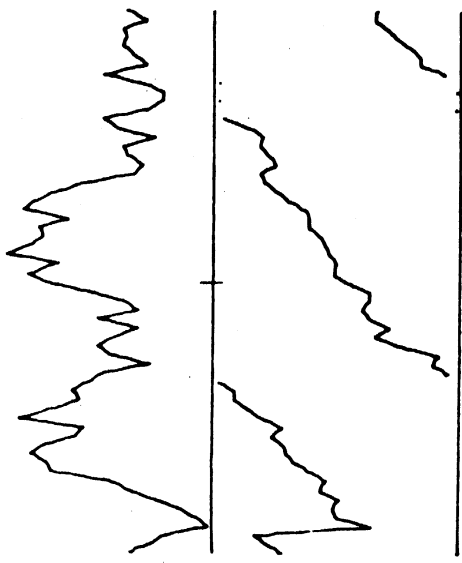
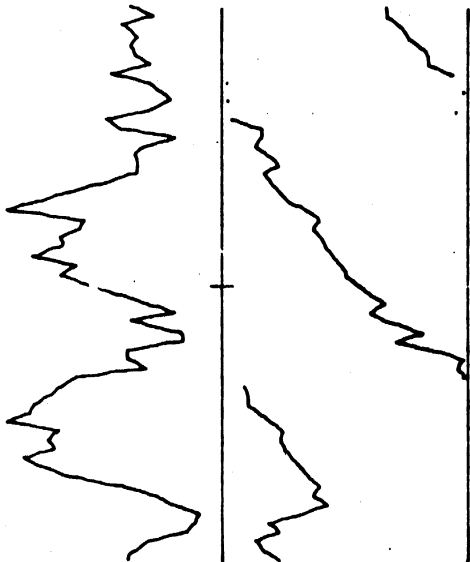
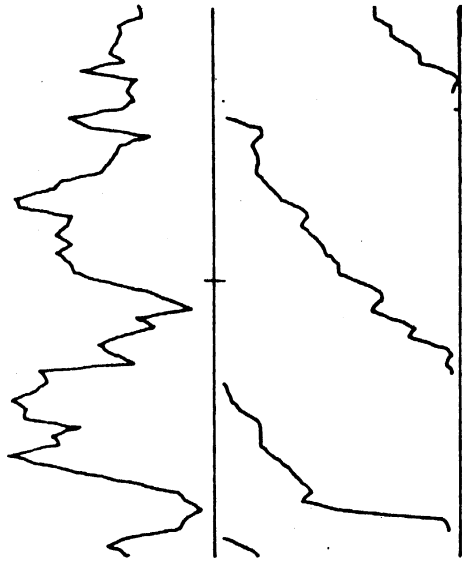


44-2317

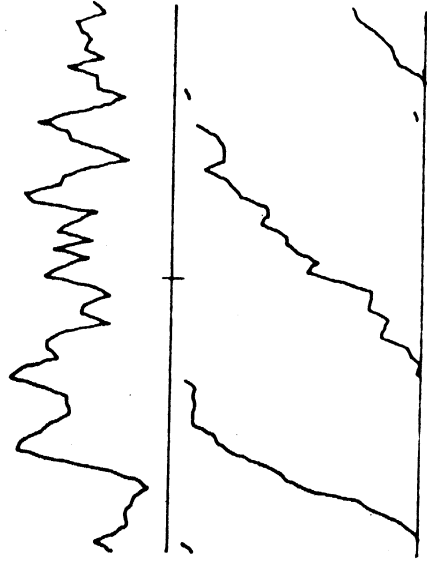
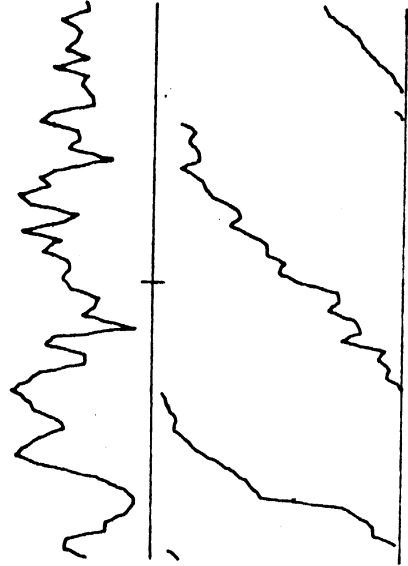
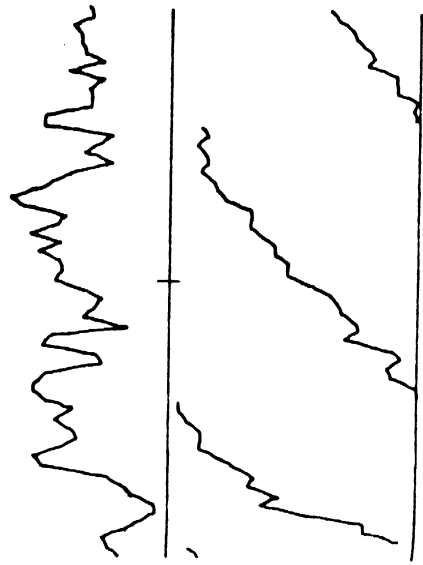
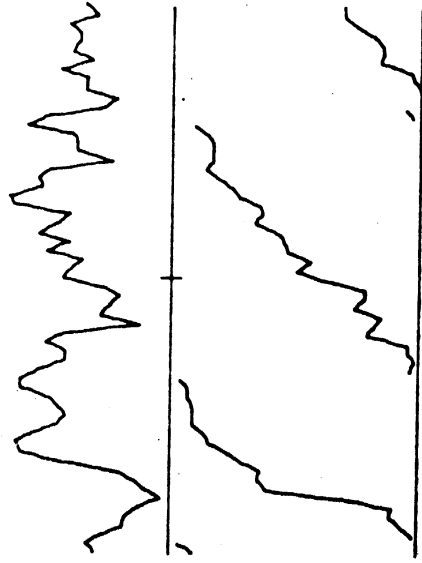
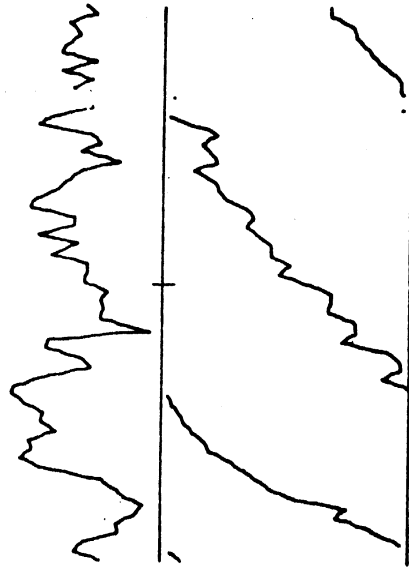
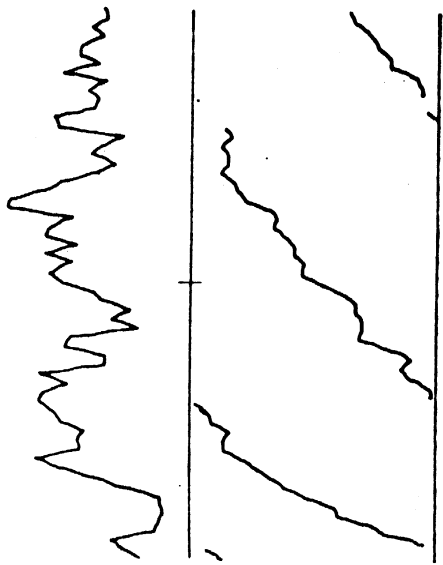




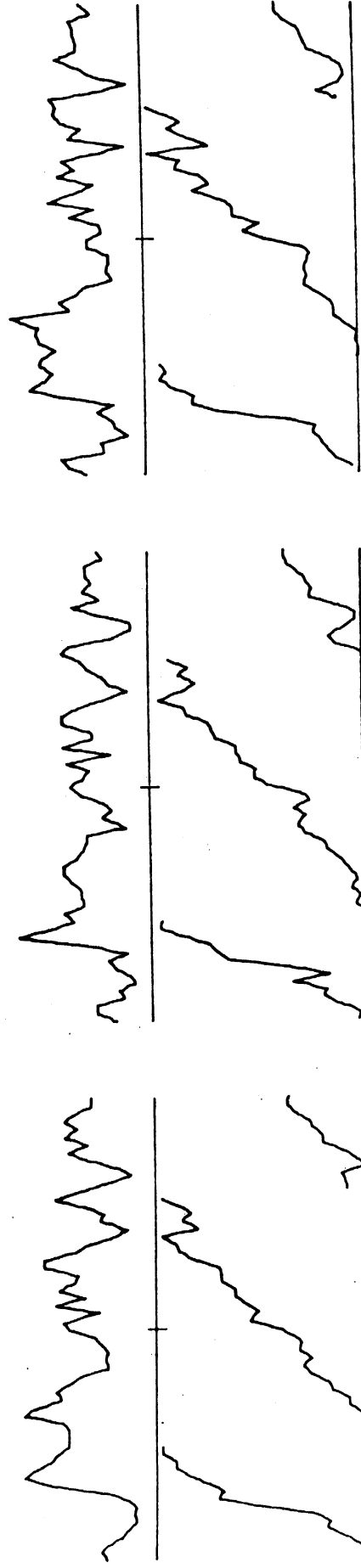
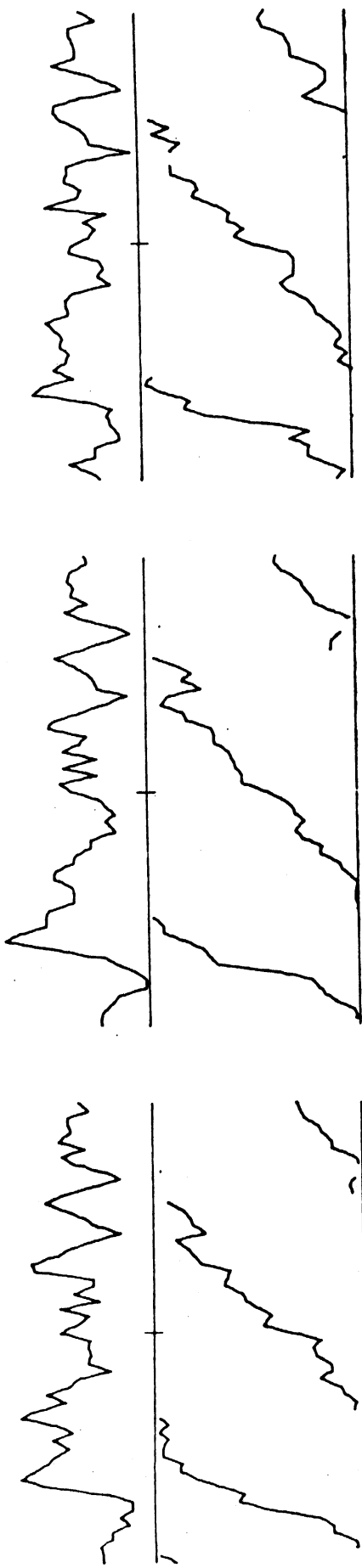
44-2363



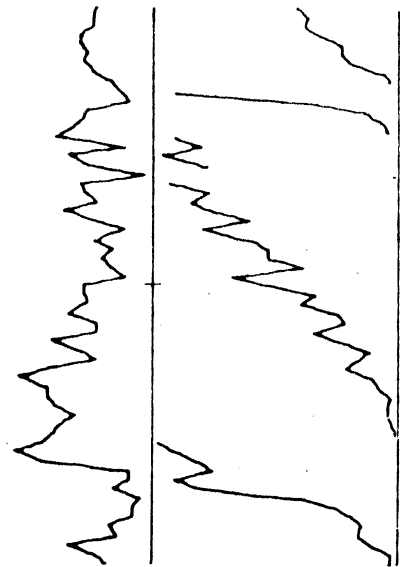
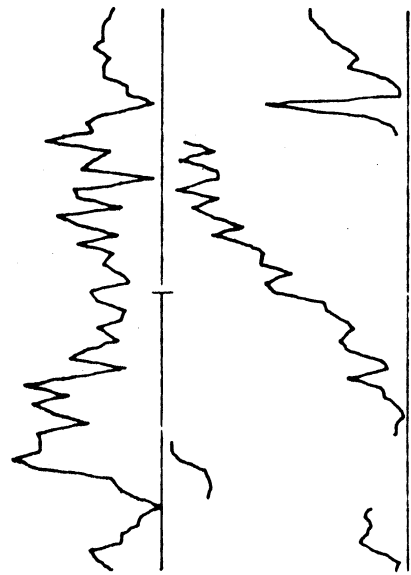
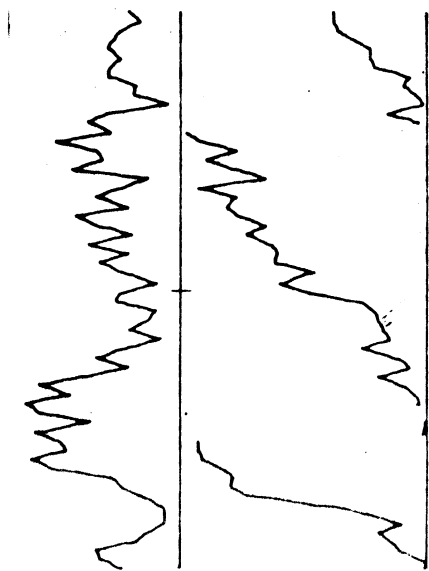
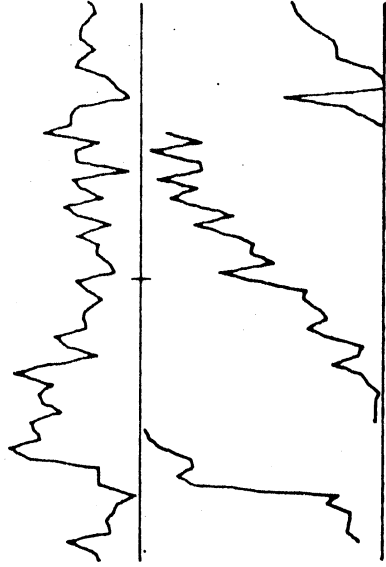
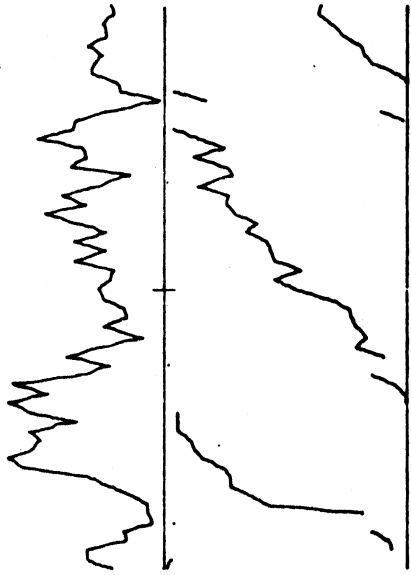
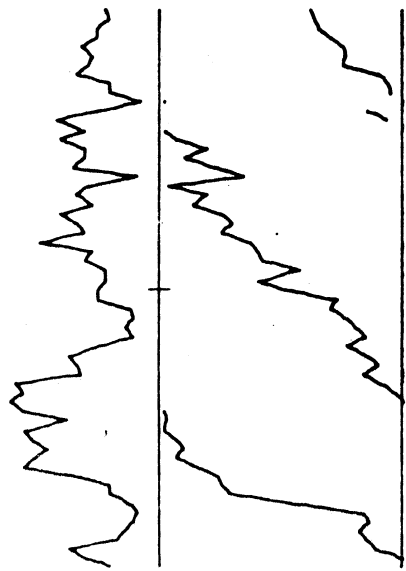
44-2430

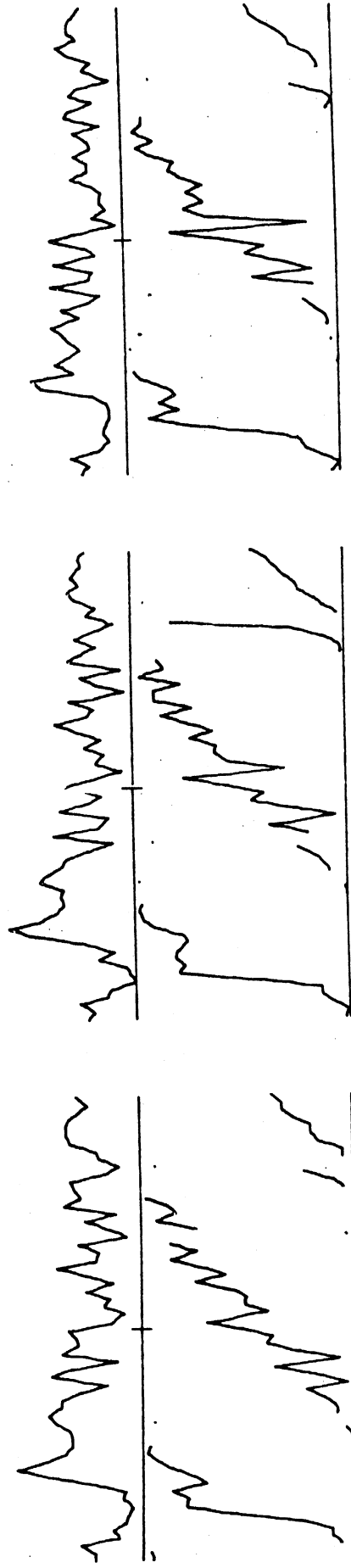
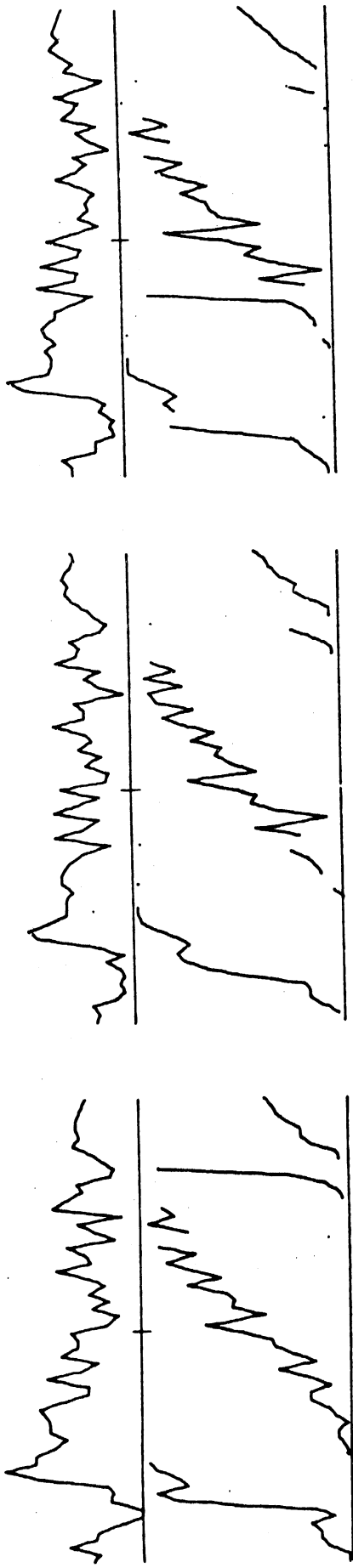


44-2474

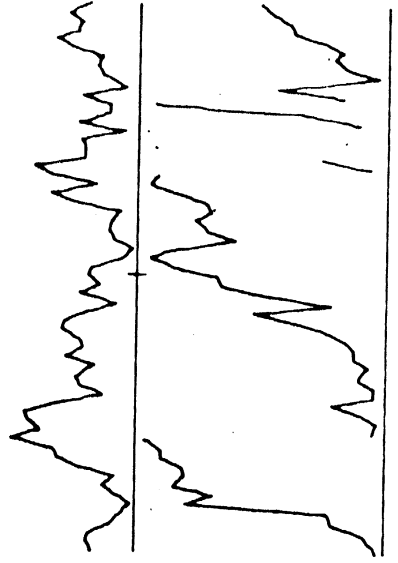
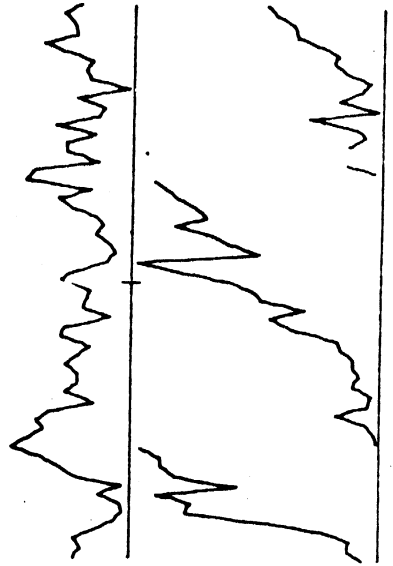
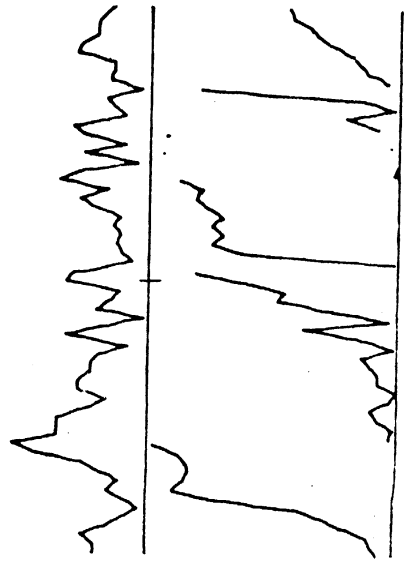
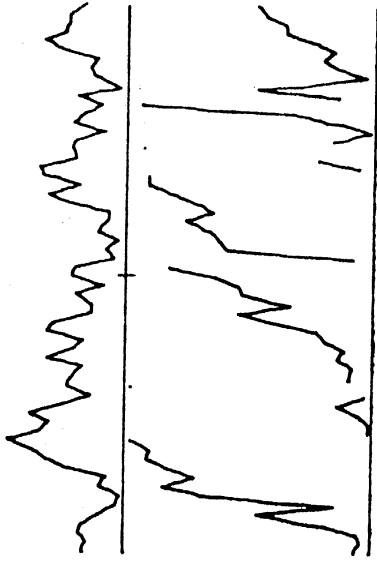
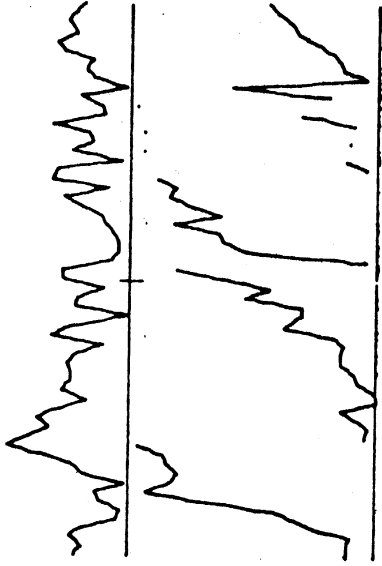
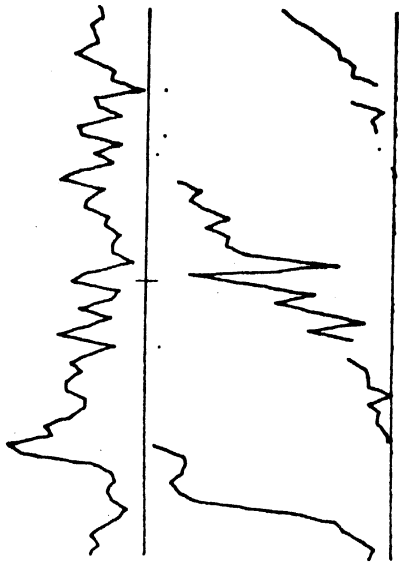


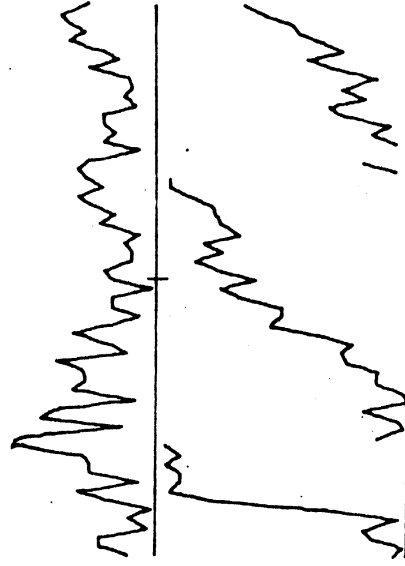
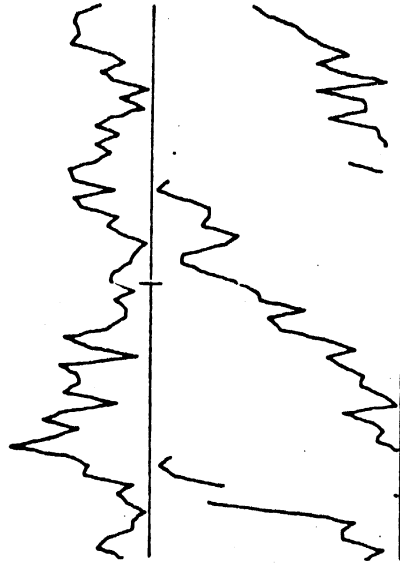
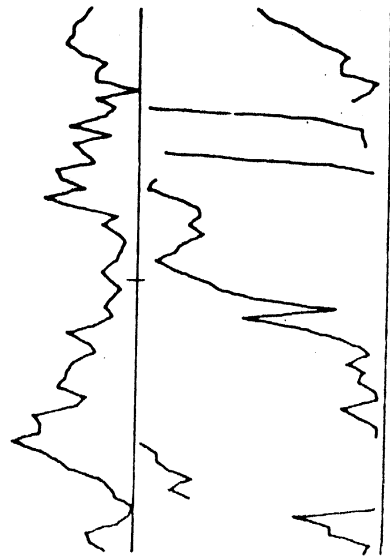
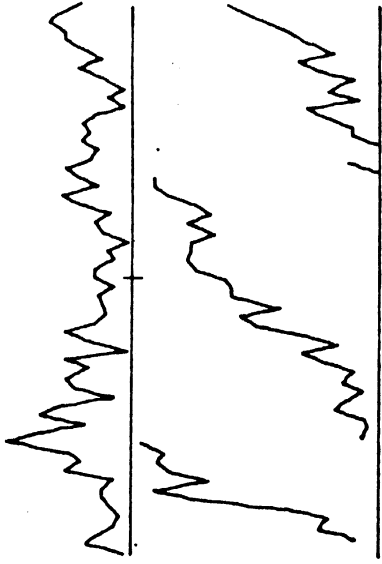
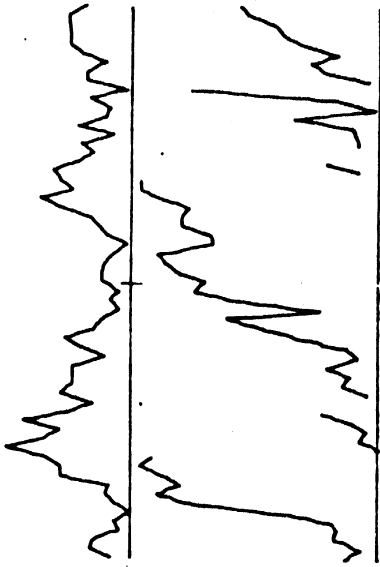
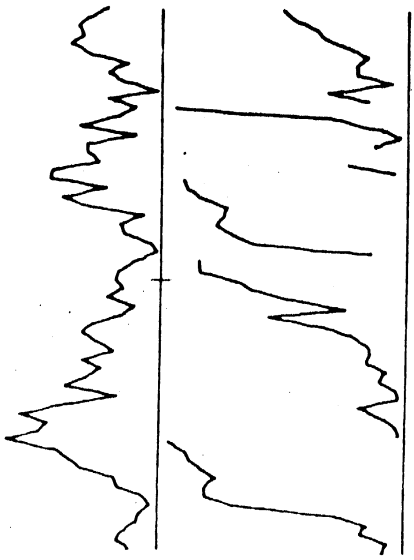
44-2541

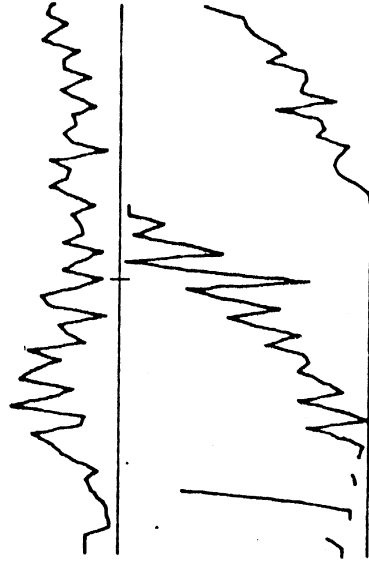
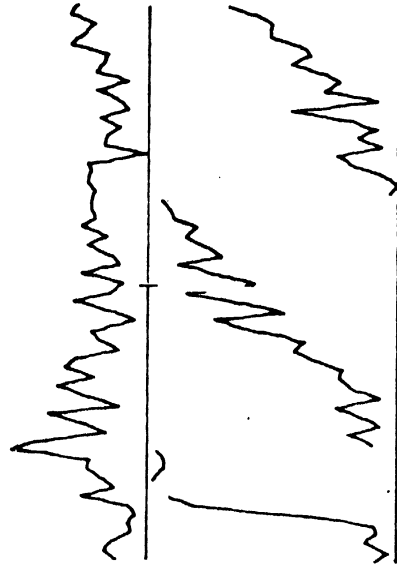
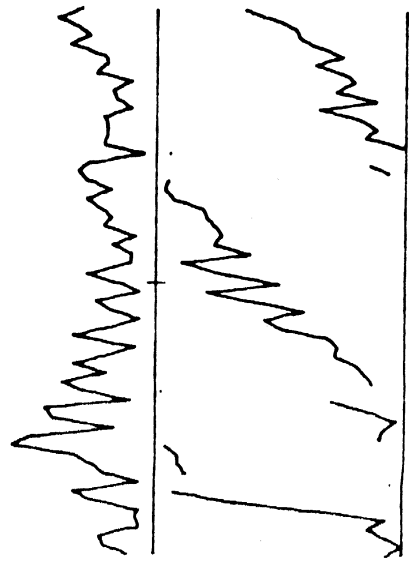
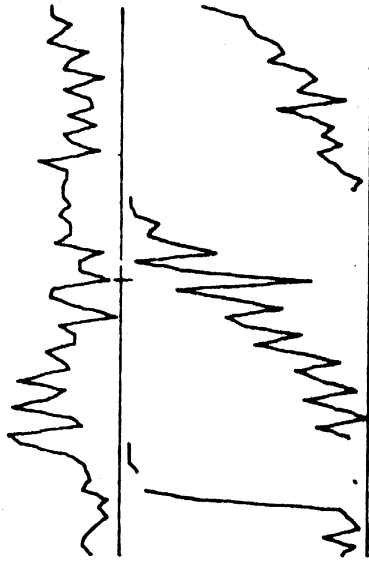
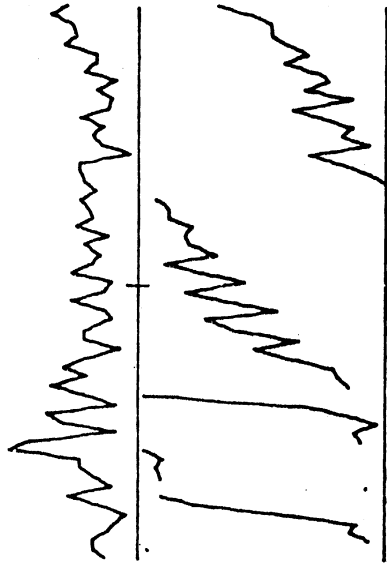
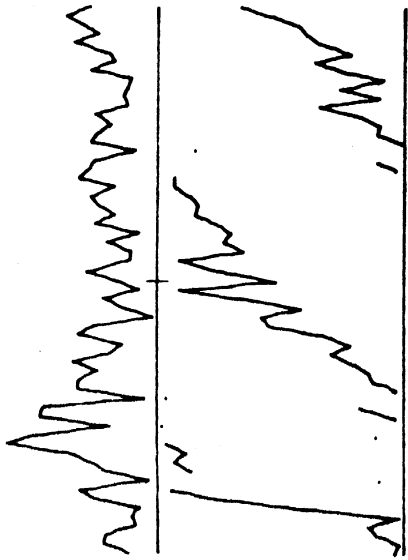




44-2651

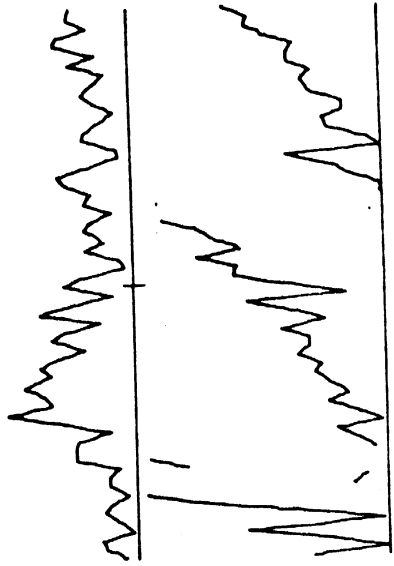
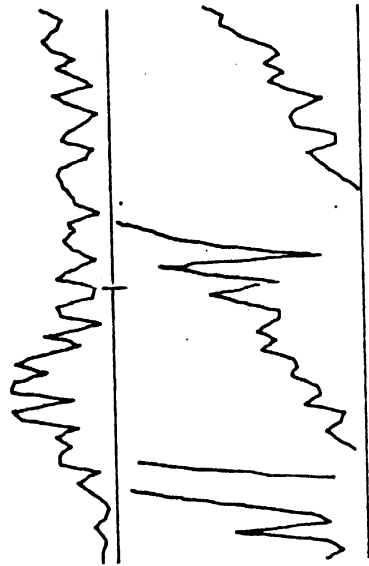
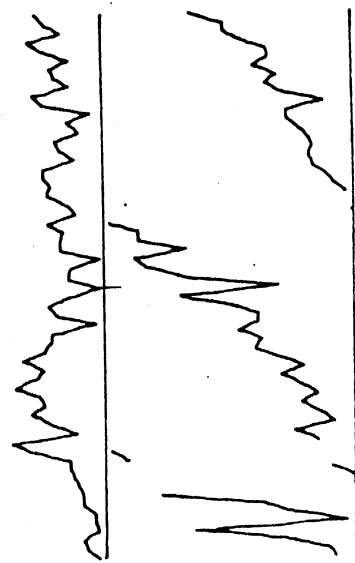
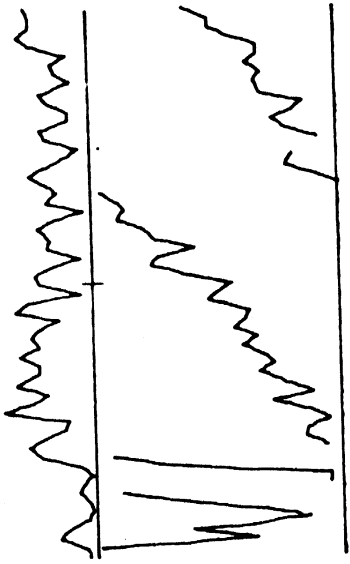
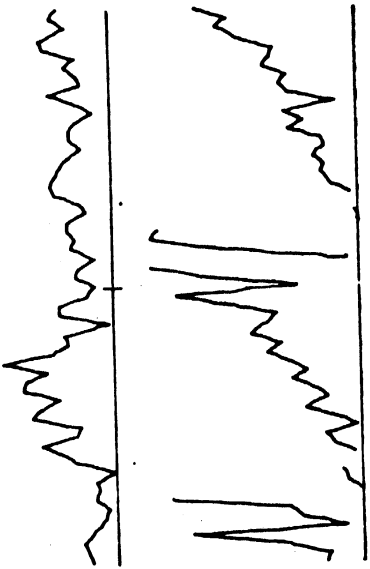
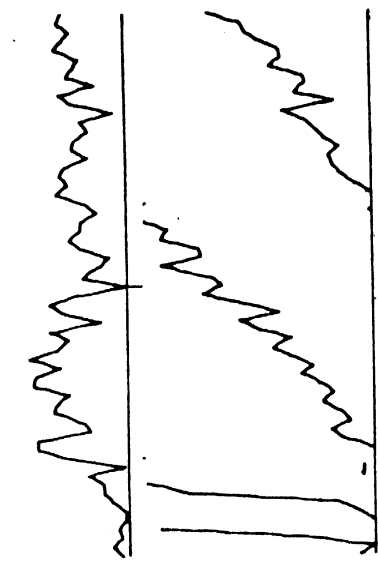


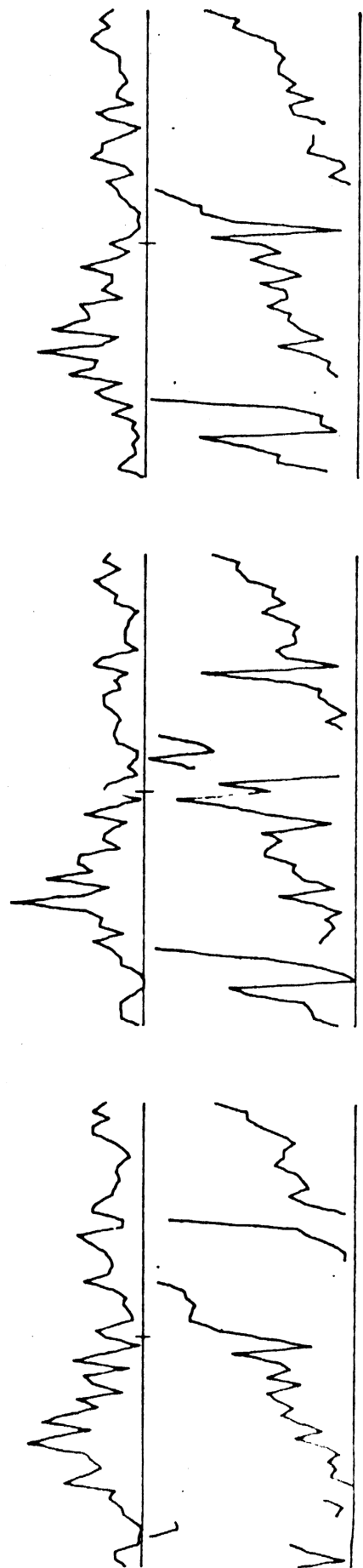
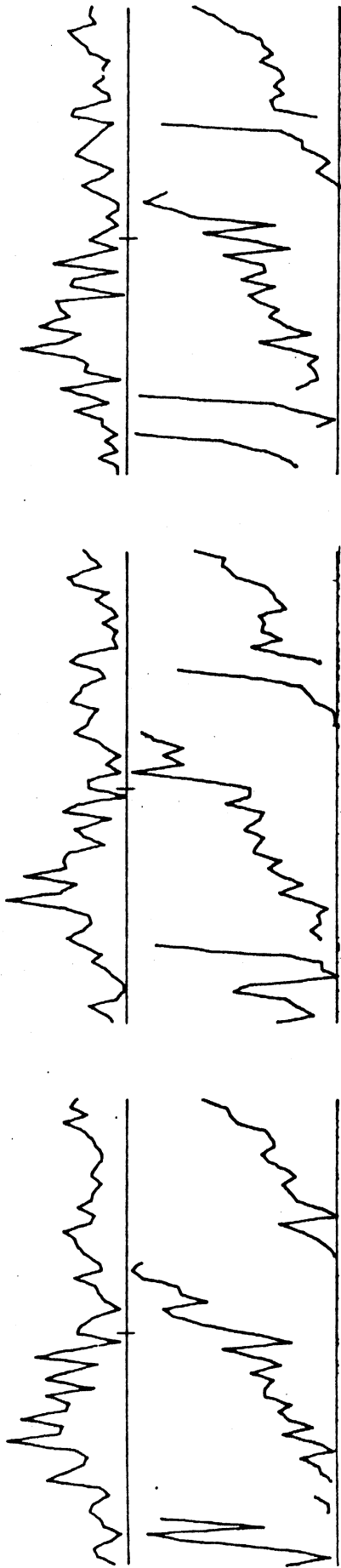




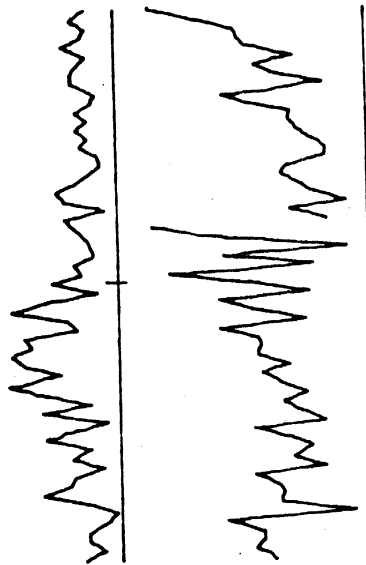
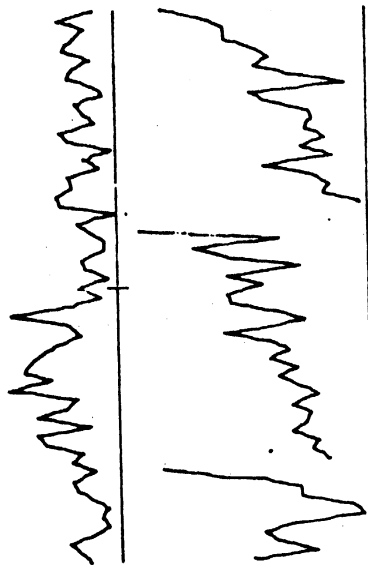
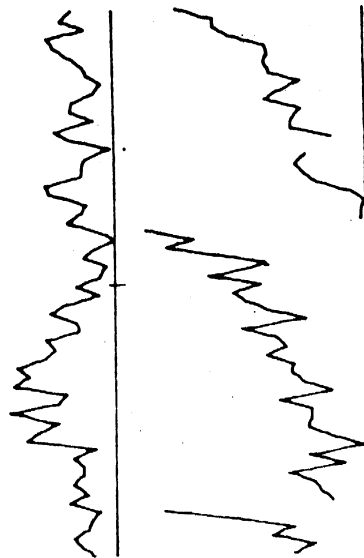
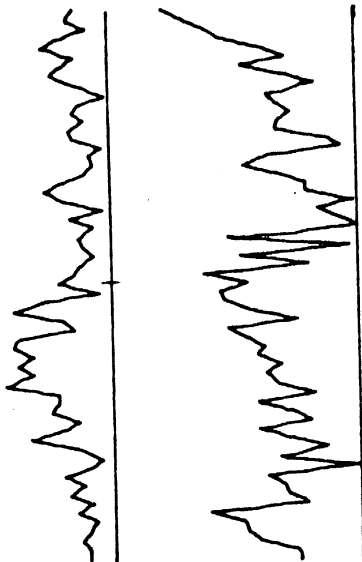
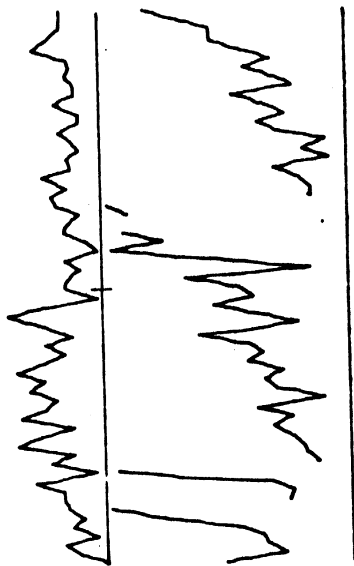
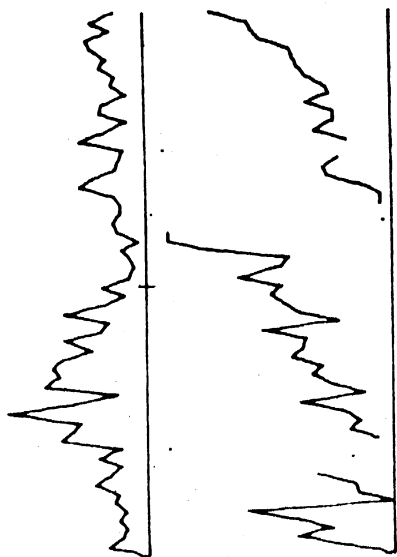


44-3027

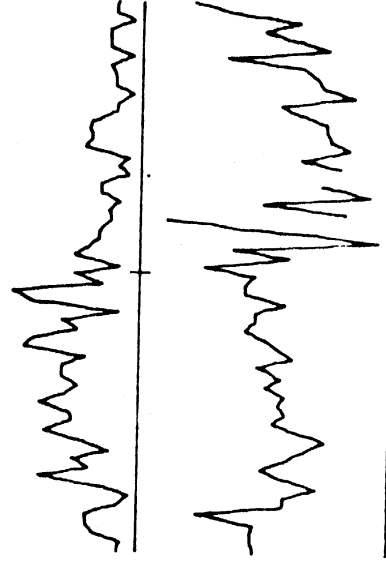
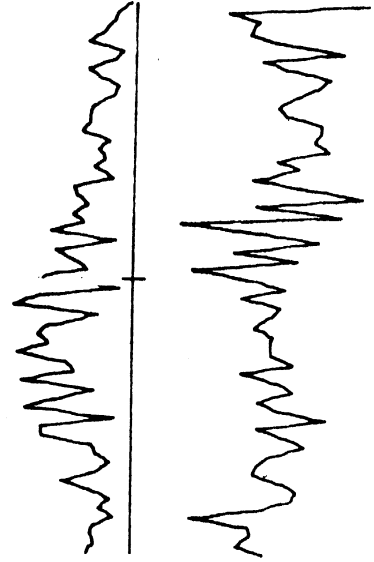
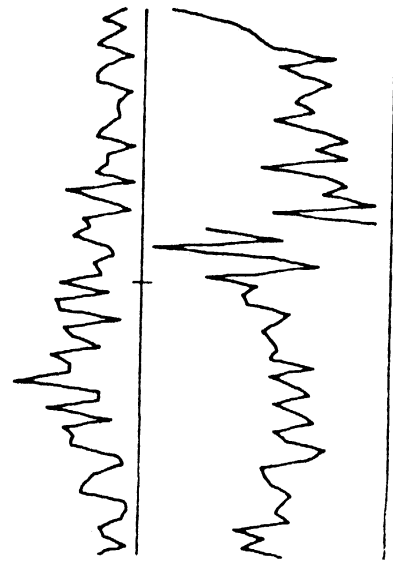
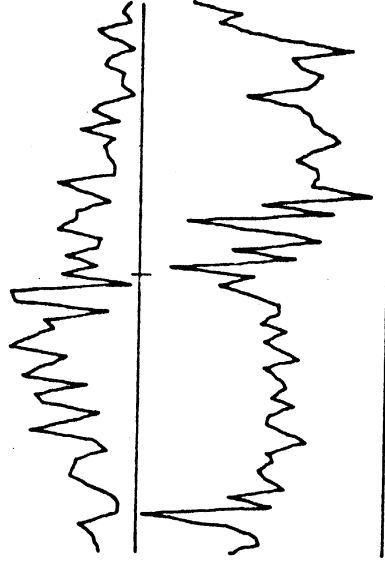
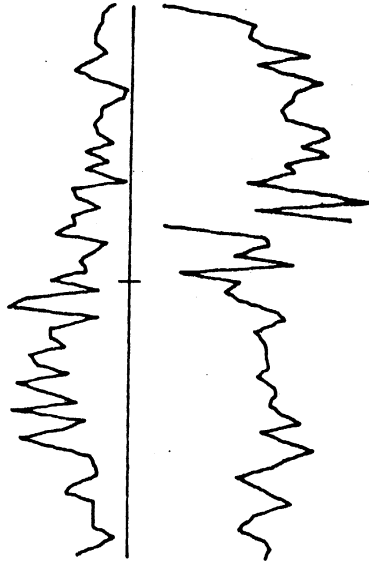
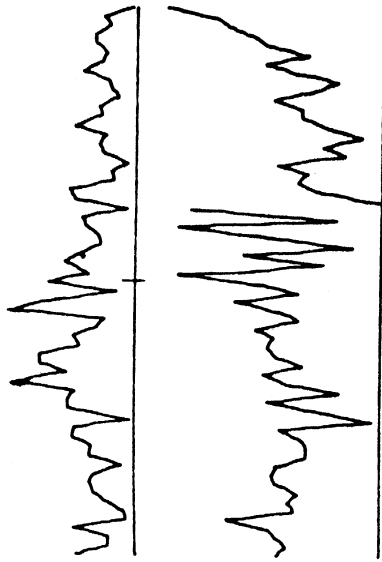




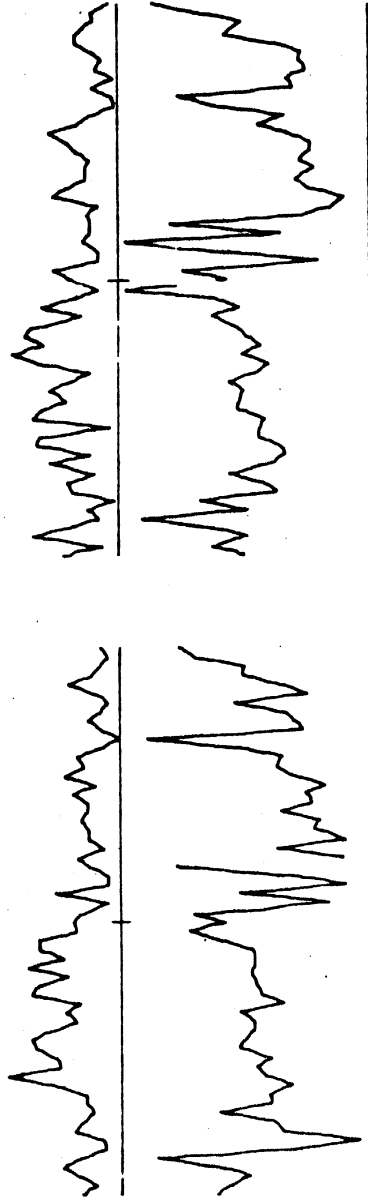
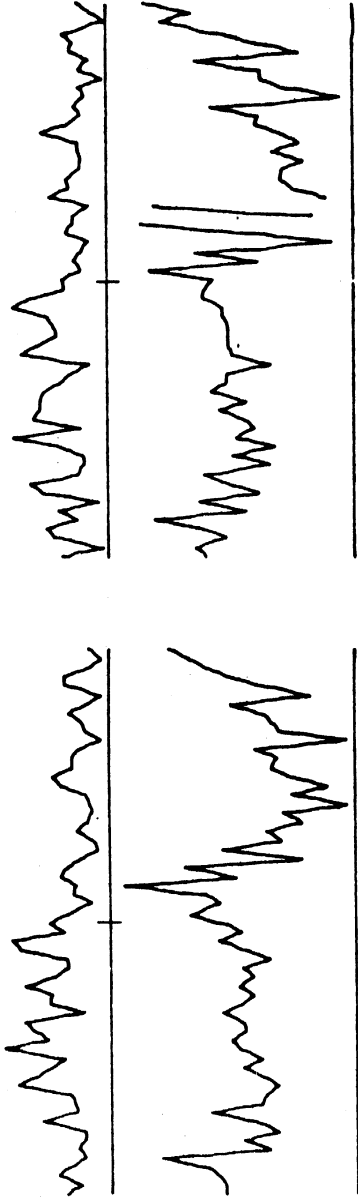
44-3137



44-3204



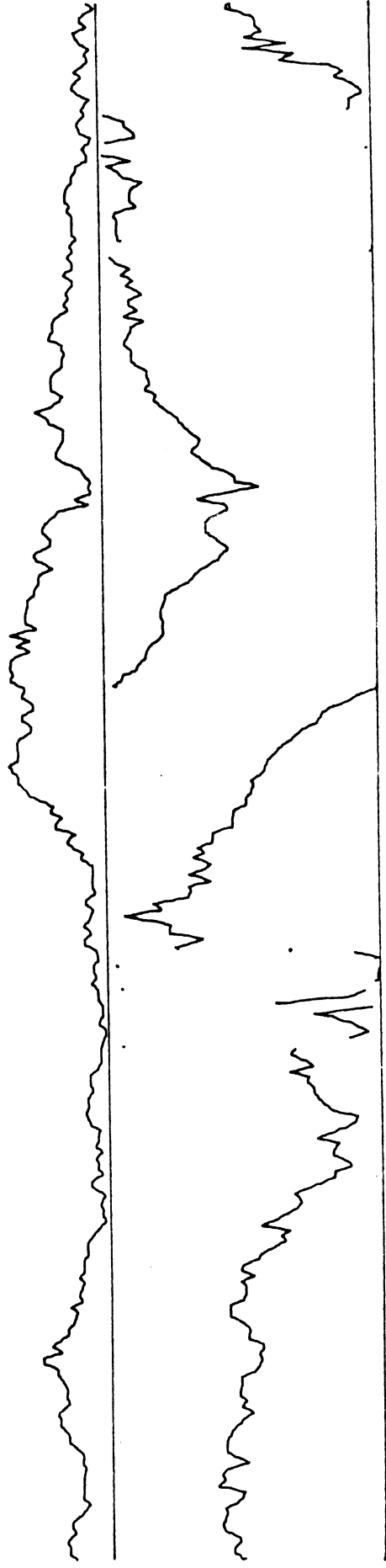
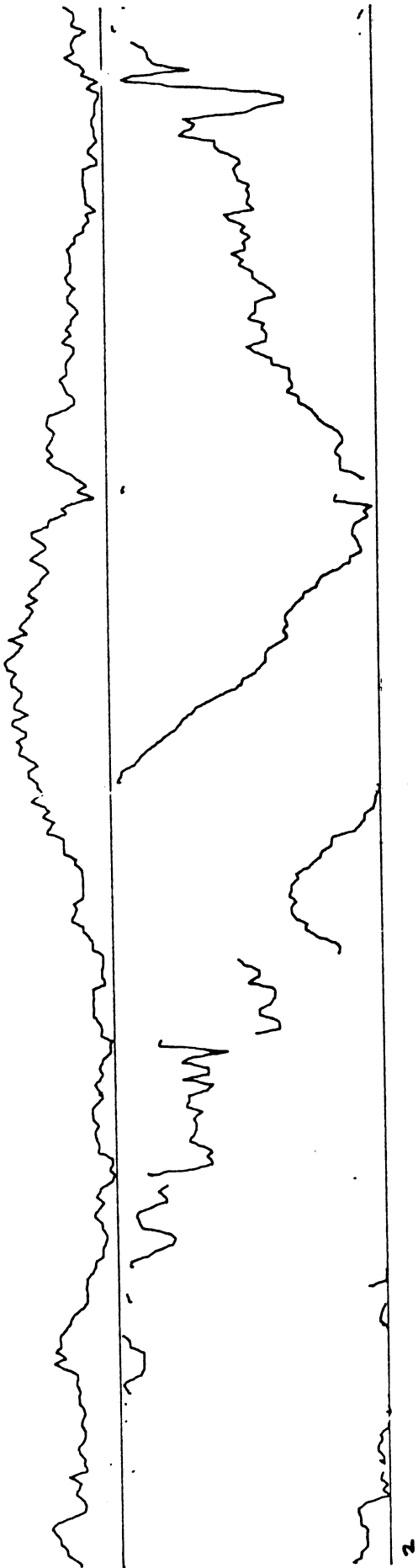
44-3250



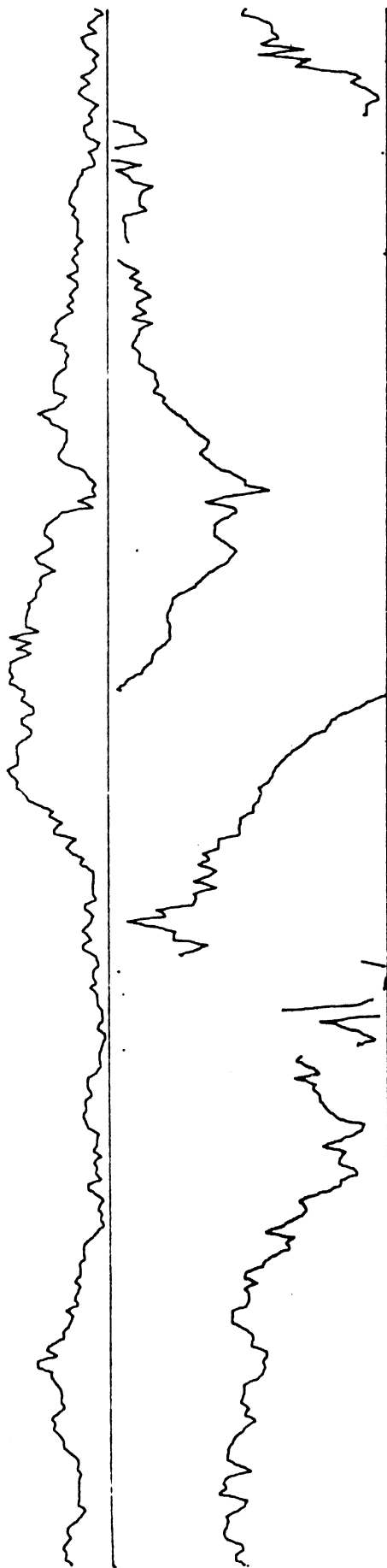
## APPENDIX B

### Constant Frequency Plots

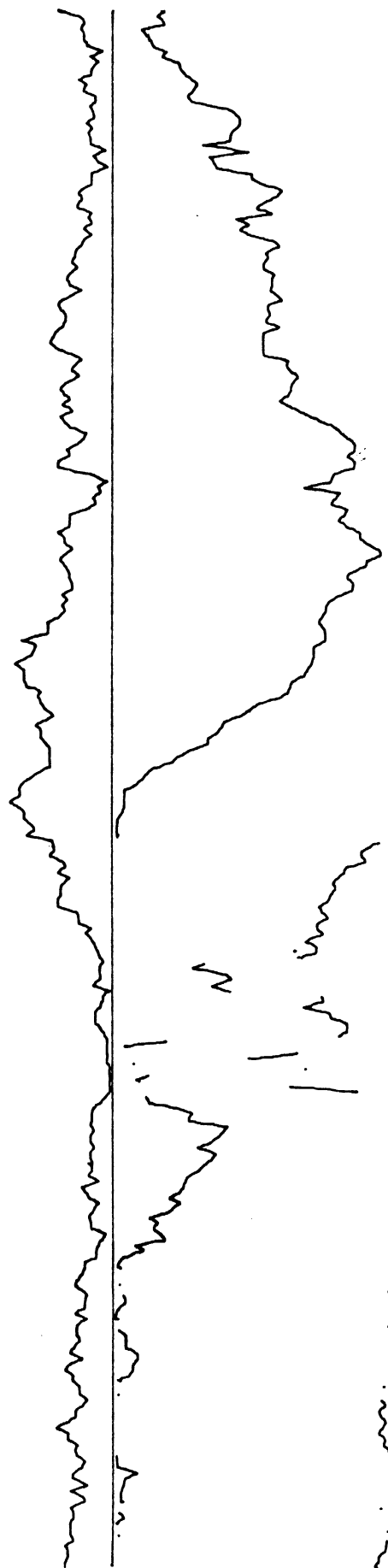
Section 4.3.2 explains how to interpret the constant frequency plots that follow.



3

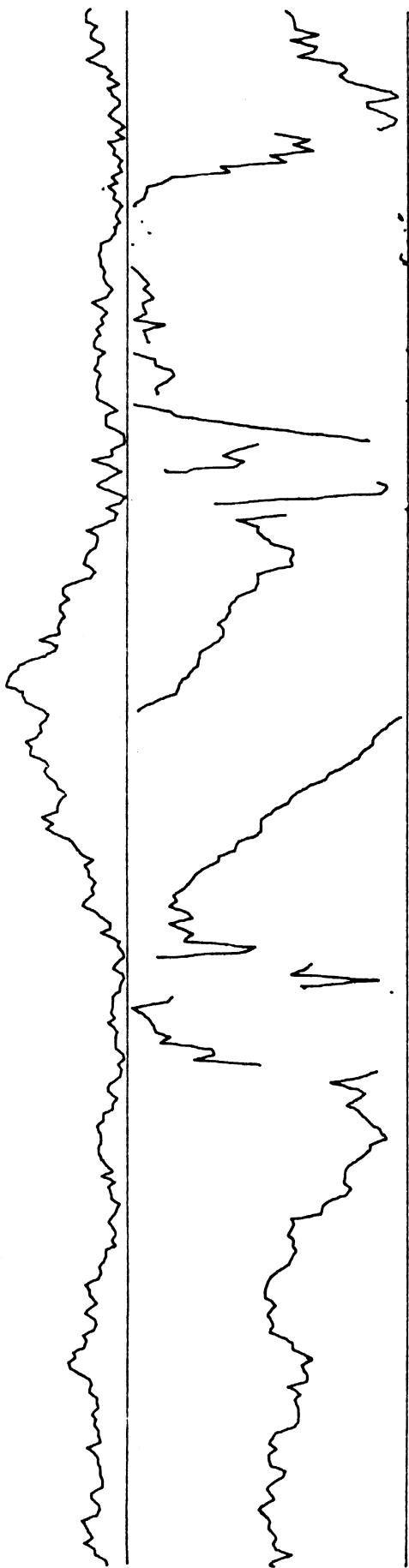


4

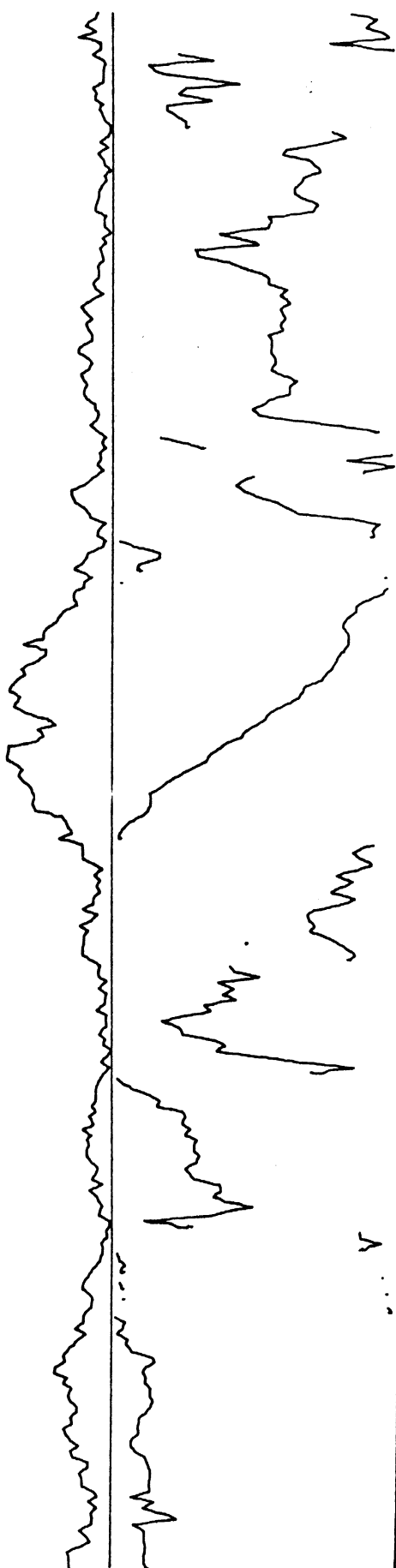




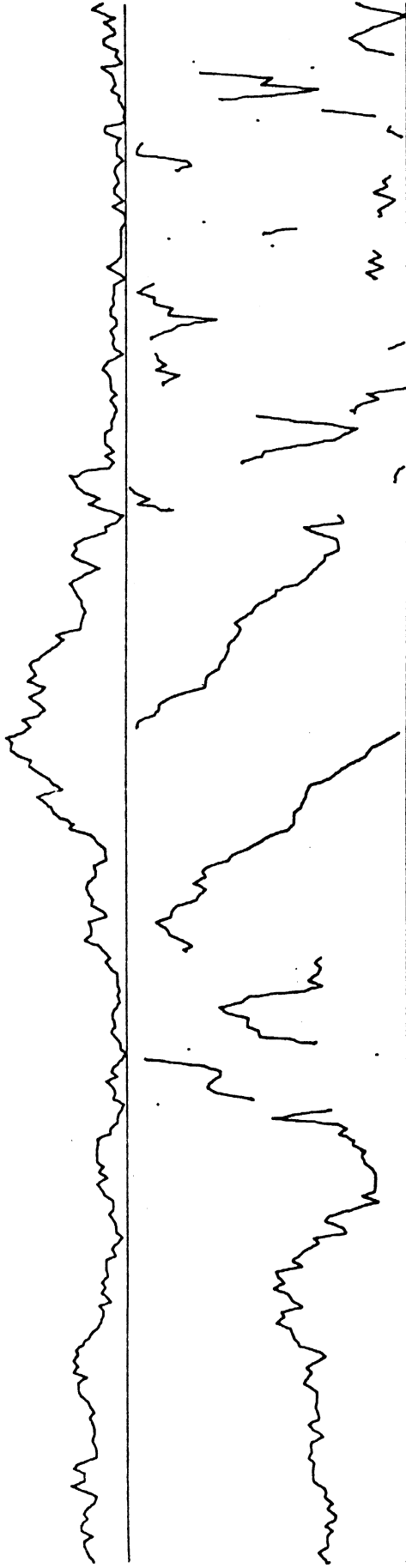
5



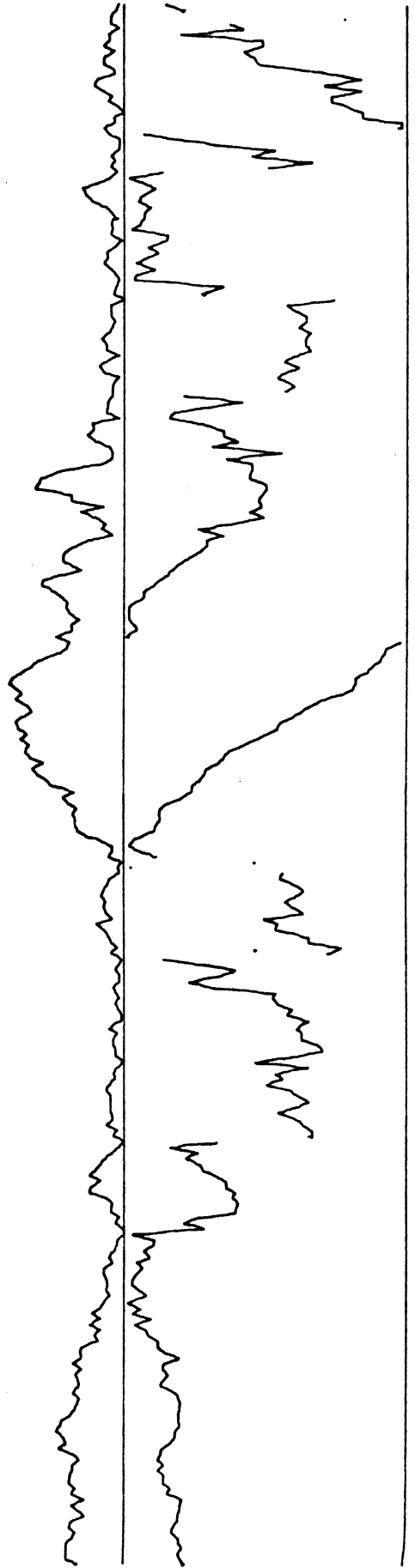
6



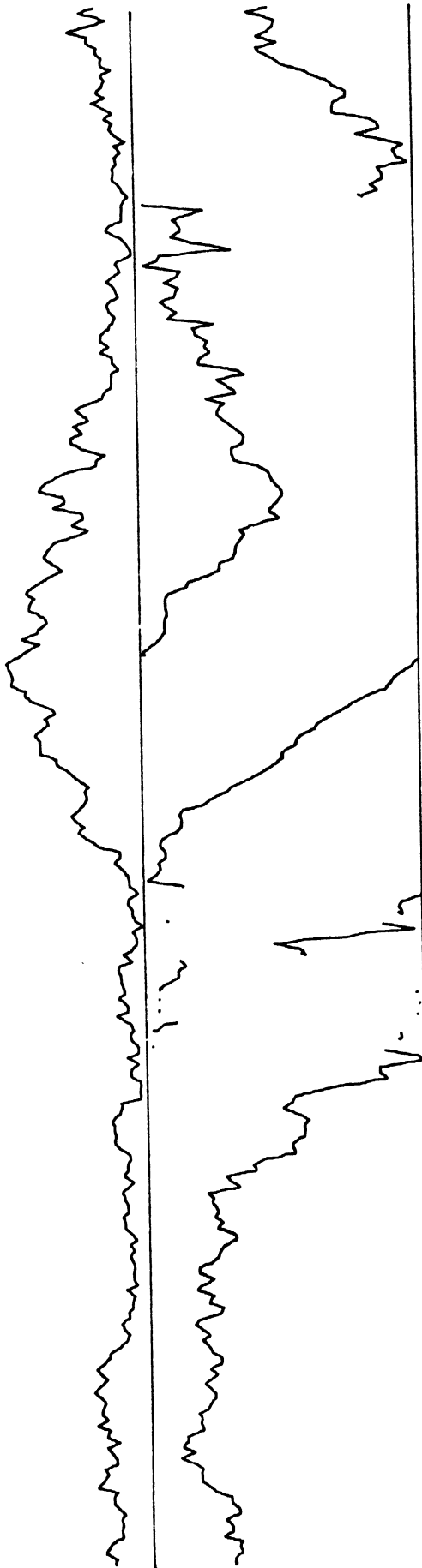
7



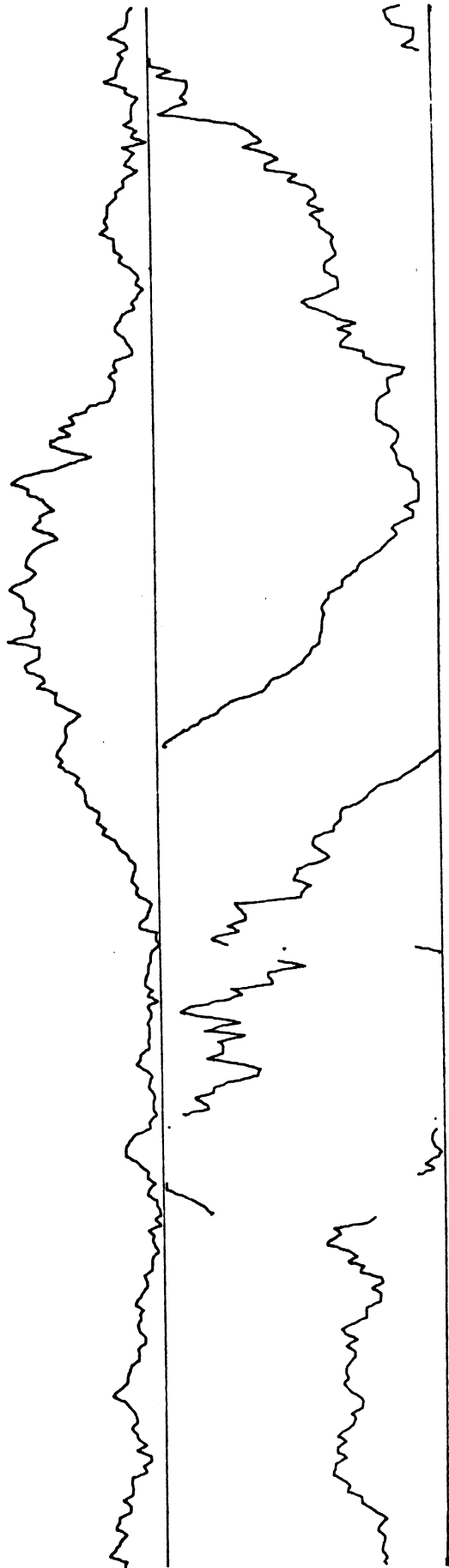
8

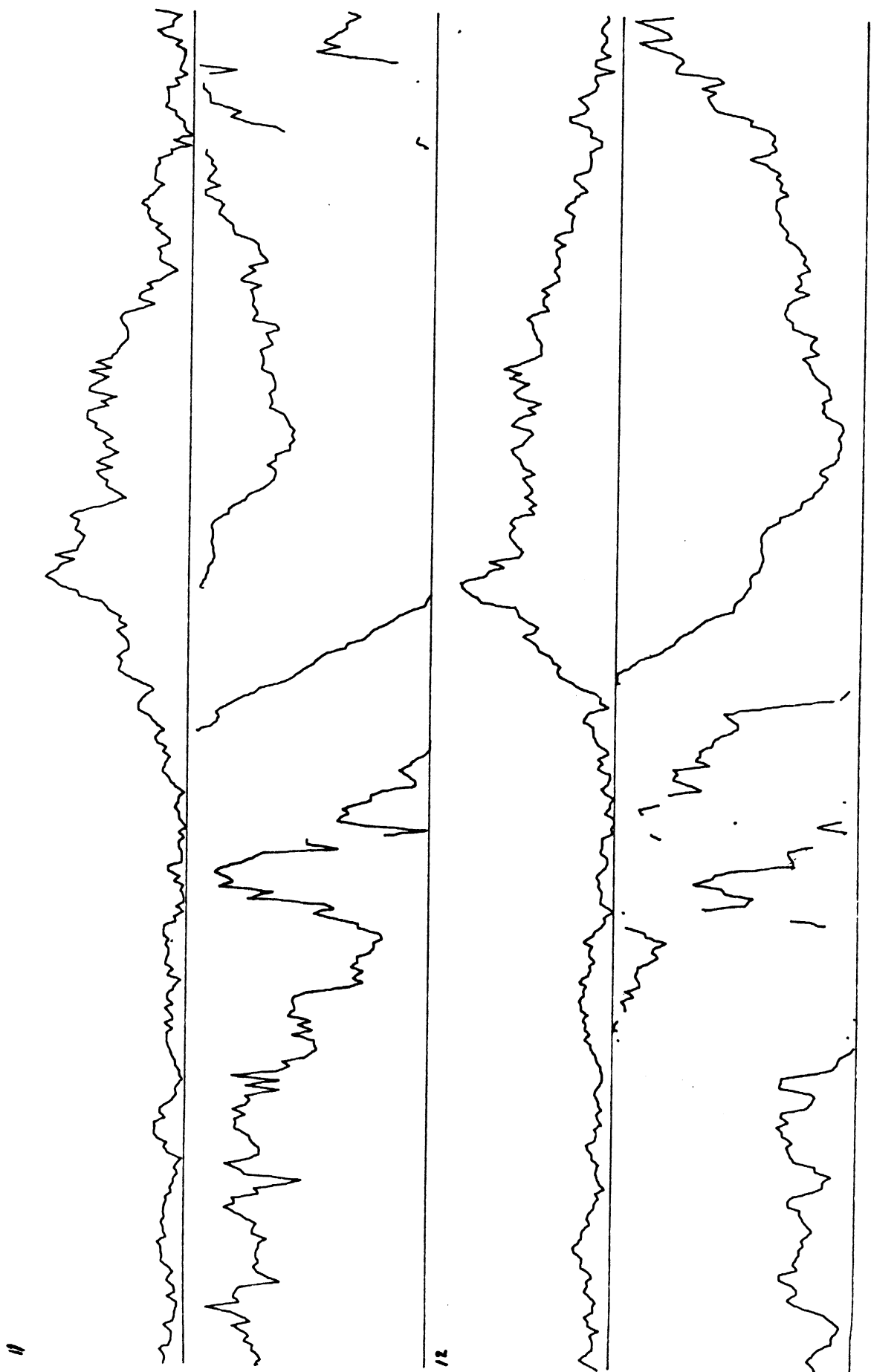


9

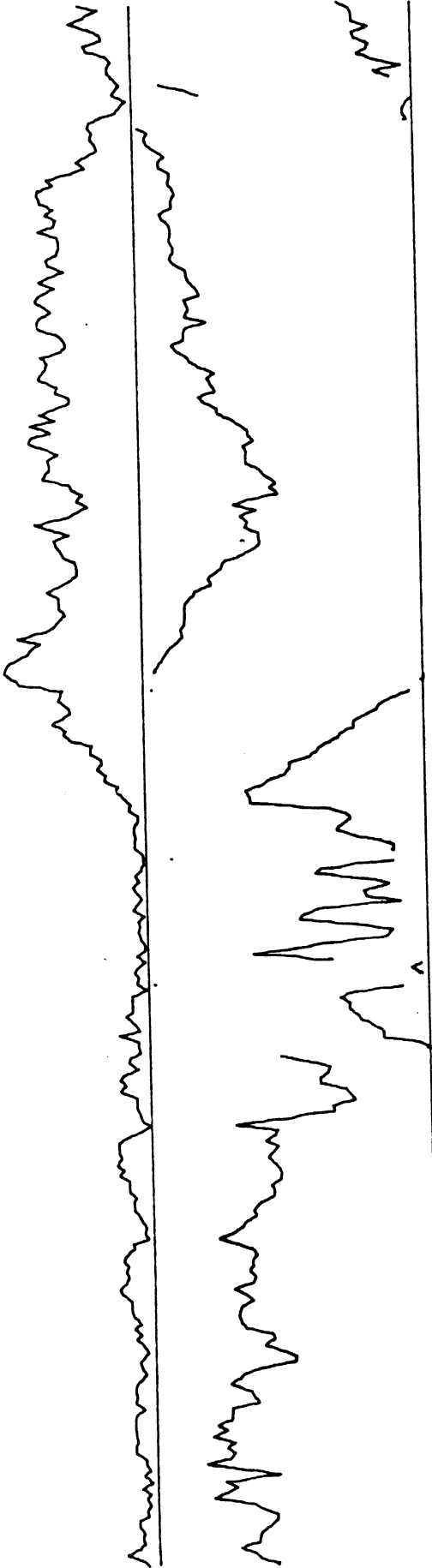


10

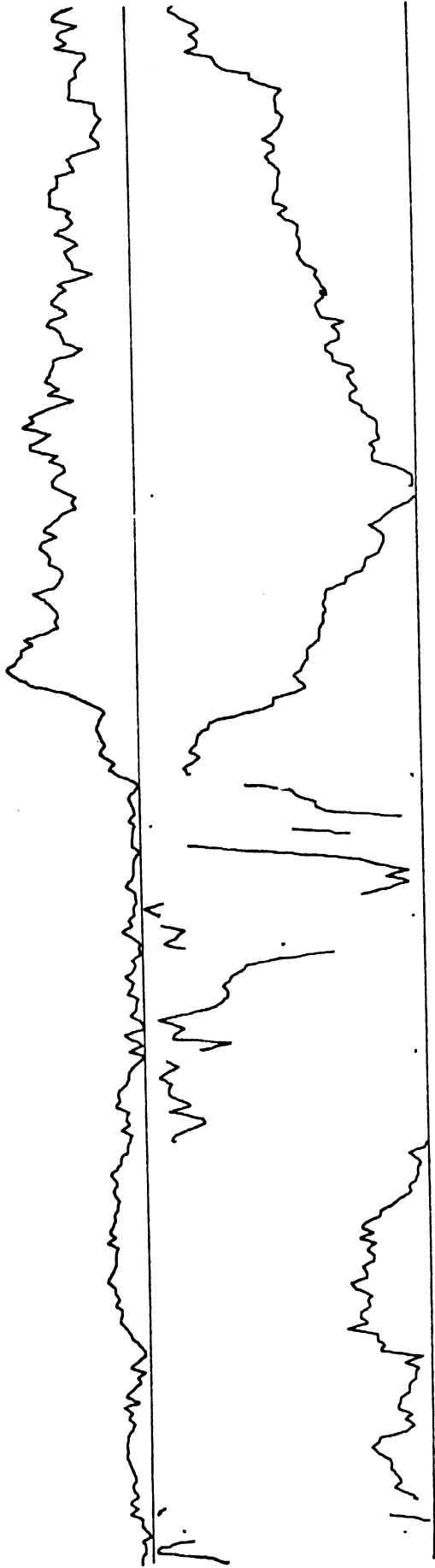




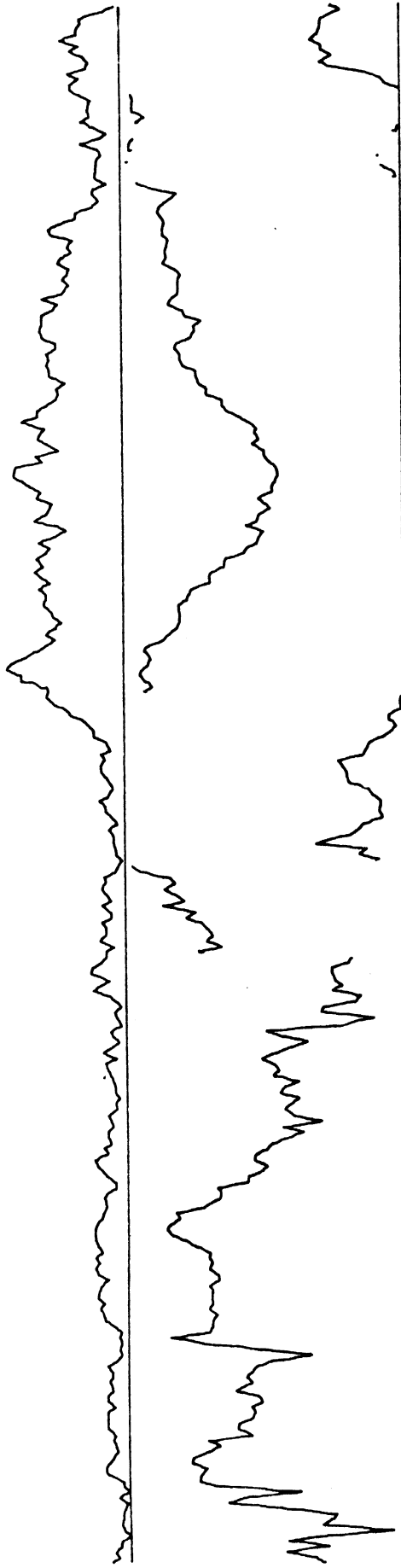
13



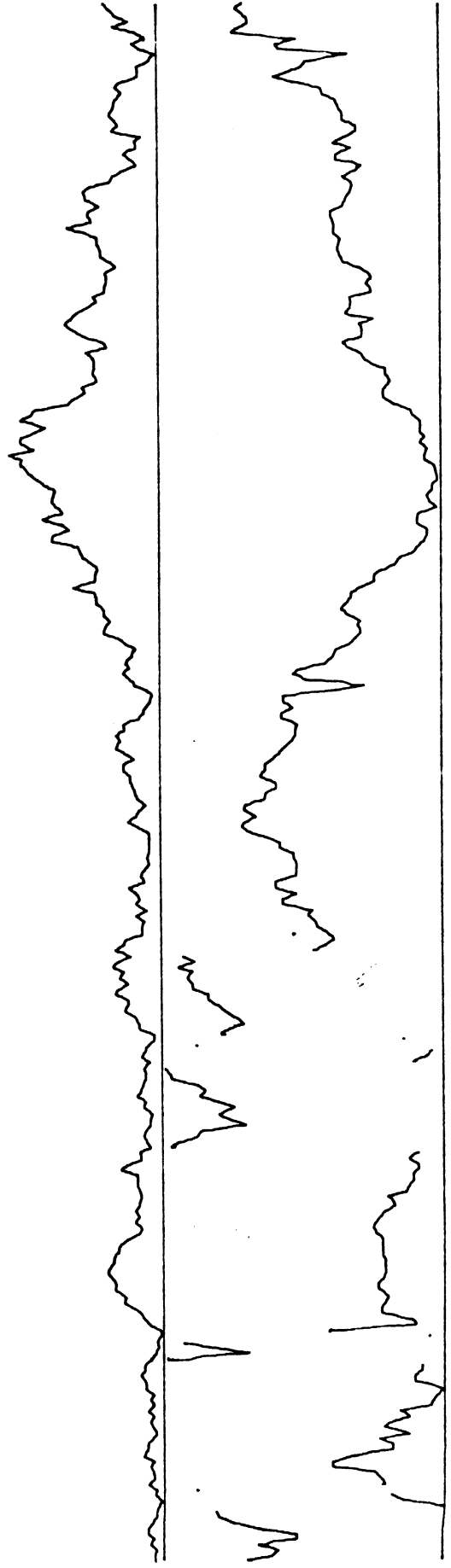
14



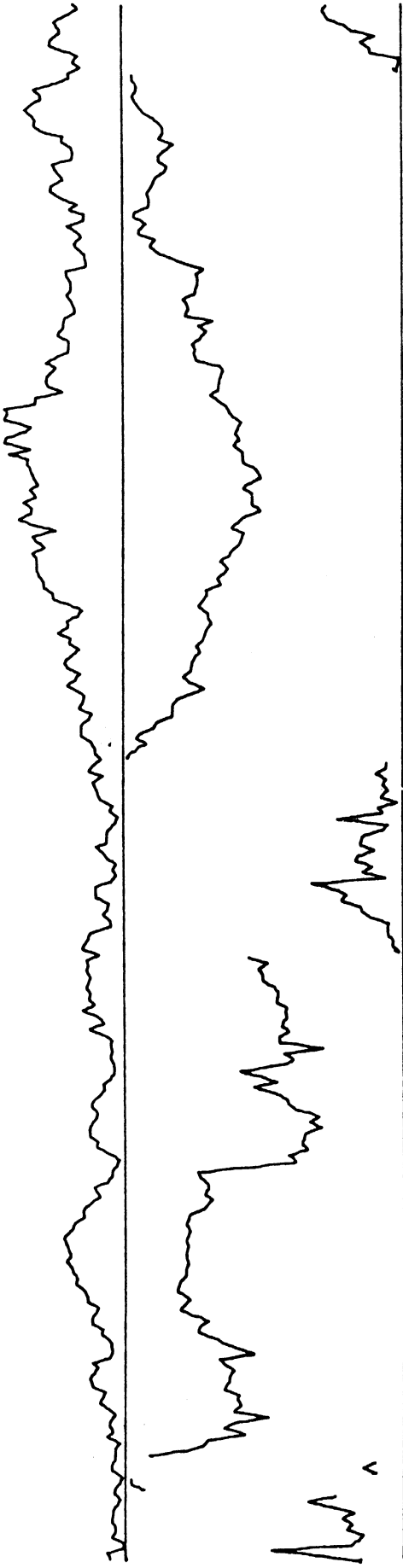
15



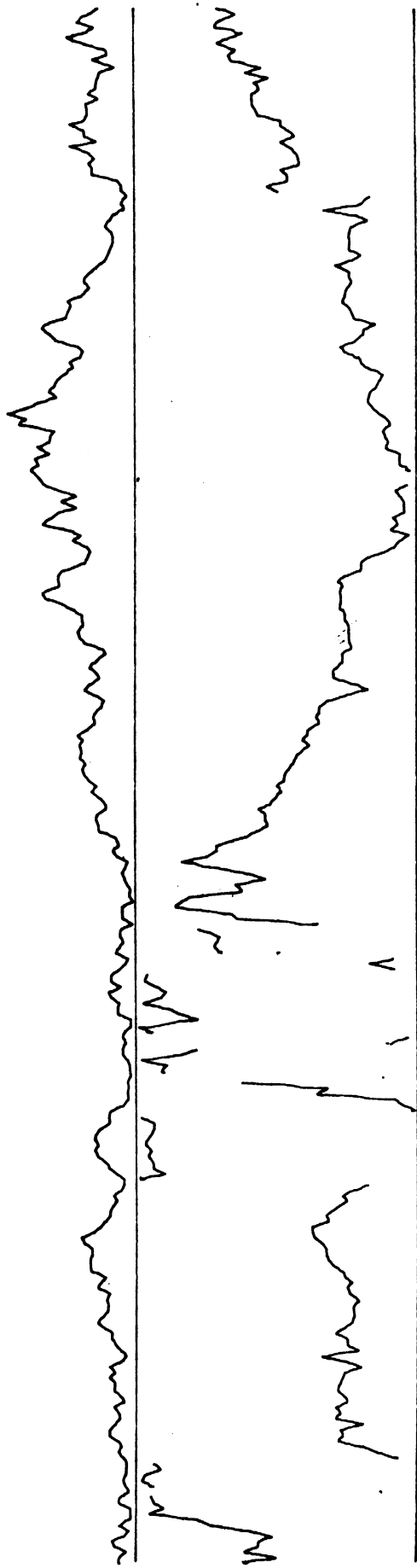
16



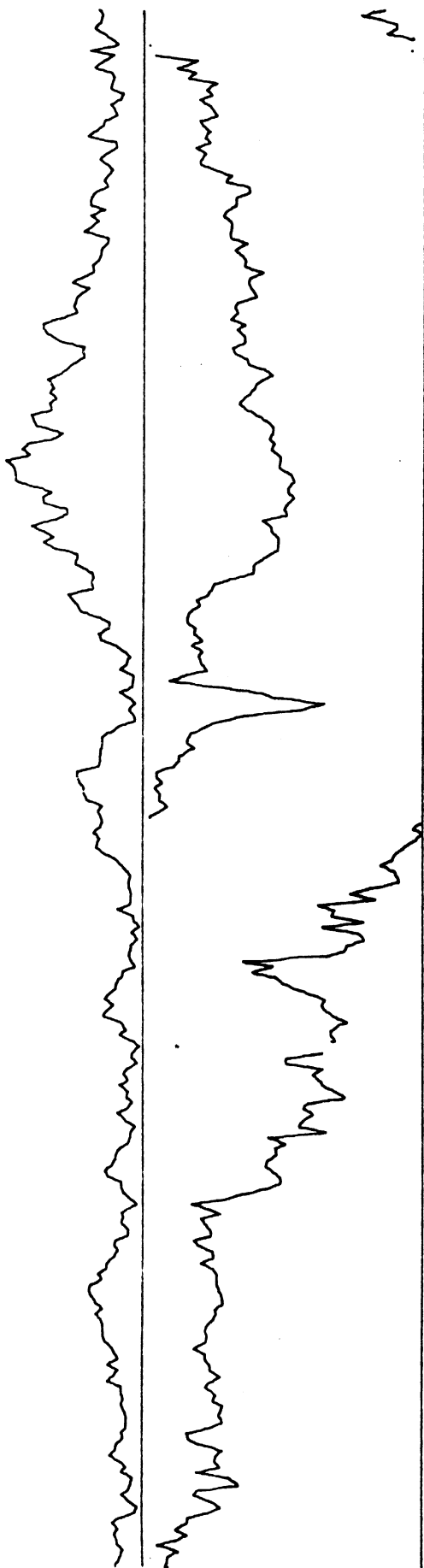
17



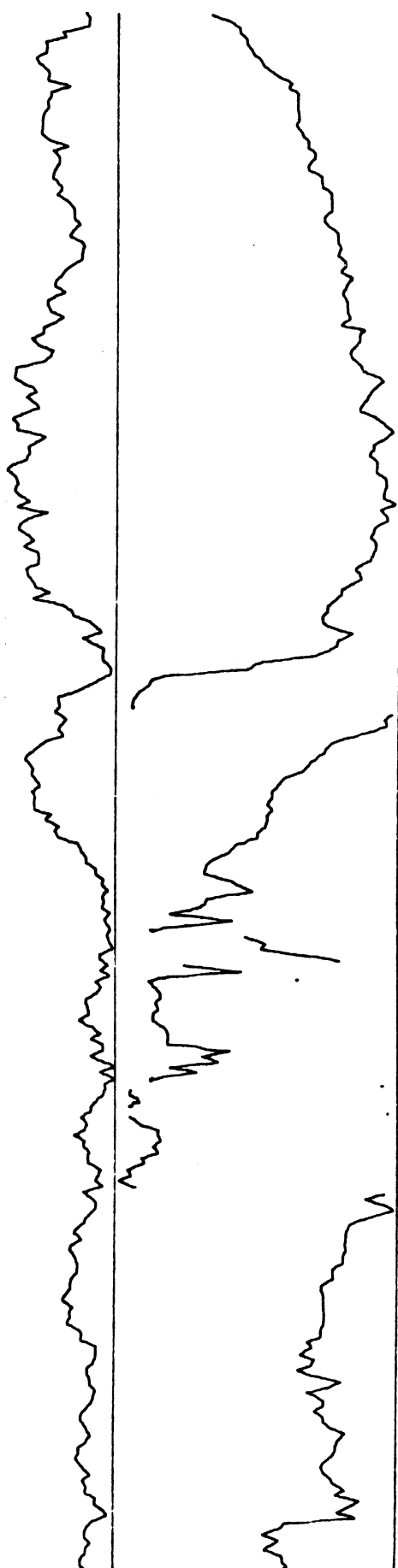
18



19

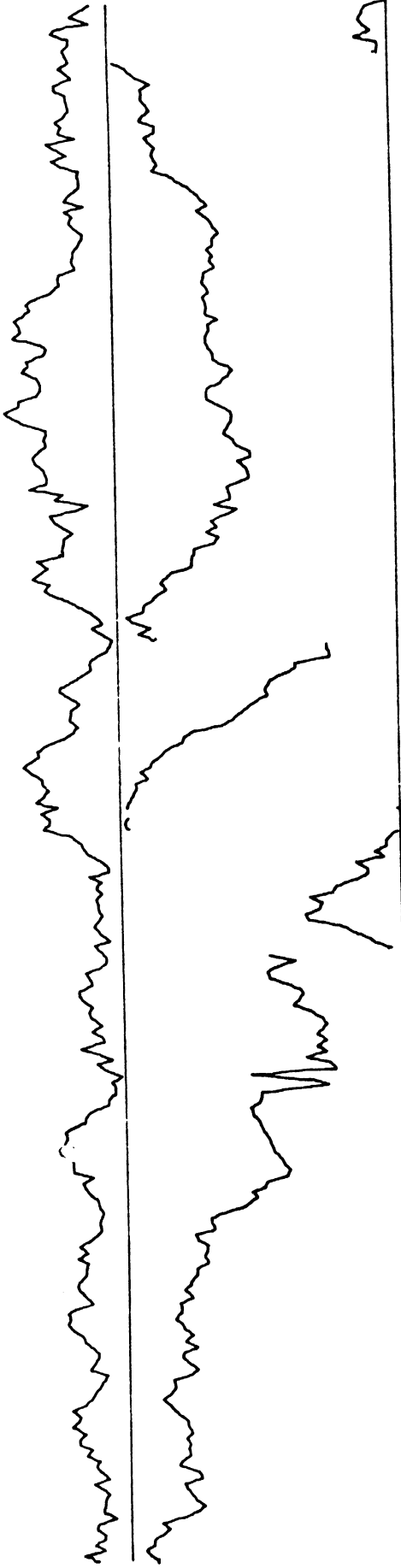


20



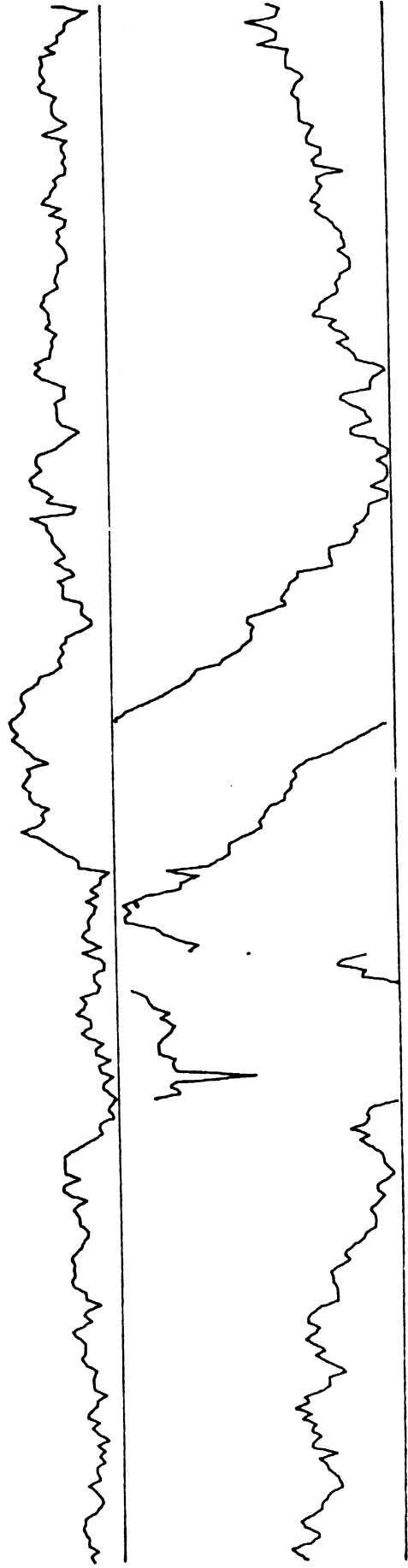


21

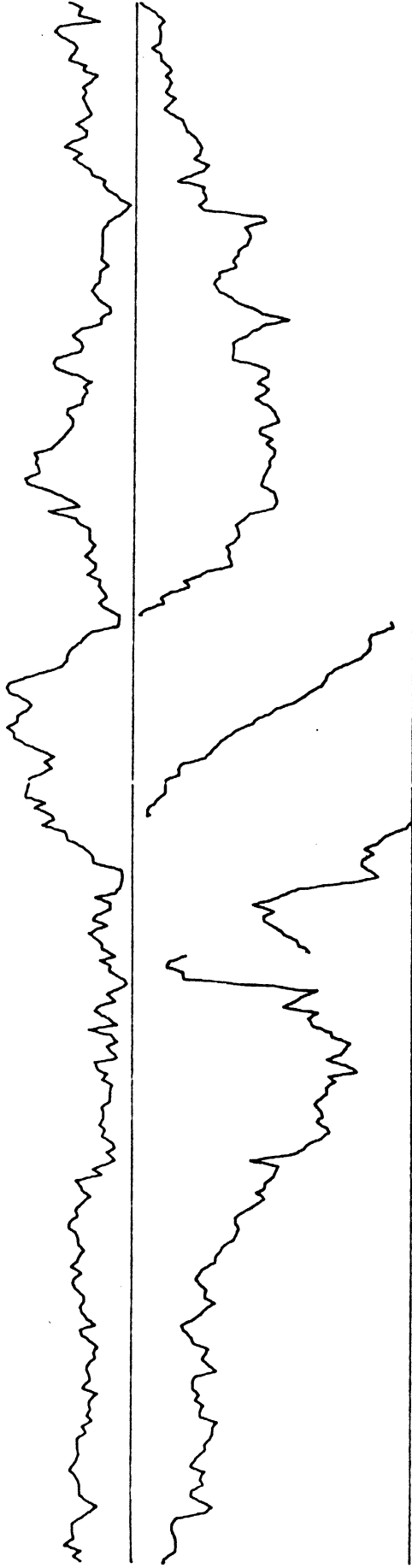


89

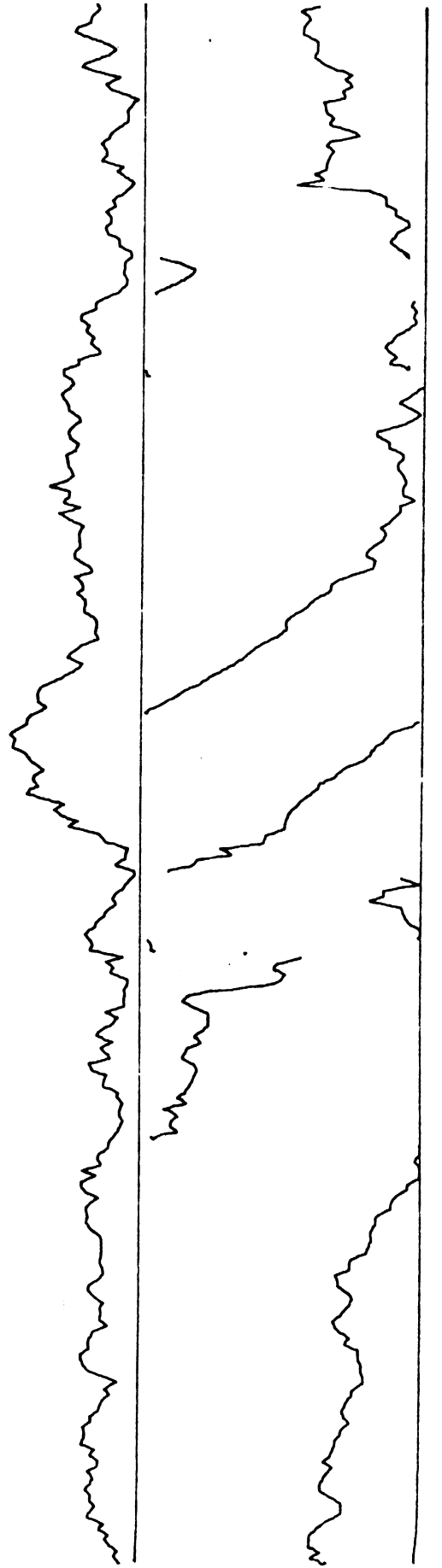
22



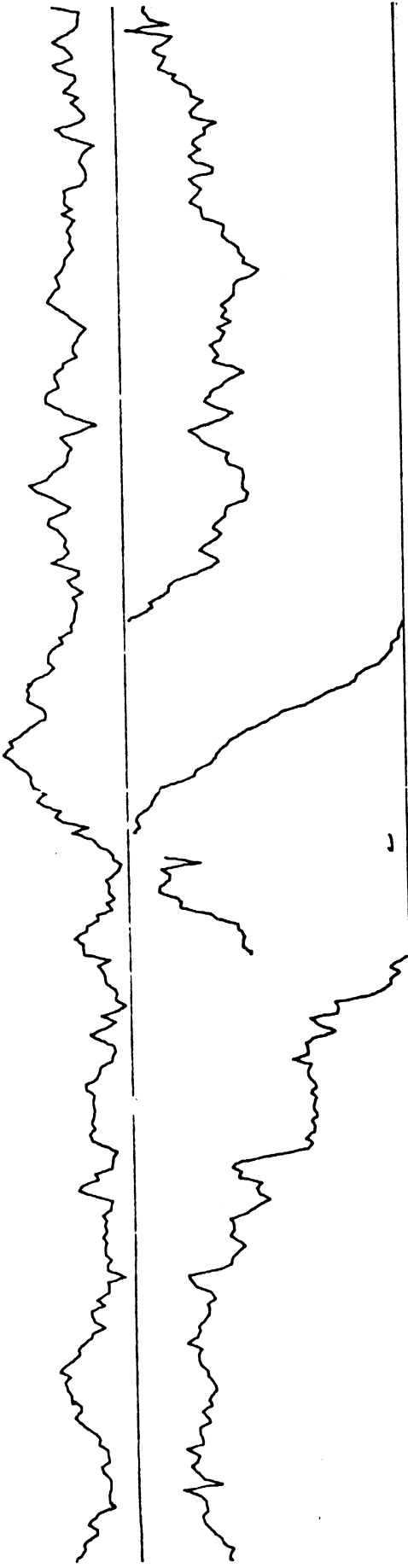
23



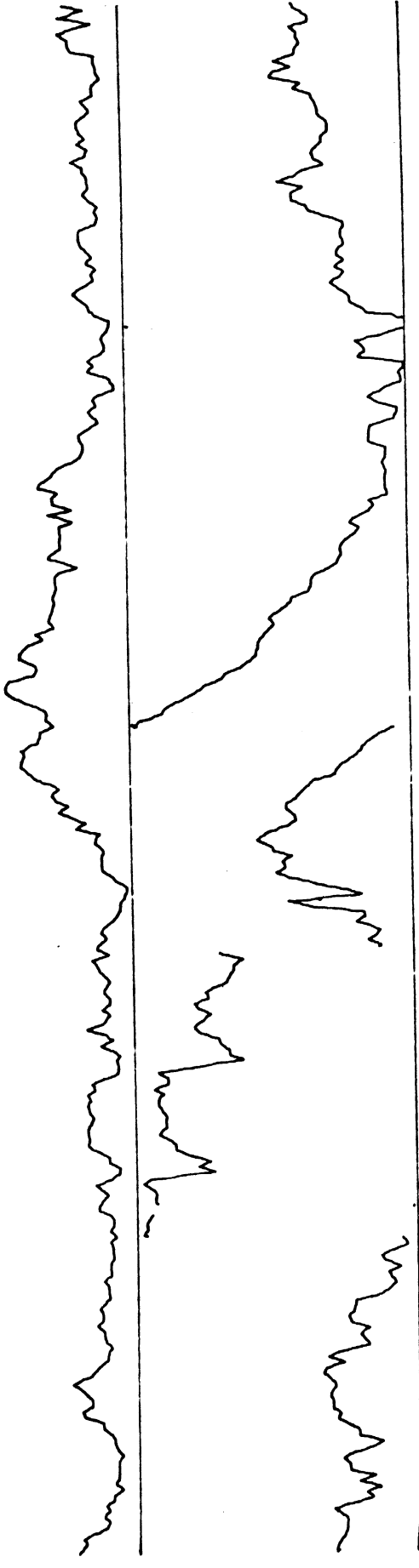
24



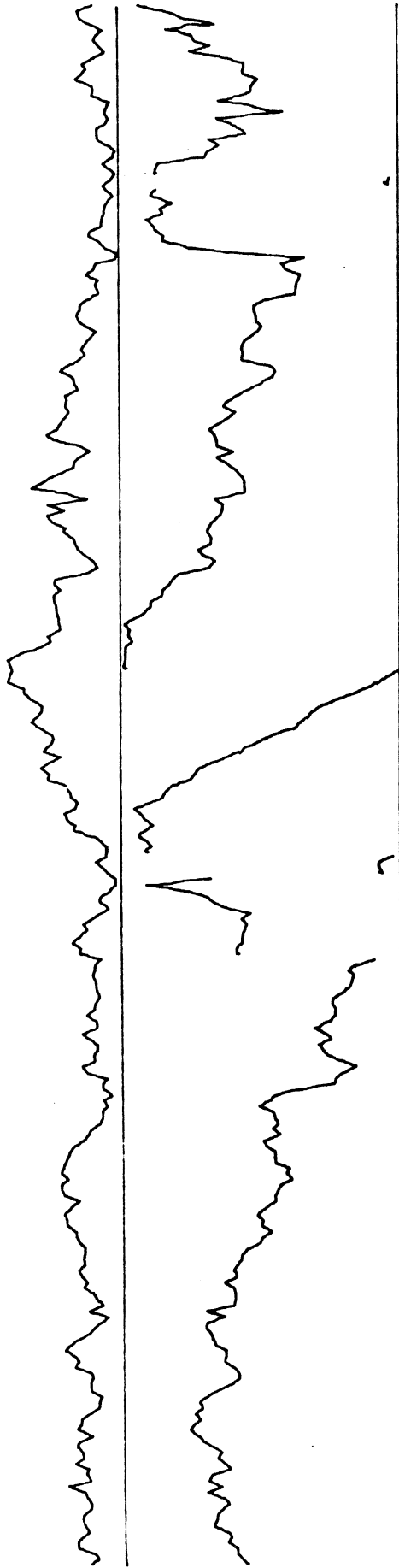
51



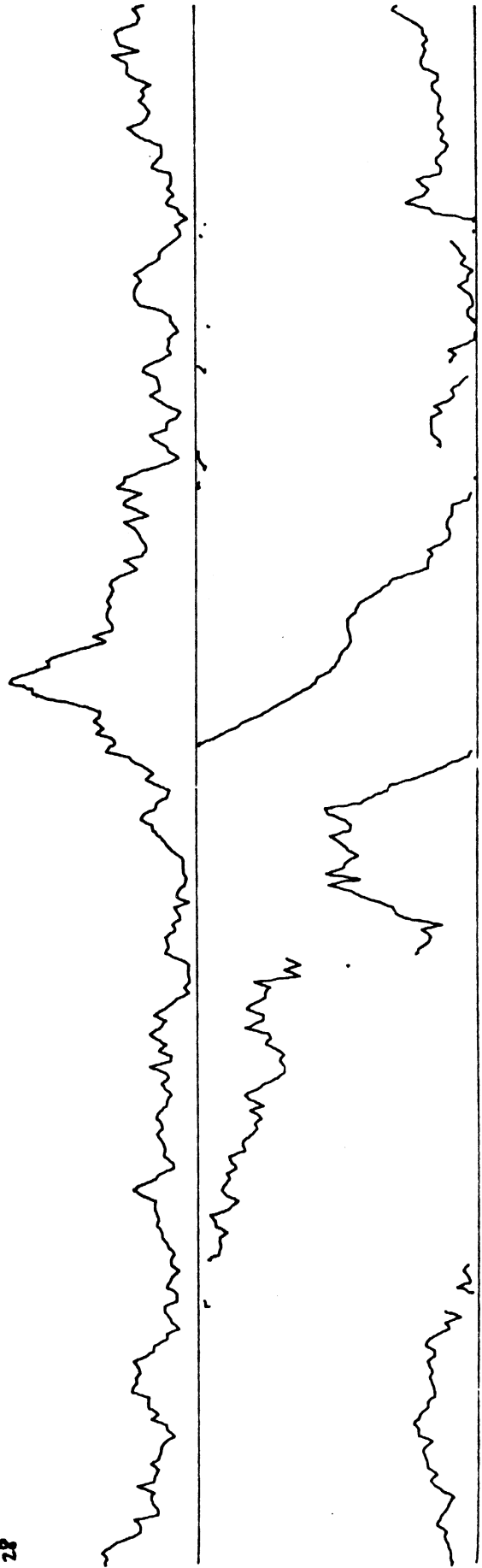
52

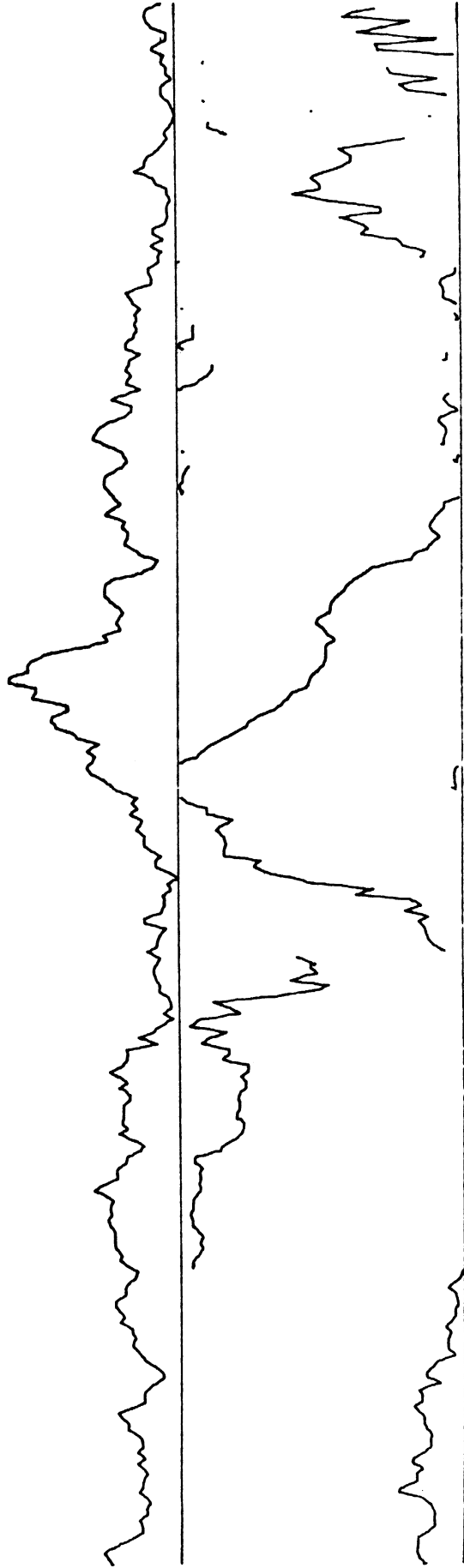
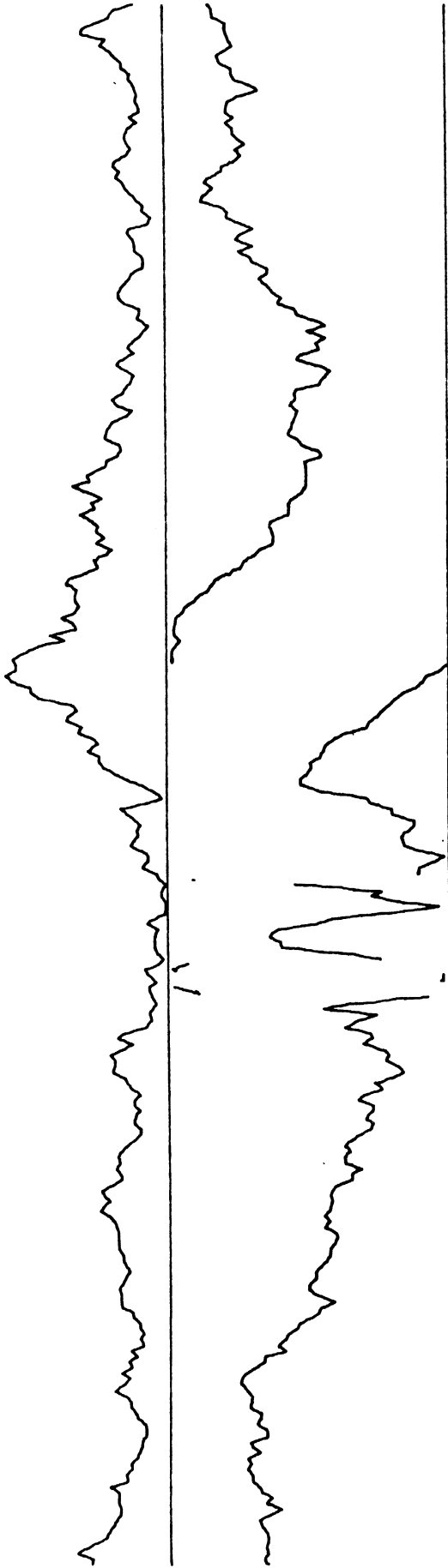


27

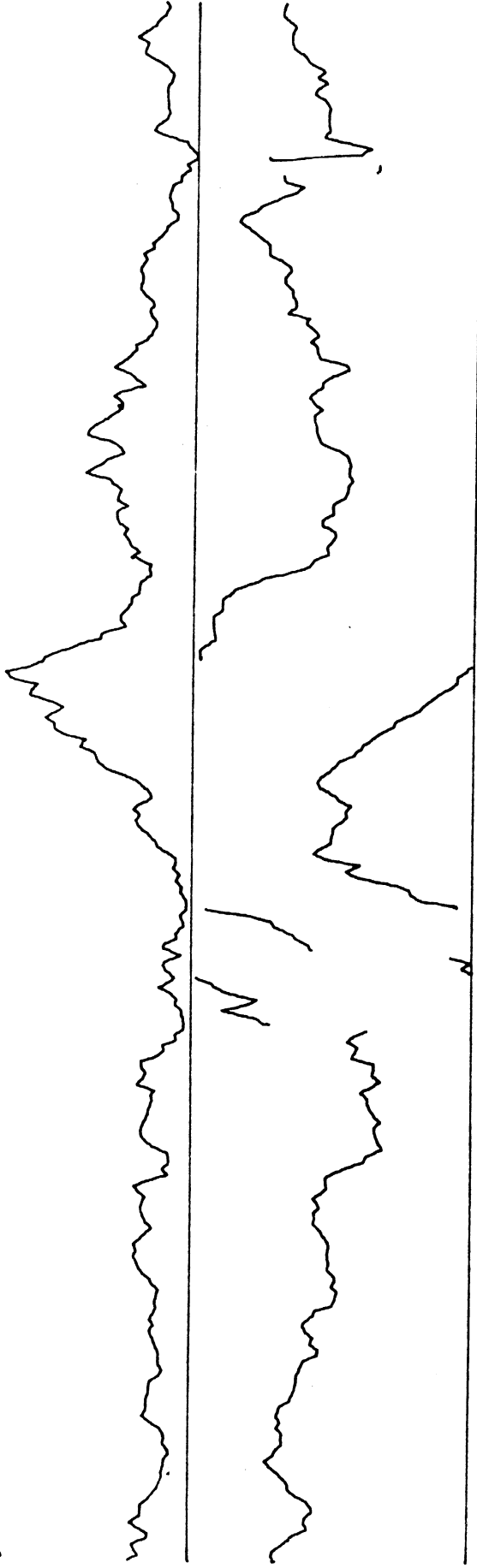


28

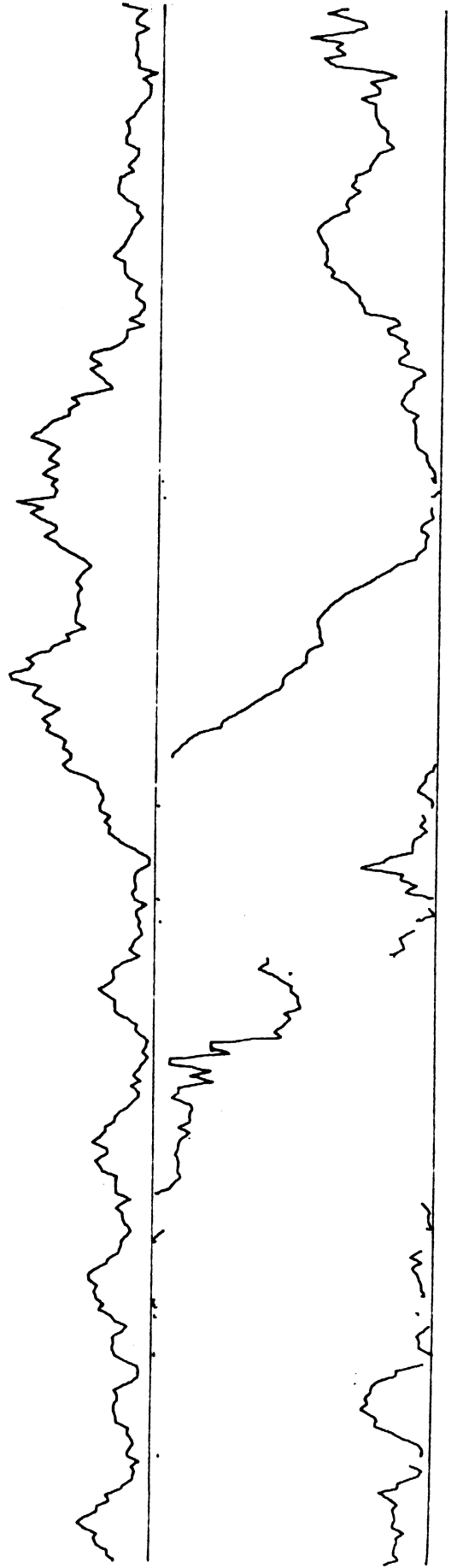




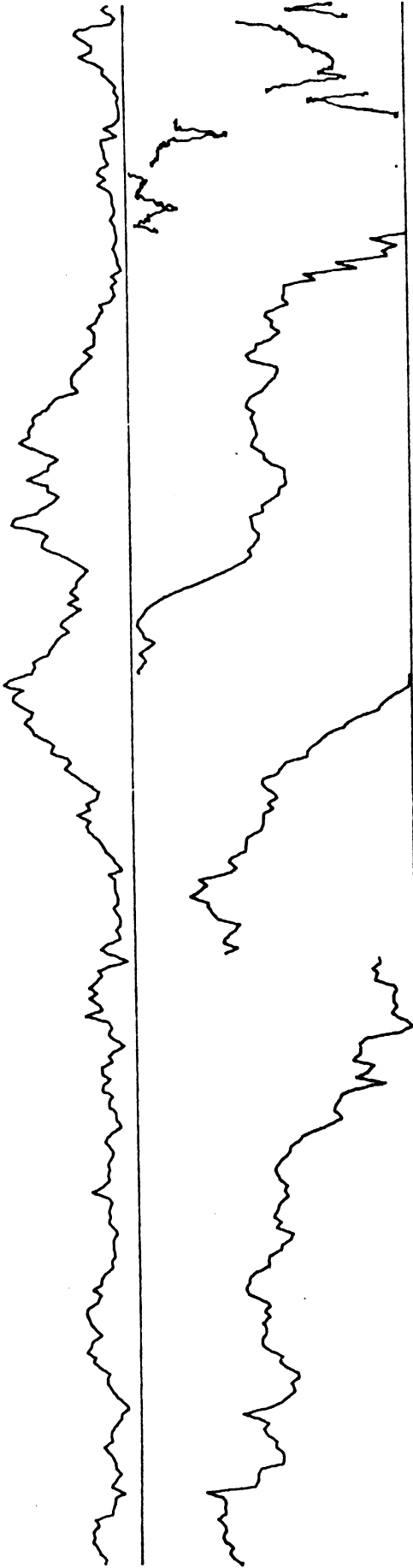
31



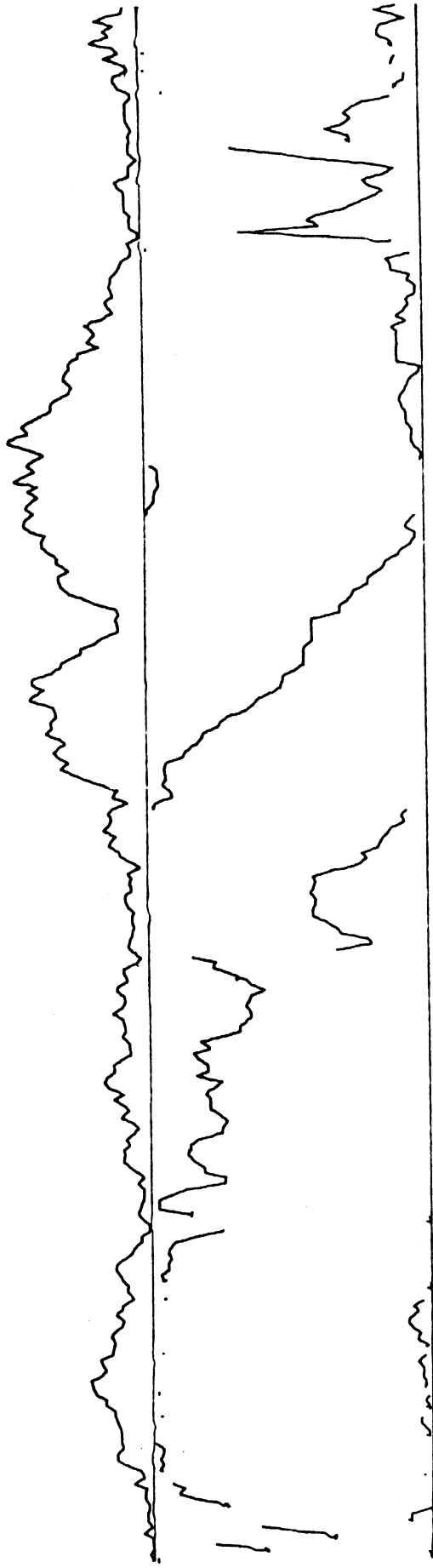
32



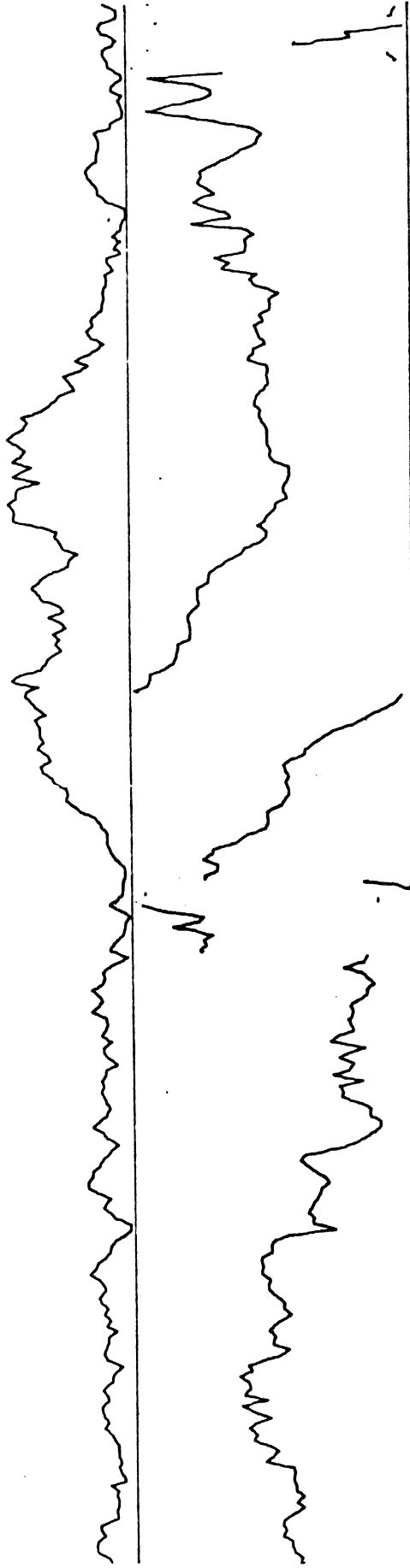
33



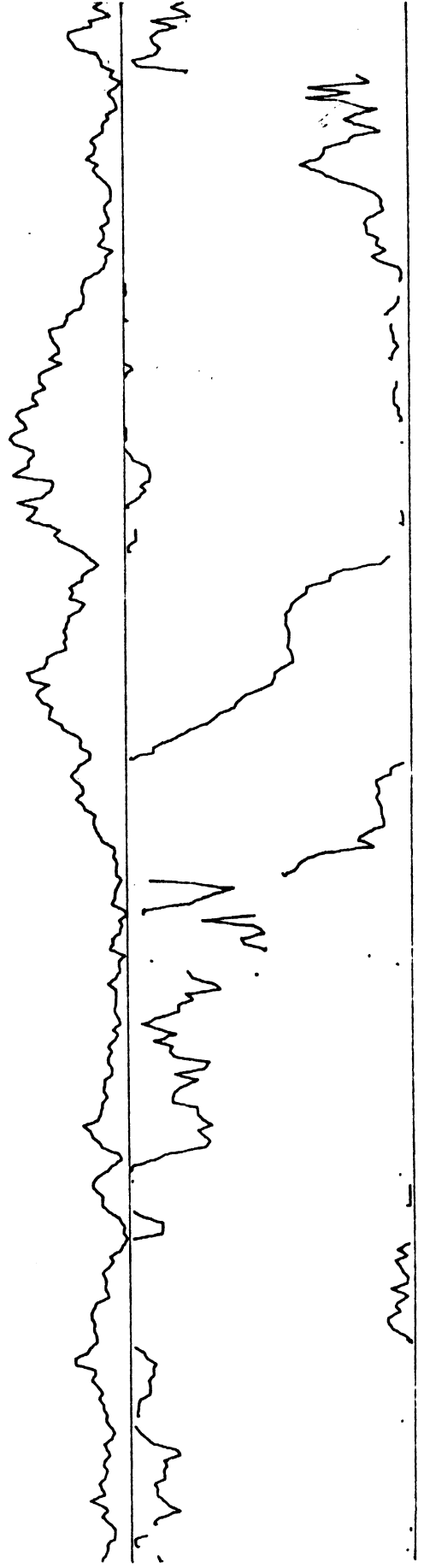
34



35

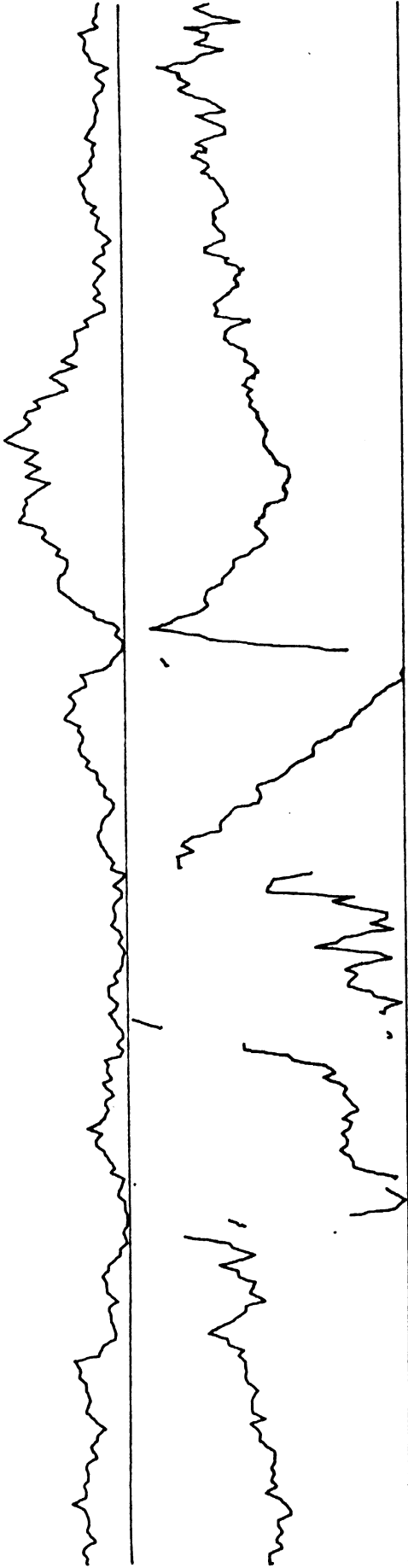


36

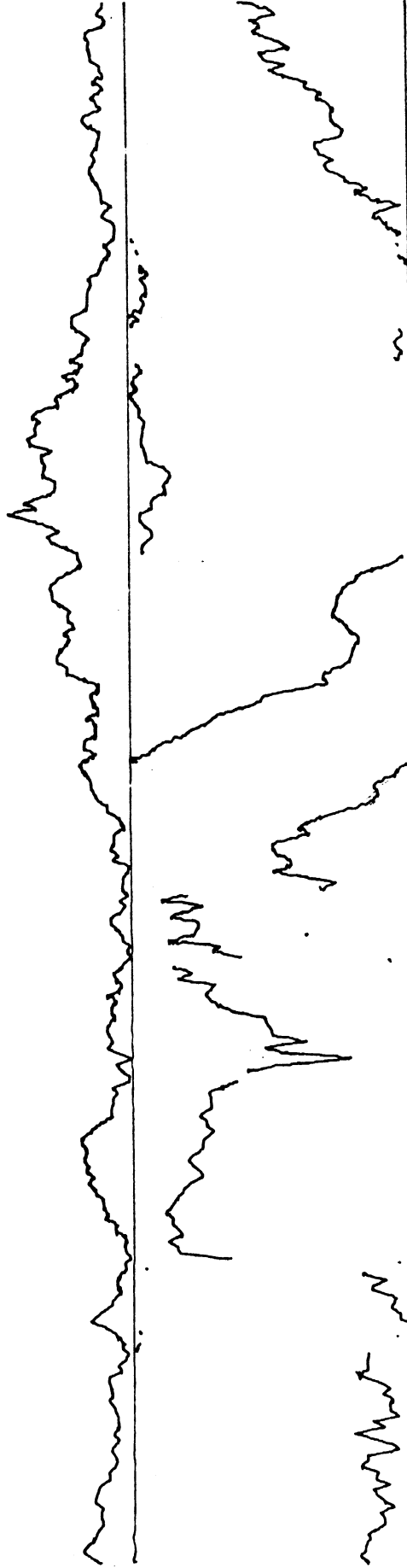




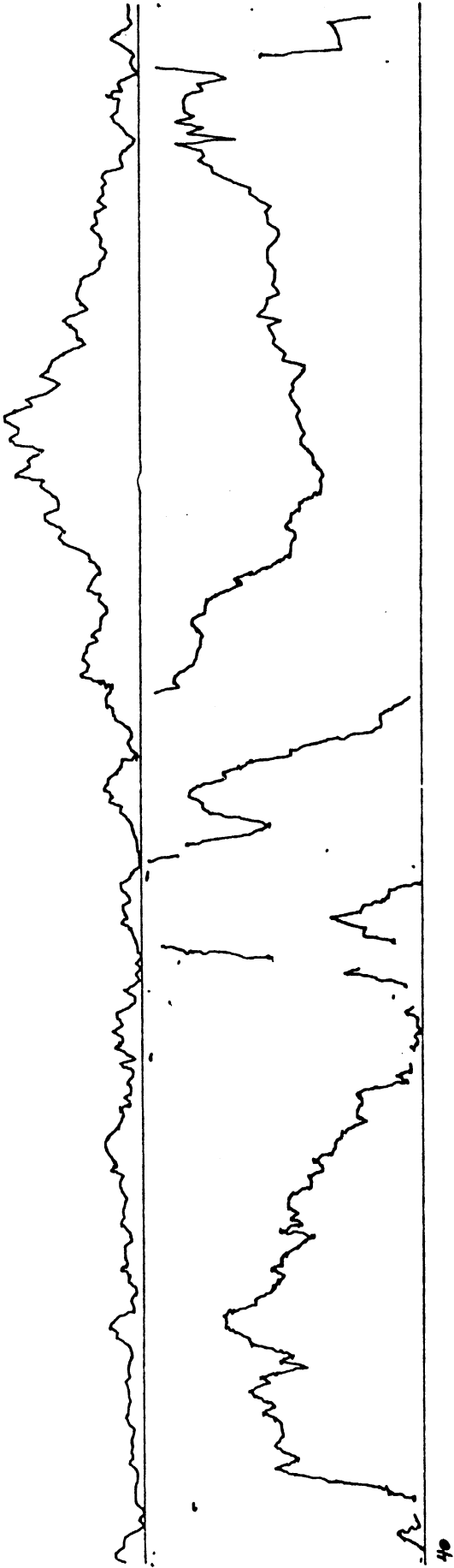
57



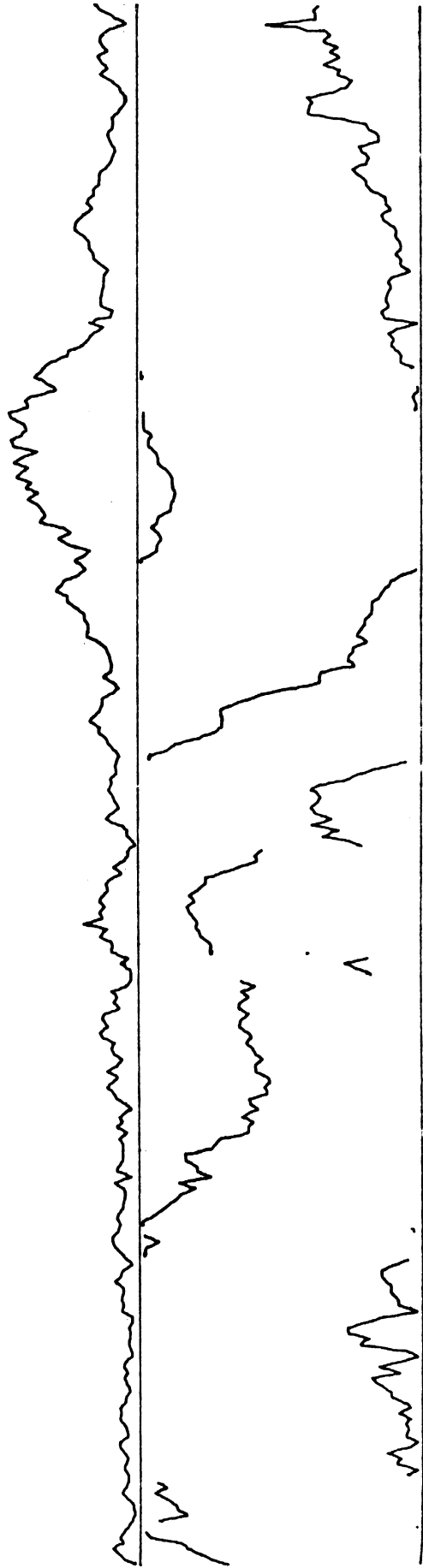
58



55



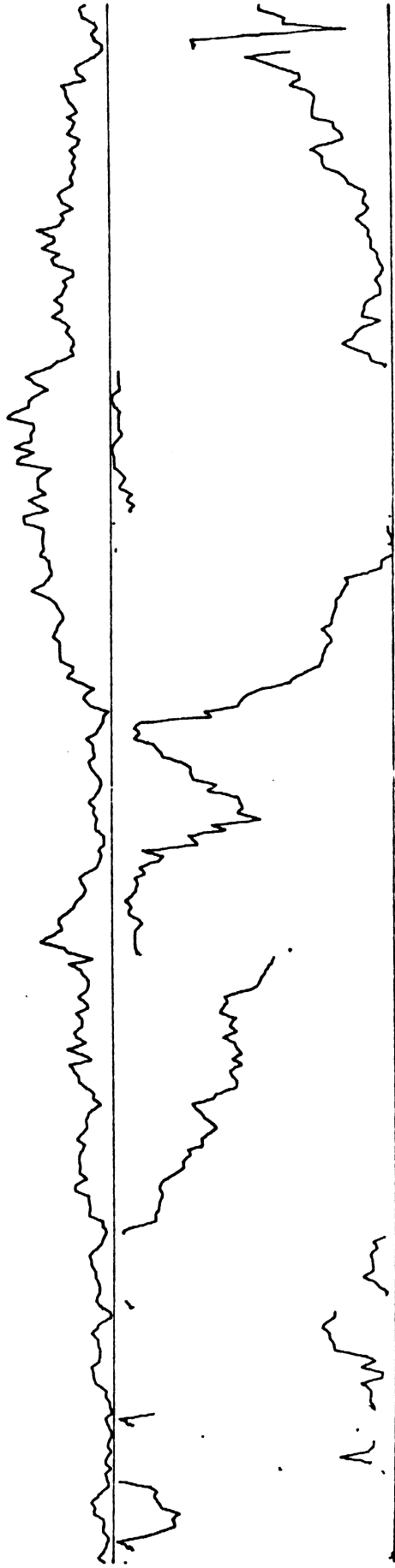
56



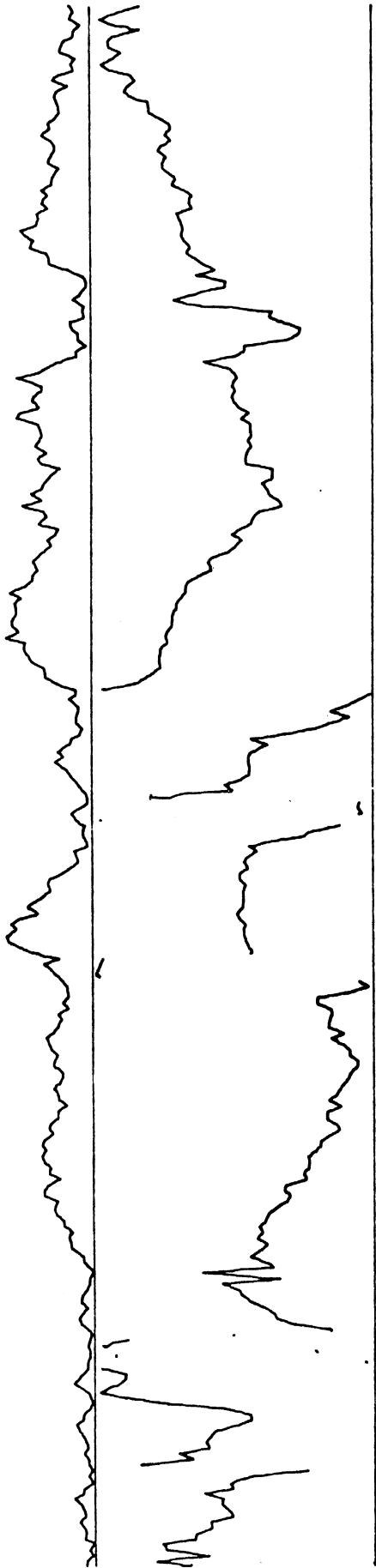
41



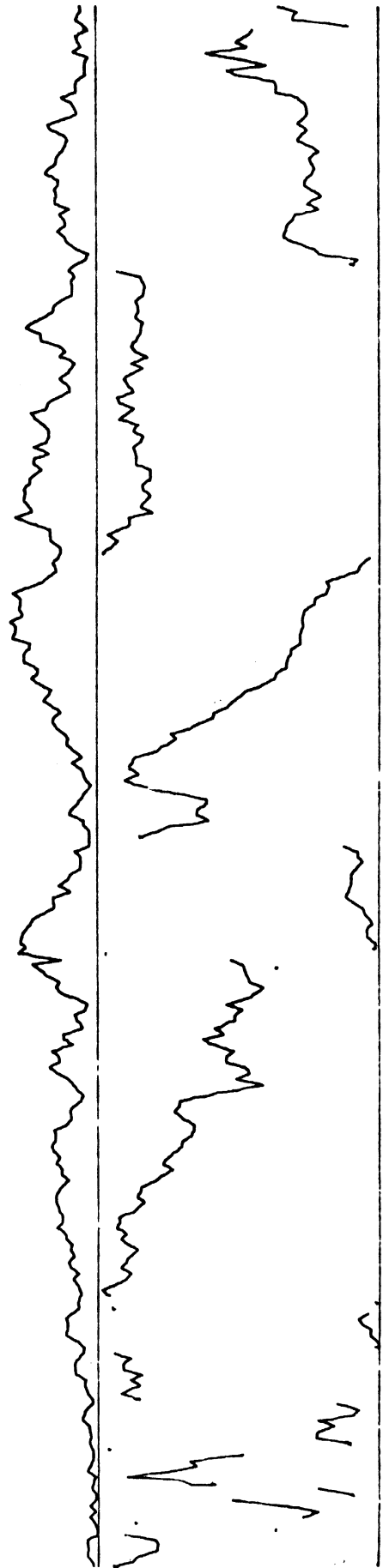
42

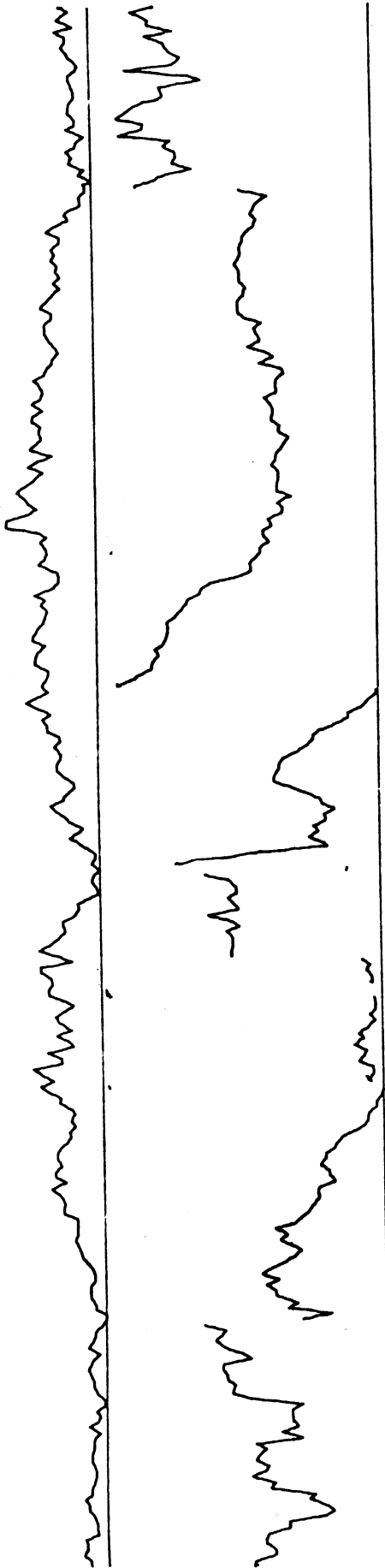


43

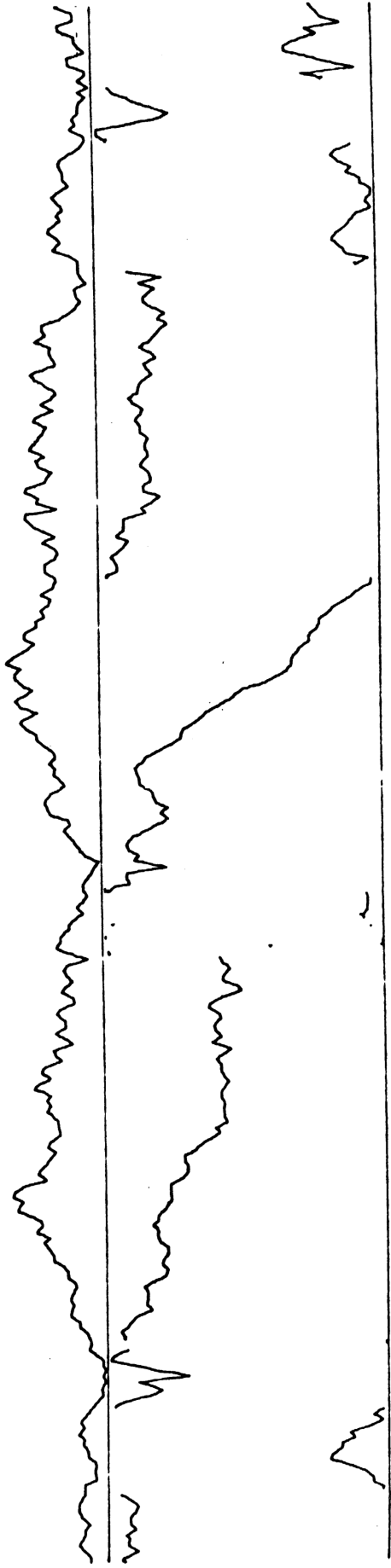


44





54

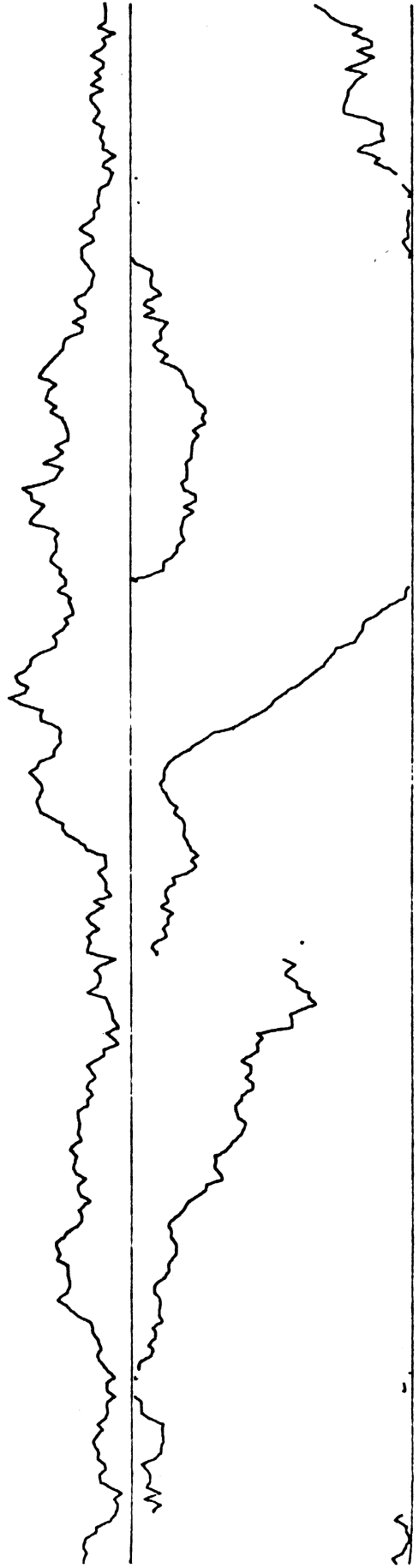


46

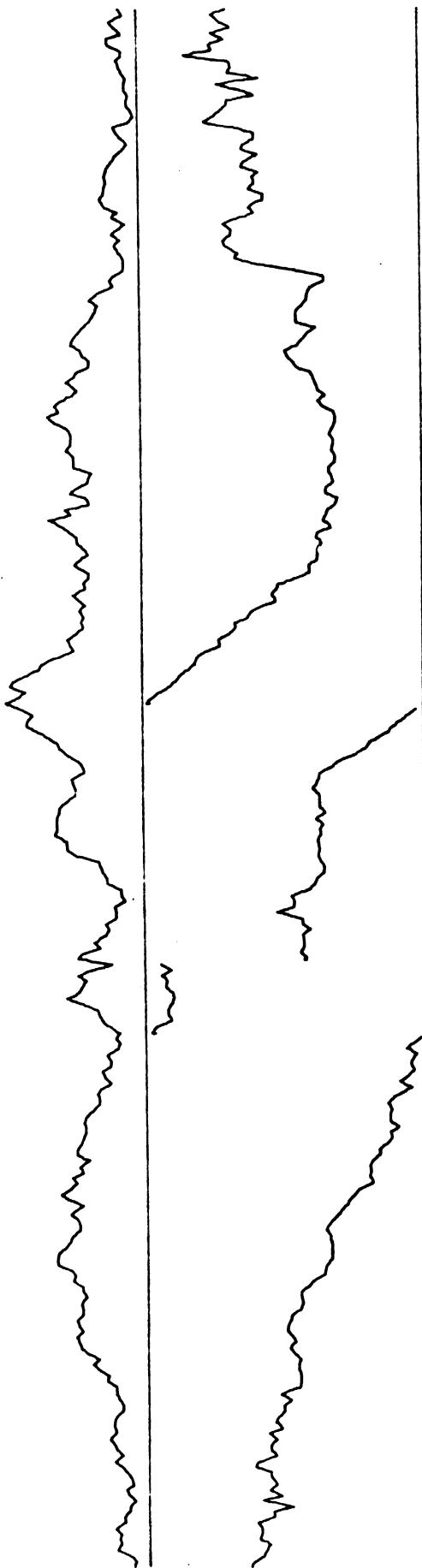
47



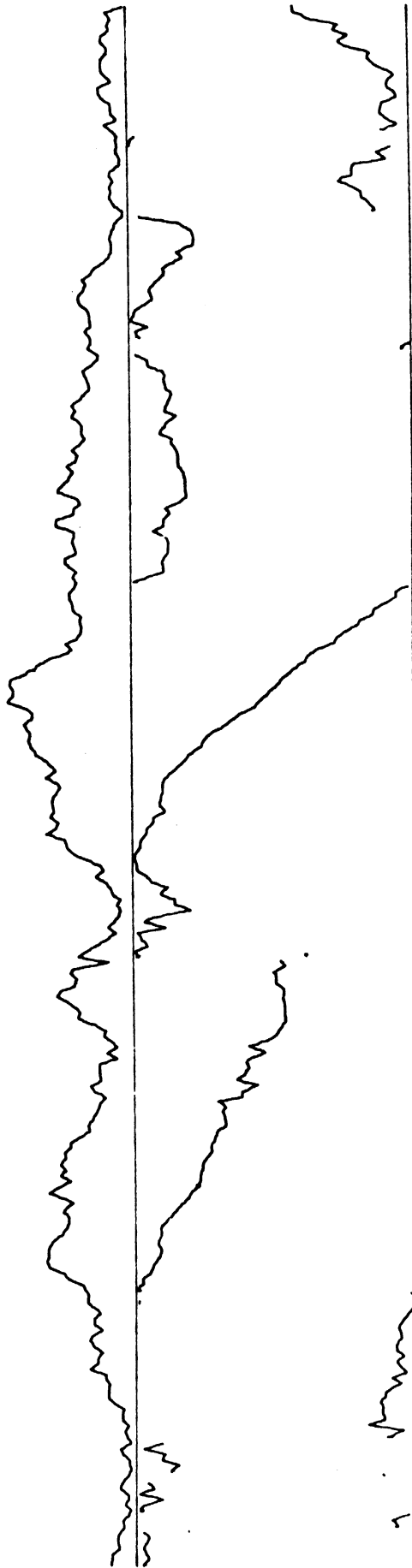
48



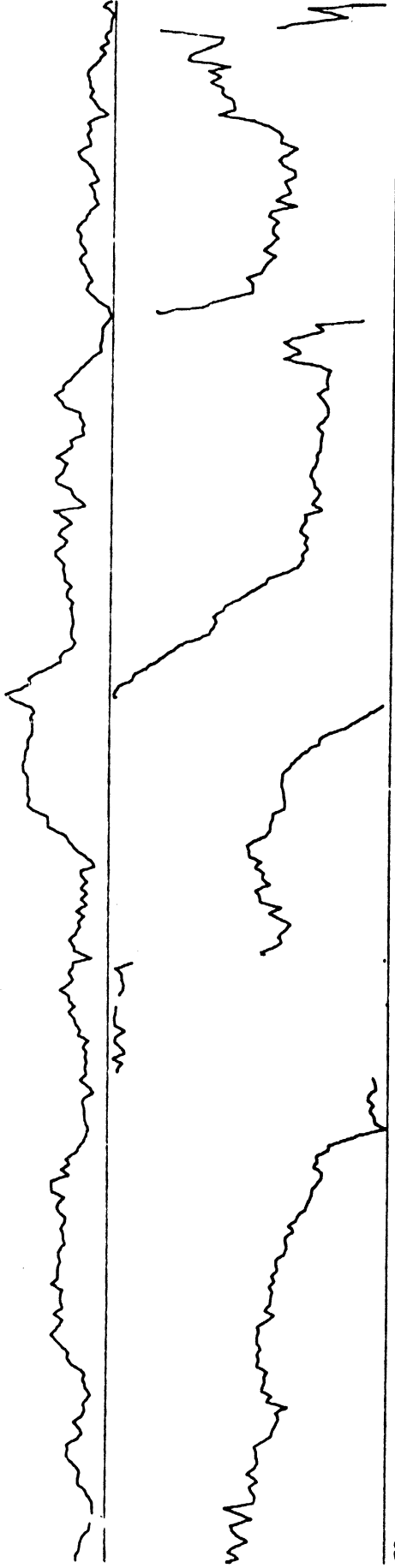
49



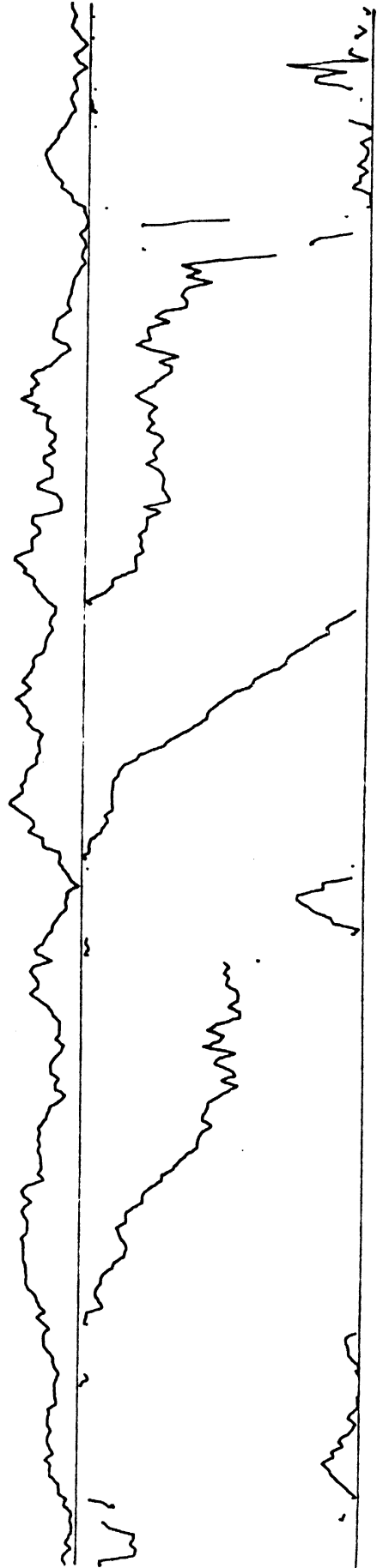
50



51

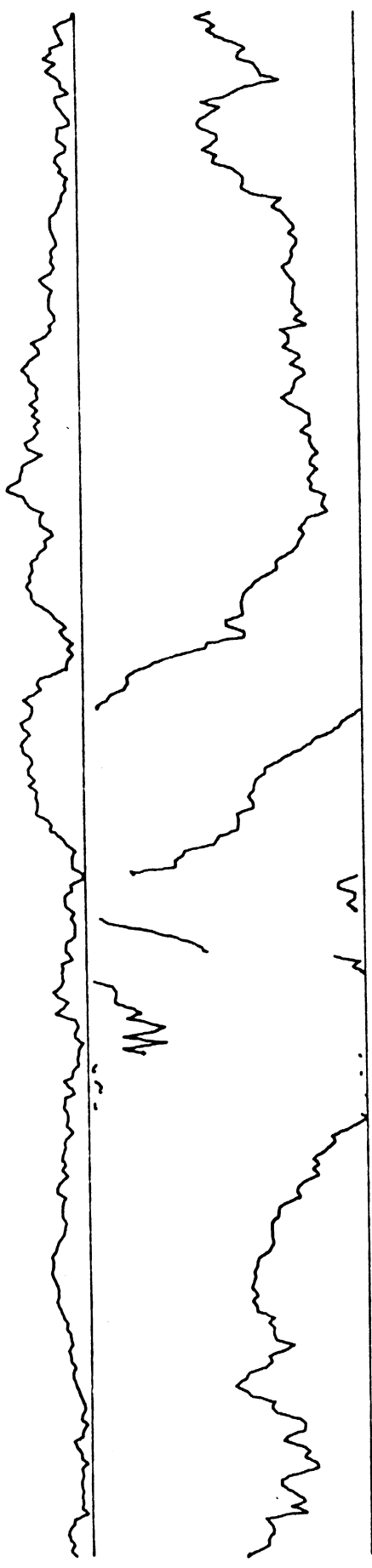


52

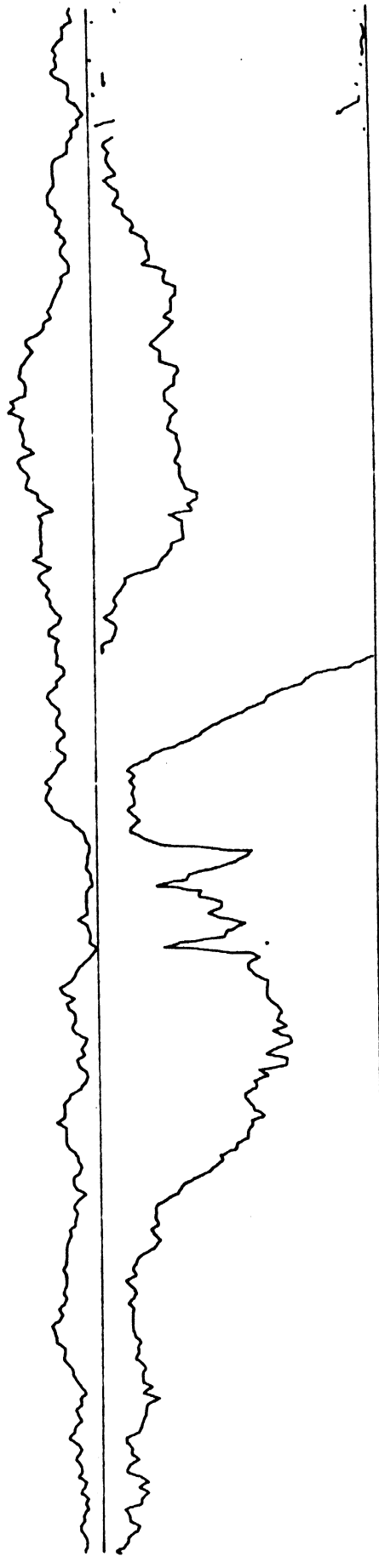




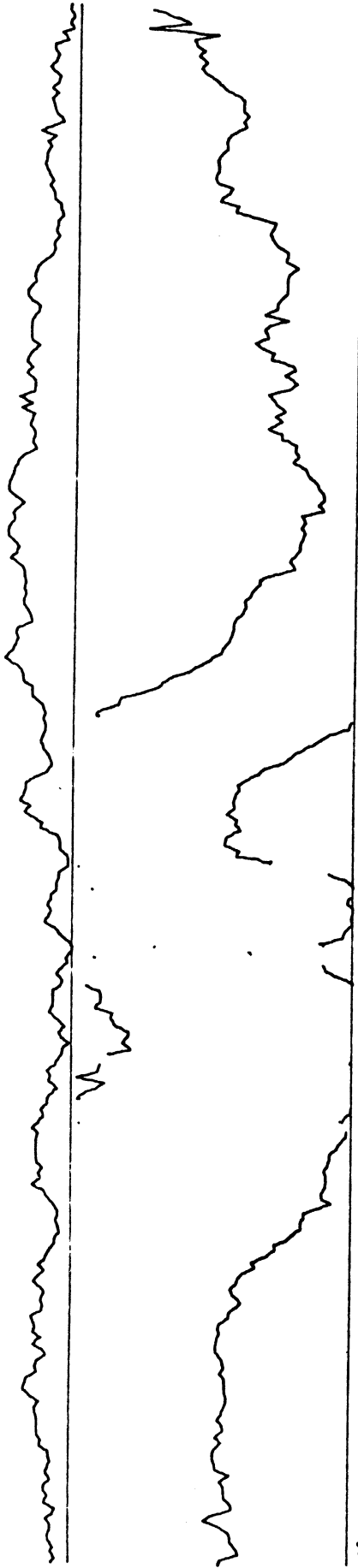
53



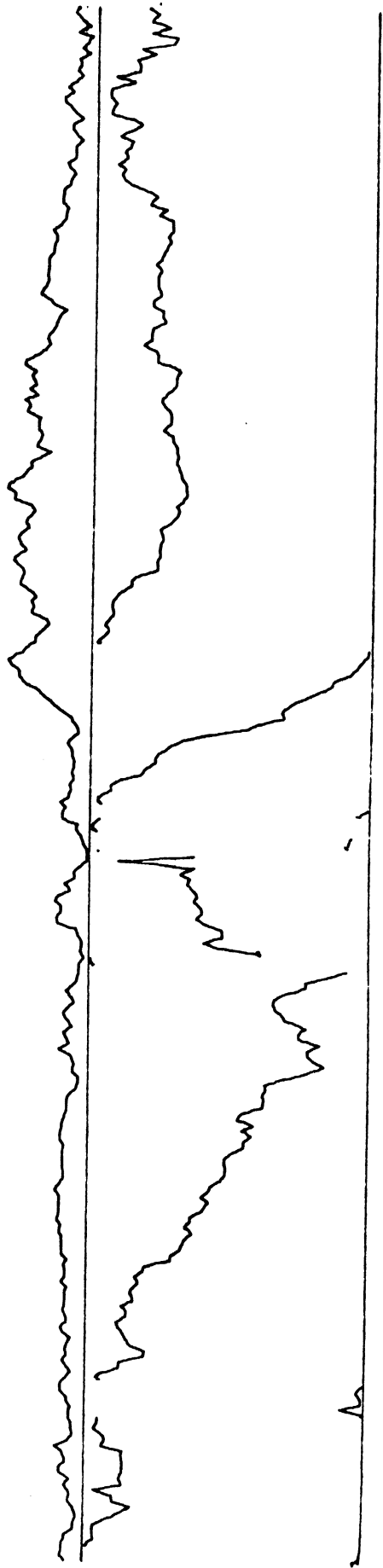
54



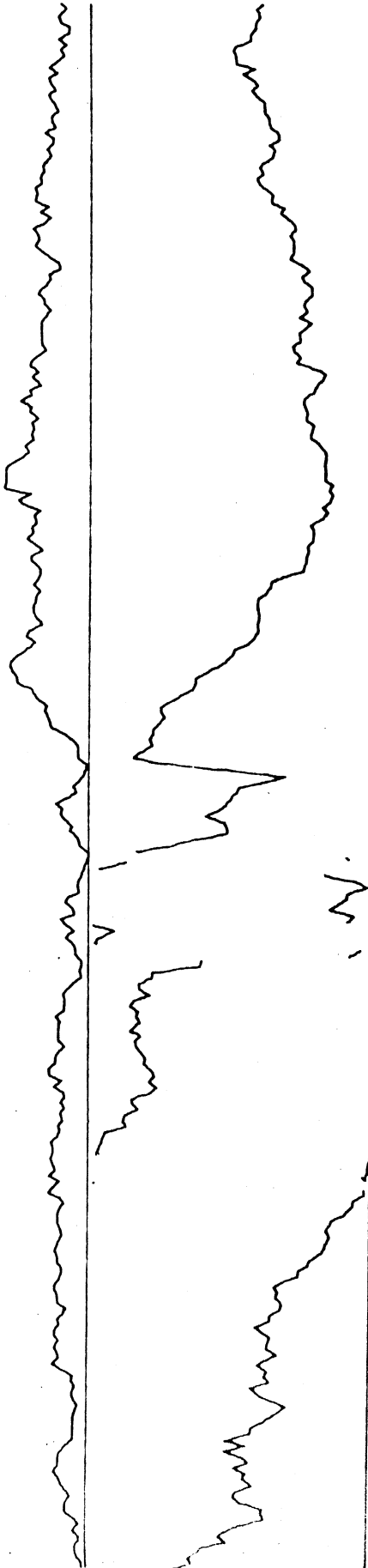
55



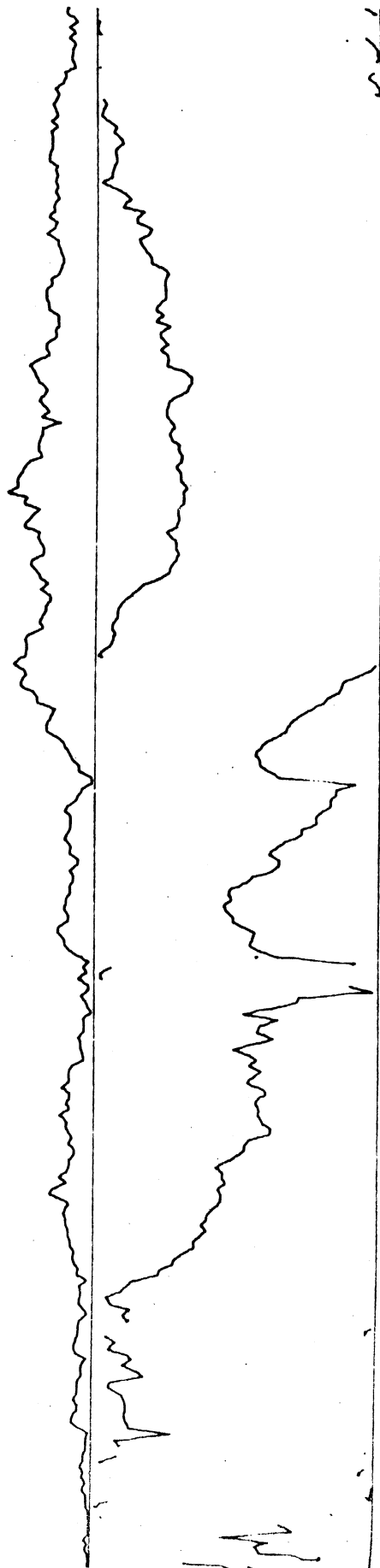
56



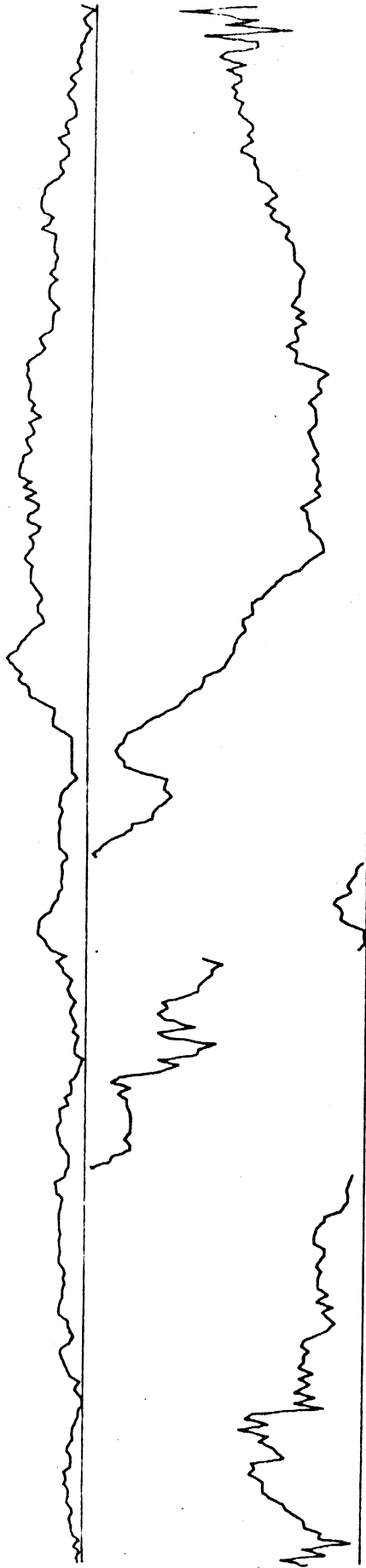
57



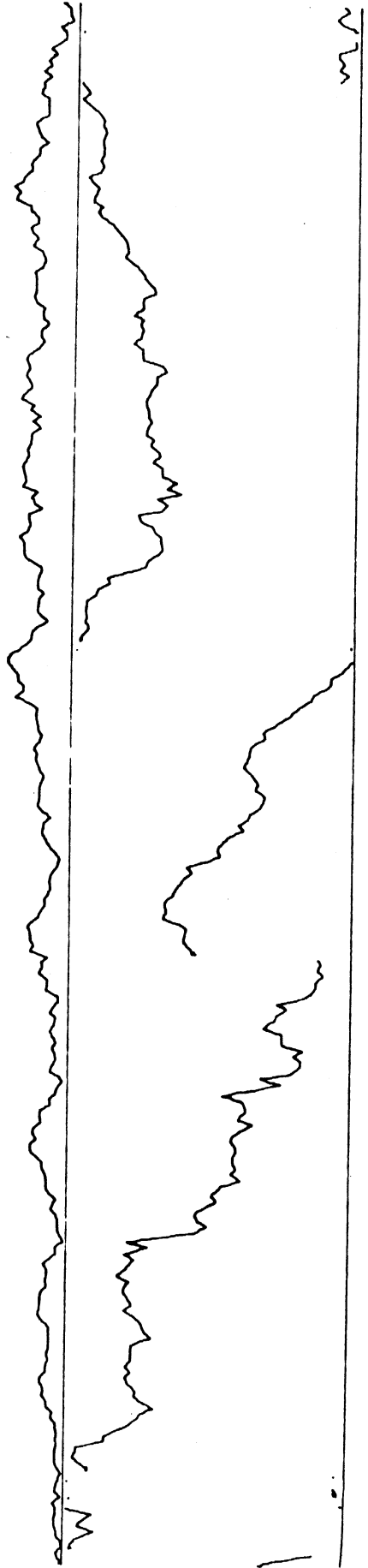
58

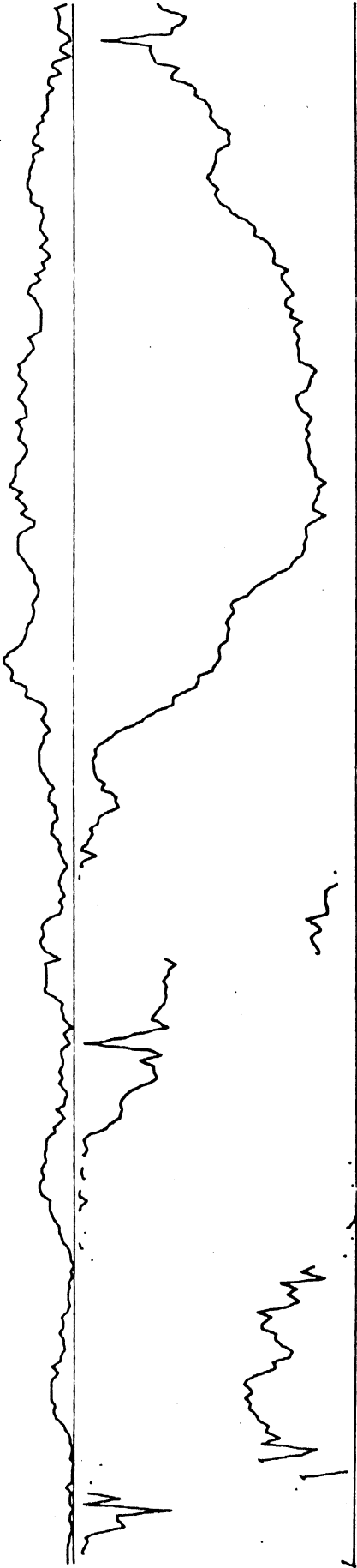


59



60





4

## REFERENCES

1. J. C. Steinberg and T. G. Birdsall, "Underwater Sound Propagation in the Straits of Florida," Acoust. Soc. Am., Vol. 39, No. 2, February 1966, pp. 301-315.
2. R. M. Heitmeyer, Underwater Sound Propagation in the Straits of Florida: The Preliminary Analysis of the MIMI Experiment of 1970, Technical Report No. 213, Cooley Electronics Laboratory, The University of Michigan, Ann Arbor, June 1971.
3. A. Papoulis, Probability, Random Variables, and Stochastic Processes, McGraw-Hill Inc., 1965, pp. 373-377.

## DISTRIBUTION LIST

	<u>No. of Copies</u>
Office of Naval Research (Code 468)	1
(Code 102-OS)	1
(Code 480)	1
Navy Department Washington, D. C. 20360	
Director, Naval Research Laboratory Technical Information Division Washington, D. C. 20390	6
Director Office of Naval Research Branch Office 1030 East Green Street Pasadena, California 91101	1
Dr. Christopher V. Kimball 8441 S. W. 142 Street Miami, Florida 33149	1
Director Office of Naval Research Branch Office 495 Summer Street Boston, Massachusetts 02210	1
Office of Naval Research New York Area Office 207 West 24th Street New York, New York 10011	1
Director Office of Naval Research Branch Office 536 S. Clark Street Chicago, Illinois 60605	1
Director Naval Research Laboratory Attn: Library, Code 2029 (ONRL) Washington, D. C. 20390	8

DISTRIBUTION LIST (Cont.)

	<u>No. of Copies</u>
Commander Naval Ordnance Laboratory Acoustics Division White Oak, Silver Spring, Maryland 20907 Attn: Dr. Zaka Slawsky	1
Commanding Officer Naval Ship Research & Development Center Annapolis, Maryland 21401	1
Commander Naval Undersea Research & Development Center San Diego, California 92132 Attn: Dr. Dan Andrews Mr. Henry Aurand	2
Chief Scientist Navy Underwater Sound Reference Division P. O. Box 8337 Orlando, Florida 32800	1
Commanding Officer and Director Navy Underwater Systems Center Fort Trumbull New London, Connecticut 06321	1
Commander Naval Air Development Center Johnsville, Warminster, Pennsylvania 18974	1
Commanding Officer and Director Naval Ship Research and Development Center Washington, D. C. 20007	1
Superintendent Naval Postgraduate School Monterey, California 93940	1
Commanding Officer & Director Naval Ship Research & Development Center* Panama City, Florida 32402	1

---

\* Formerly Mine Defense Lab.



DISTRIBUTION LIST (Cont.)

	<u>No. of Copies</u>
Naval Underwater Weapons Research & Engineering Station Newport, Rhode Island 02840	1
Superintendent Naval Academy Annapolis, Maryland 21401	1
Scientific and Technical Information Center 4301 Suitland Road Washington, D. C. 20390 Attn: Dr. T. Williams Mr. E. Bissett	2
Commander Naval Ordnance Systems Command Code ORD-03C Navy Department Washington, D. C. 20360	1
Commander Naval Ship Systems Command Code SHIPS 037 Navy Department Washington, D. C. 20360	1
Commander Naval Ship Systems Command Code SHIPS 00V1 Washington, D. C. 20360 Attn: CDR Bruce Gilchrist Mr. Carey D. Smith	2
Commander Naval Undersea Research & Development Center 3202 E. Foothill Boulevard Pasadena, California 91107	1
Commanding Officer Fleet Numerical Weather Facility Monterey, California 93940	1

## DISTRIBUTION LIST (Cont.)

	<u>No. of Copies</u>
Defense Documentation Center Cameron Station Alexandria, Virginia 22314	5
Dr. James Probus Office of the Assistant Secretary of the Navy (R&D) Room 4E741, The Pentagon Washington, D. C. 20350	1
Mr. Allan D. Simon Office of the Secretary of Defense DDR&E Room 3E1040, The Pentagon Washington, D. C. 20301	1
Capt. J. Kelly Naval Electronics Systems Command Code EPO-3 Washington, D. C. 20360	1
Chief of Naval Operations Room 5B718, The Pentagon Washington, D. C. 20350 Attn: Mr. Benjamin Rosenberg	1
Chief of Naval Operations Rm 4C559, The Pentagon Washington, D. C. 20350 Attn: CDR J. M. Van Metre	1
Chief of Naval Operations 801 No. Randolph St. Arlington, Virginia 22203	1
Dr. Melvin J. Jacobson Rensselaer Polytechnic Institute Troy, New York 12181	1
Dr. Charles Stutt General Electric Co. P. O. Box 1088 Schenectady, New York 12301	1

DISTRIBUTION LIST (Cont.)

	<u>No. of Copies</u>
Dr. Alan Winder EDO Corporation College Point, New York 11356	1
Dr. T. G. Birdsall Cooley Electronics Lab. The University of Michigan Ann Arbor, Michigan 48105	1
Mr. Morton Kronengold Director, Institute for Acoustical Research 615 S.W. 2nd Avenue Miami, Florida 33130	1
Mr. Robert Cunningham Bendix Corporation 11600 Sherman Way North Hollywood, California 91606	1
Dr. H. S. Hayre University of Houston Cullen Boulevard Houston, Texas 77004	1
Dr. Robert R. Brockhurst Woods Hole Oceanographic Institute Woods Hole, Massachusetts 02543	1
Dr. Stephen Wolff Johns Hopkins University Baltimore, Maryland 21218	1
Dr. Bruce P. Bogert Bell Telephone Laboratories Whippany Road Whippany, New Jersey 07981	1
Dr. Albert Nuttall Navy Underwater Systems Center Fort Trumbull New London, Connecticut 06320	1

DISTRIBUTION LIST (Cont.)

	<u>No. of Copies</u>
Dr. Philip Stocklin Raytheon Company P. O. Box 360 Newport, Rhode Island 02841	1
Dr. H. W. Marsh Navy Underwater Systems Center Fort Trumbull New London, Connecticut 06320	1
Dr. David Middleton 35 Concord Ave., Apt. #1 Cambridge, Massachusetts 02138	1
Mr. Richard Vesper Perkin-Elmer Corporation Electro-Optical Division Norwalk, Connecticut 06852	1
Dr. Donald W. Tufts University of Rhode Island Kingston, Rhode Island 02881	1
Dr. Loren W. Nolte Dept. of Electrical Engineering Duke University Durham, North Carolina 27706	1
Dr. Thomas W. Ellis Texas Instruments, Inc. 13500 North Central Expressway Dallas, Texas 75231	1
Mr. Robert Swarts Honeywell, Inc. Marine Systems Center 5303 Shilshole Ave., N.W. Seattle, Washington, 98107	1
Mr. Charles Loda Institute for Defense Analyses 400 Army-Navy Drive Arlington, Virginia 22202	1

DISTRIBUTION LIST (Cont.)

	<u>No. of Copies</u>
Mr. Beaumont Buck General Motors Corporation Defense Research Division 6767 Holister Ave. Goleta, California 93017	1
Dr. M. Weinstein Underwater Systems, Inc. 8121 Georgia Avenue Silver Spring, Maryland 20910	1
Dr. Harold Saxton 1601 Research Blvd. TRACOR, Inc. Rockville, Maryland 20850	1
Dr. Thomas G. Kincaid General Electric Company P. O. Box 1088 Schenectady, New York 12305	1
Applied Research Laboratories The University of Texas at Austin Austin, Texas 78712 Attn: Dr. Loyd Hampton Dr. Charles Wood	3
Dr. Paul McElroy Woods Hole Oceanographic Institution Woods Hole, Massachusetts 02543	1
Dr. John Bouyoucos Hydroacoustics, Inc. P. O. Box 3818 Rochester, New York 14610	1
Dr. Joseph Lapointe Systems Control, Inc. 260 Sheridan Avenue Palo Alto, Calif. 94306	1
Cooley Electronics Laboratory University of Michigan Ann Arbor, Michigan 48105	25

DISTRIBUTION LIST (Cont.)

	<u>No. of Copies</u>
Mr. Ray Veenkant Texas Instruments, Inc. North Central Expressway Dallas, Texas 75222 Mail Station 208	1

## DOCUMENT CONTROL DATA - R &amp; D

*(Security classification of title, body of abstract and indexing annotation must be entered when the overall report is classified)*

1. ORIGINATING ACTIVITY (Corporate author) Cooley Electronics Laboratory University of Michigan Ann Arbor, Michigan 48105		2a. REPORT SECURITY CLASSIFICATION Unclassified	
		2b. GROUP	
3. REPORT TITLE A MIMI Propagation Study: Coherent Spectra of Wideband Underwater Acoustic Receptions in the Straits of Florida, 25 November 1970			
4. DESCRIPTIVE NOTES (Type of report and inclusive dates) Technical Report May 1973			
5. AUTHOR(S) (First name, middle initial, last name) Gerald N. Cederquist			
6. REPORT DATE May 1973	7a. TOTAL NO. OF PAGES 128	7b. NO. OF REFS 3	
8a. CONTRACT OR GRANT NO. N00014-67-A-0181-0035	9a. ORIGINATOR'S REPORT NUMBER(S) TR 215		
b. PROJECT NO.	9b. OTHER REPORT NO(S) (Any other numbers that may be assigned this report) 004860-1-T		
c.			
d.			
10. DISTRIBUTION STATEMENT  Approved for public release; distribution unlimited.			
11. SUPPLEMENTARY NOTES		12. SPONSORING MILITARY ACTIVITY Office of Naval Research Department of the Navy Arlington, Virginia 22217	
13. ABSTRACT  In an underwater acoustic propagation experiment conducted in November 1970 a periodic broadband signal, centered about 420 Hz, was transmitted across the Straits of Florida continuously for 19 days. This report presents the preliminary results from spectral analysis of the acoustic reception of this signal at Bimini, Bahamas, during a 7.61-hour period on 25 November 1970. The spectra are noteworthy for their slow rate of change during this period. Plots of the spectral amplitude and phase of the reception are presented for a 50 Hz bandwidth centered about 420 Hz.			

KEY WORDS	LINK A		LINK B		LINK C	
	ROLE	WT	ROLE	WT	ROLE	WT
Signal processing Underwater sound Multipath Surface reverberation Acoustic propagation						



UNIVERSITY OF MICHIGAN



3 9015 02086 6433